選択的溶出法による新規H型層状ペロブスカイトの合成とその高機能光触媒への変換

課題番号：14350462

平成14年度～平成16年度科学研究費補助金（基盤研究(B)）
研究成果報告書

平成18年3月

研究代表者　菅原 義之
（早稲田大学理工学術院教授）

はしがき

研究組織

研究代表者：菅原　義之（早稲田大学理工学術院教授）

研究分担者：安盛　敦雄（東京理科大学基礎工学部教授）

研究期間　　平成14年度　～　平成16年度

研究経費

金額単位：千円

	直接経費	間接経費	合　計
平成　14　年度	10,700	0	10,700
平成　15　年度	2,200	0	2,200
平成　16　年度	2,300	0	2,300
総　計	15,200	0	15,200

研究概要

光触媒は太陽エネルギーの有効利用の観点から注目を集め、原子の規則配列に基づいたバンド構造に起因することから、構造・組成が重要である。ペロブスカイト関連構造を有する物質群も光触媒活性を示すものがあり、中でも、ペロブスカイト構造を有するナノシートに交換性のカチオンが挟み込まれたイオン交換性層状ペロブスカイトは、酸処理することで層間に水素イオンを有するH型層状ペロブスカイトに変換する。H 型層状ペロブスカイトは光触媒能などのペロブスカイト構造に由来する物性を示すだけでなく、層間に有機分子を取り込ませることや、層を剥離させ単一のナノシートとして用いることができる。一方、層間に酸化ビスマスシートが挟まれたAurivillius相は酸処理により酸化ビスマス層だけが選択的に溶出し、イオン交換性層状ペロブスカイトから合成されるH型層状ペロブスカイトとは異なる組成を持つ新しいH型層状ペロブスカイトが合成できる。

そこで、本研究ではAurivillius相中の酸化ビスマス層の選択的溶出により新しいH型層状ペロブスカイトを合成して、これらの光触媒活性を調査することを目的とする。

1) H 型層状ペロブスカイトの光触媒特性

Aurivillius 相 $Bi_2ANaNb_3O_{12}$ (A = Ca or Sr)と $Bi_2CaNaTa_3O_{12}$ を酸処理して酸化ビスマス層を選択的に溶出することで H 型層状ペロブスカイトの合成を行い、これらの光触媒活性について検討した。光触媒活性は紫外線照射下、エタノール水溶液(20wt%)から発生する水素量で見積もった。酸処理前では水素発生に活性を示さなかったが、酸処理後は水素発生に活性を示した。UV-Vis 測定の結果、酸化ビスマス層の溶出により電子構造が変化し、伝導帯の位置が変化したため光触媒活性を示したと考えられる。また、光触媒調査後の試料の XRD パターンは層間隔が増加しており、水素発生に層間が有効に使用されていると考えられ、酸化ビスマス層の溶出が表面積を増加させ光触媒活性を向上させたと考えられる。

2) 新しい 2 層構造をもつ層状タングステン酸の合成

層状ペロブスカイトと類似構造を有するナノシートに酸化ビスマス層が挟まれた Aurivillius 相、$Bi_2W_2O_9$ の酸処理を行った。XRD、ICP、TG、TEM により、酸化ビスマス層のみが選択的溶出されたことを確認し、光触媒活性を示す可能性がある $H_2W_2O_7{\cdot}nH_2O$ を合成できることを示した。

3) H 型層状ペロブスカイトとアルコールとの相互作用

光触媒による水からの水素発生の犠牲試薬である *n*-アルコールと $HCa_2Nb_3O_{10}{\cdot}xH_2O$ の相互作用を調査したところ、Nb-O-C 結合を形成したアルコキシ基修飾体を形成することが分かった。

上述の結果を基に光触媒活性の向上のため、ピラー化(層間内架橋)による表面積の増加の手法を検討した。XRD、IR、NMR より、CH_2=CH$(CH_2)_n$O-修飾 $HLaNb_2O_7{\cdot}xH_2O$ (n = 3, 8)とクロロシラン、オリゴシロキサンとのヒドロシリル化反応が層間で起こることを確認し、光触媒活性を示す層状ペロブスカイトにシリカを段階的に導入する新たなプロセスを開発した。

また、新しい光触媒材料の合成のため、アルコキシ基修飾体を用いシロキサン系高分子との複合化を行った。アルコキシ基修飾体と金属アルコキシド、シロキサン系高分子を共加水分解(ゾルゲル反応)を行うことで、H 型層状ペロブスカイトが剥離し、光触媒活性を示すペロブスカイトナノシートが高分子中に分散したハイブリッドを合成した。

研究発表

(A) 本研究に関する論文

[1] M. Kudo, S. Tsuzuki, K. Katsumata and A. Yasumori and Y. Sugahara, "Effects of selective leaching of bismuth oxide sheets in triple-layered Aurivillius phases on their photocatalytic activities", *Chemical Physics Letters*, **393**, 12–16 (2004).

[2] M. Kudo, H. Ohkawa, W. Sugimoto, N. Kumada, Z. Liu, O. Terasaki, and Y. Sugahara, "A layered tungstic acid $H_2W_2O_7 \cdot nH_2O$ with a double-octahedral sheet structure: Conversion process from an Aurivillius phase $Bi_2W_2O_9$ and structural characterization", *Inorganic Chemistry*, **42**, 4479–4484 (2003).

[3] S. Tahara and Y. Sugahara, "Interlayer surface modification of the protonated triple-layered perovskite $HCa_2Nb_3O_{10} \cdot xH_2O$ with *n*-alcohols", *Langmuir*, **19**, 9473–9478 (2003).

[4] S. Yoshioka, Y. Takeda, Y. Uchimaru and Y. Sugahara, "Hydrosilylation in the 2D interlayer space between inorganic layers: reaction between immobilized C=C groups on the interlayer surface of layered perovskite $HLaNb_2O_7 \cdot xH_2O$ and chlorohydrosilanes", *Journal of Organometallic Chemistry*, **686**, 145–150 (2003).

[5] S. Tahara and Y. Sugahara, "Novel materials derived from layered perovskites using a *Chimie Douce* approach", *Recent Research Development in Inorganic Chemistry*, **4**, 13–34 (2004.)

[6] S. Tahara, Y. Takeda and Y. Sugahara, "Preparation of organic-inorganic hybrids possessing nanosheets with perovskite-related structures *via* exfoliation during a sol-gel process", *Chemistry of Materials*, **17**, 6198–6204 (2005).

[7] S. Tahara, K. Ohta, S. Yoshioka, Y. Takeda, Y. Uchimaru and Y. Sugahara, "Hydrosilylation of the CH_2=CH- groups immobilized on the interlayer surface of ion-exchangeable layered perovskite with hydorochlorosilanes and oligosiloxanes", *Progress in Organometallic Chemistry Research*, in press.

B) 口頭発表

[1] 工藤学, 続佐紀, 勝又健一, 安盛敦雄, 菅原義之, "Aurivillius 相の酸処理により合成した3層構造を持つH型層状ペロブスカイトの光触媒特性", 第15回日本セラミックス協会秋季シンポジウム, 秋田大学, 1H03, 2002 年 9 月.

[2] 谷晋輔, 津野田悠, 小森佳彦, 林繁信, 菅原義之, "$Bi_2SrTa_2O_9$から得たH型層状ペロブスカイトにおける層間Hの環境および運動性", 第18回日本セラミックス協会関東支部研究発表会, 浜松市, 1B17, 2002 年 7 月.

[3] 梶原剛, 田原聖一, 菅原義之, "Ruddlesden-Popper 相層状ペロブスカイト $H_2La_2Ti_3O_{10}$ へのアルキルアミンのインターカレーション", 第 15 回日本セラミックス協会秋季シンポジウム, 秋田大学, 2H04, 2002 年 9 月

[4] 田原聖一, 菅原義之, "層状ペロブスカイトとポリジメチルシロキサンからの有機誘導体型層状ペロブスカイトポリマーナノハイブリッドの合成", 第51回高分子討論会, 九州工業大学, IIH05, 2002 年 10 月.

[5] 中曽根文, 熊田伸弘, 菅原義之, "ソフト化学的手法による低酸化層状タングステン酸 $H_xW_2O_7$ の合成", 第41回セラミックス基礎科学討論会, 鹿児島市, 2F7, 2003 年 1 月.

[6] 田原聖一, 菅原義之, "層表面へのオルガノシロキサンの固定化による層状ペロブスカイト-ポリシロキサンハイブリッドの合成", 第 41 回セラミックス基礎科学討論会, 鹿児島市, 2F8, 2003 年 1 月.

[7] 谷晋輔, 津野田悠, 小森佳彦, 林繁信, 菅原義之, "H型層状ペロブスカイト層間における酸性プロトンの特性評価", 第 41 回セラミックス基礎科学討論会, 鹿児島市, 2F9, 2003 年 1 月.

[8] 田原聖一, 菅原義之, "*n*-アルキルアミン層間化合物を中間体として用いた層状ペロブスカイト有機誘導体の合成", 日本セラミックス協会 2003 年年会, 東京都立大学, 2K22, 2003 年 3 月.

[9] 大田和督, 田原聖一, 菅原義之, "ヒドロシリル基末端ポリジメチルシロキサンと層状ペロブスカイト $HLaNb_2O_7$ 層表面に固定化された C=C 結合とのヒドロシリル化反応", 日本セラミックス協会 2003 年年会, 2K23, 東京都立大学, 2003 年 3 月.

[10] 谷晋輔, 工藤学, 小森佳彦, 林繁信, 原晋治, 宮山勝, 菅原義之, "NMR 及び伝導度測定を用いた層状タングステン酸 $H_2W_2O_7{\cdot}nH_2O$ における水素環境の調査", 日本セラミックス協会 2003 年年会, 東京都立大学, 2K24, 2003 年 3 月.

[11] 中曽根文, 工藤学, 大川肇, 杉本渉, 熊田伸弘, 劉崢, 寺崎治, 菅原義之, "Aurivillius 相 $Bi_2W_2O_9$ の酸処理により得られる層状タングステン酸 $H_2W_2O_7$ の透過型顕微鏡観察", 日本セラミックス協会 2003 年年会, 東京都立大学, 2I32, 2003 年 3 月.

[12] 梶原剛, 山下貴史, 菅原義之, "$Bi_2SrTa_2O_9$ を酸処理して得られる H 型層状ペロブスカイト $H_{1.8}[Sr_{0.8}Bi_{0.2}Ta_2O_7]$ へのジアミンのインターカレーション", 日本化学会第 83 春季年会, 早稲田大学, 3PC076, 2003 年 3 月.

[13] 杉本渉, 工藤学, 津野田悠, 白田雅史, 菅原義之, "Bi 層状ペロブスカイトの酸化ビスマス層の溶解による新規 H 型 層状ペロブスカイトの創製と化学的性質", 日本化学会第 83 春季年会, 早稲田大学, 3C9-11, 2003 年 3 月.

[14] 田原聖一, 菅原義之, "層状ペロブスカイトの反応性を利用したハイブリッド材料の作製", 粉体粉末冶金協会平成 15 年度春季大会, 早稲田大学, 3-37A, 2003 年 5 月.

[15] Y. Sugahara, "Nano-structured Inorganic-Organic Hybrids Based on Ion-exchangeable Layered Perovskites", 5th U.S.-Japan Joint Seminar on Inorganic and Organometallic Polymers "NANO 2003 -Nanotechnology Hybrids", Mishima, Japan, May 2003.

[16] 鈴木裕美, 野津和也, 竹田洋介, 杉本渉, 菅原義之, "層状ペロブスカイト有機誘導体のアルコール交換型反応とその反応機構", 第19回日本セラミックス協会関東支部研究発表会, 千葉県長柄町, 2B05, 2003 年 7 月.

[17] 菅原義之, 田原聖一, 竹田洋介, 鈴木裕美, "層状ペロブスカイトの層表面修飾によるハイブリッド材料の合成", 第 52 回高分子討論会, 山口大学, II K07, 2003 年 9 月.

[18] Y. Sugahara, M. Kudo, H. Ohkawa, W. Sugimoto, N. Kumada, Z. Liu, O. Terasaki, "A Novel Layered Tungstic Acid $H_2W_2O_7 \cdot nH_2O$ Prepared from an Aurivillius Phase $Bi_2W_2O_9$ *via Chimie Douce* approach", IUMRS-ICAM 2003, Yokohama, Japan, C2-11-O34, Oct. 2003.

[19] 大田和督, 田原聖一, 内丸祐子, 菅原義之, "層状ペロブスカイト層間内に固定化されたC=C結合と末端にSi-H基を有するポリマーとのヒドロシリル化反応による無機−有機複合体の合成", 第 22 回無機高分子研究討論会, 東京理科大学, 35, 2003 年 11 月.

[20] S. Ishikawa, Y. Tsunoda, M. Kudo, Y. Sugahara, "Preparation of New Ion-Exchangeable Layered Perovskites via Selective eaching of Bismuth Oxide Sheets in Aurivillius Phases and Their Intercalation Behavior", Nano-structured Materials based on Layered Inorganics, University of Tokyo, P17, JAPAN, Feb. 2004.

[21] K. Ohta, S. Yoshioka, H. Suzuki, S. Tahara, Y. Sugahara, "Nano-scaled Inoraganic-Organic Hybrids Prepared through Grafting Reactions of Ion-Exchangeable Layered Perovskite", Nano-structured Materials based on Layered Inorganics, University of Tokyo, P18, JAPAN, Feb. 2004.

[22] 大田和督, 田原聖一, 内丸祐子, 菅原義之, "層状ペロブスカイト層間内に固定化されたC=C結合とヒドロオリゴシロキサンとのヒドロシリル化反応による無機/有機複合体の合成", 第 20 回日本セラミックス協会関東支部研究発表会, 埼玉県伊奈町, 1A28, 2004 年 7 月.

[23] 田原聖一, 菅原義之, "イオン交換性層状ペロブスカイトと *n*-アルコールによる層表面修飾体の合成", 第 20 回日本セラミックス協会関東支部研究発表会, 埼玉県伊奈町, 1A29, 2004 年 7 月.

[24] 田原聖一, 菅原義之, "共加水分解反応による金属オキソアルコキシドナノシート-ポリシロキサンハイブリッドの調製", 日本ゾル-ゲル学会第 2 回討論会, 関西大学, 62, 2004 年 7 月.

[25] 田原聖一, 菅原義之, "ゾルゲル法を用いたナノシート分散によるポリシロキサンハイブリッドの合成", 第 53 回高分子討論会討論会, 北海道大学, 3J07, 2004 年 9 月.

[26] 菅原義之, 鈴木裕美, 竹田洋介, 田原聖一, 吉岡聰, 内丸祐子, "イオン交換性層状ペロブスカイトの層表面修飾による 2 次元有機-無機ハイブッリッドの合成",セラミックス協会第 17 回秋季シンポジウム, 北陸先端科学技術大学院大学, 2F05, 2004 年 9 月.

[27] 梶原剛, 田原聖一, 菅原義之, "イオン交換性層状ペロブスカイト $H_2La_2Ti_3O_{10}$ へのアルキルアミンのインターカレーション反応機構",第 23 回無機高分子研究討論会, 東京理科大学, 15, 2004 年 11 月.

[28] 菅原義之, 田原聖一, 鈴木裕美, 竹田洋介, "イオン交換性層状ペロブスカイトの層表面修飾による有機一無機ハイブリッドの合成",第 23 回無機高分子研究討論会, 東京理科大学, 16, 2004 年 11 月.

[29] 大田和督, 田原聖一, 菅原義之, 内丸祐子, "層状ペロブスカイト層間内に固定化した C=C 結合の付加反応", 日本化学会第 85 春季年会, 神奈川大学, 1PC120, 2005 年 3 月.

Available online at www.sciencedirect.com
SCIENCE DIRECT
Chemical Physics Letters 393 (2004) 12–16
CHEMICAL PHYSICS LETTERS
www.elsevier.com/locate/cplett

Effects of selective leaching of bismuth oxide sheets in triple-layered Aurivillius phases on their photocatalytic activities

Manabu Kudo [a], Saki Tsuzuki [a], Ken-ichi Katsumata [b], Atsuo Yasumori [b,1], Yoshiyuki Sugahara [a,*]

[a] Department of Applied Chemistry, School of Science and Engineering, Waseda University, Ohkubo-3, Shinjuku-ku, Tokyo 169-8555, Japan
[b] Department of Metallurgy and Ceramics Science, Tokyo Institute of Technology, O-Okayama-2, Meguro, Tokyo 152-8552, Japan

Received 29 March 2004; in final form 3 June 2004
Available online 19 June 2004

Abstract

The photocatalytic activities of triple-layered Aurivillius phases, $Bi_2A'NaNb_3O_{12}$ ($A' = Sr$, Ca) and $Bi_2CaNaTa_3O_{12}$, and of protonated forms prepared from these Aurivillius phases through selective leaching of bismuth oxide sheets were investigated. UV–Vis diffuse reflectance spectra showed blue shifts of the adsorption edges upon selective leaching. Although none of the triple-layered Aurivillius phases were active for photocatalytic H_2 evolution from a 20 vol% ethanol solution, all the corresponding protonated forms showed photocatalytic activities for H_2 evolution. The effects of the changes in electronic structures and interlayer surface creation on photocatalytic activities are discussed.

1. Introduction

Ion-exchangeable layered perovskites consist of exchangeable interlayer cations and perovskite-like slabs, whose interlayer surface corresponds to the (1 0 0) plane of cubic perovskites [1]. These are classified into Dion–Jacobson phases ($M[A_{n-1}B_nO_{3n+1}]$) and Ruddlesden–Popper phases ($M_2[A_{n-1}B_nO_{3n+1}]$) based on their layer charge. The interlayer cations (M) can be exchanged with protons through acid treatment to give their protonated forms ($H_x[A_{n-1}B_nO_{3n+1}]$, $x = 1, 2$). Because only a few kinds of metal ions can be present at the A- and B-sites of the $[A_{n-1}B_nO_{3n+1}]$ slabs, the number of protonated phases possible has been limited in the past.

Aurivillius phases ($Bi_2A_{n-1}B_nO_{3n+3}$), another series of layered perovskites, consist of bismuth oxide sheets and perovskite-like slabs, the latter of which are essentially identical to those in the ion-exchangeable layered perovskites [2–4]. We recently reported that the Aurivillius phase $Bi_2SrNaNb_3O_{12}$ can be converted into the corresponding protonated form $H_{1.8}[Sr_{0.8}Bi_{0.2}NaNb_3O_{10}]$ through selective leaching of bismuth oxide sheets by hydrochloric acid treatment [5–7]. Additional Aurivillius phases, $Bi_2SrTa_2O_9$, [8] $Bi_2CaNaNb_3O_{12}$, [7], $Bi_2Sr_2Nb_2MnO_{12}$, [1] and $Bi_2W_2O_9$, [9,10] have been converted into protonated forms and layered tungstic acid in a similar fashion. This route can potentially provide a variety of new protonated forms of ion-exchangeable layered perovskites, permitting extension of their compositional limitations.

Photocatalysts are attracting considerable attention as solar energy conversion materials [11,12]. Some ion-exchangeable layered perovskites, Dion–Jacobson-type niobates and Ruddlesden–Popper-type titanates (and their reduced-charge forms) are known to show photocatalytic activities for water splitting as well as H_2 and/or O_2 evolution from water containing sacrificial reagents [11,13,14]. Ion exchange of interlayer cations with protons, [13,15] loading of Pt or Ni, [13,16] pillaring, [17] and combining of exfoliation with restacking [18] were reported to be effective in enhancing photo-

* Corresponding author. Fax: 81-3-5286-3204.
E-mail address: ys6546@waseda.jp (Y. Sugahara).
[1] Present address: Faculty of Industrial Science and Technology, Tokyo University of Science, Yamazaki, Noda, Chiba 278-8510, Japan.

0009-2614/$ - see front matter © 2004 Elsevier B.V. All rights reserved.
doi:10.1016/j.cplett.2004.06.010

catalytic activity. Dion–Jacobson-type tantalates, $M'LnTa_2O_7$ ($M' = Cs$, Rb, Na, H; Ln = La, Pr, Nd, Sm), also showed photocatalytic activities for water splitting without the presence of sacrificial reagents, but all of the protonated forms showed relatively low photocatalytic activities [19–21]. In addition to these ion-exchangeable layered perovskites, some Aurivillius phases, Bi_2WO_6, $Bi_2W_2O_9$, and Bi_3TiNbO_9, also showed moderate photocatalytic activities [22].

We report here the effect of selective leaching of bismuth oxide sheets on the photocatalytic H_2 evolution behavior of Aurivillius phases. Aurivillius phases with triple-layered perovskite-like slabs [$A_2B_3O_{10}$], $Bi_2A'NaNb_3O_{12}$ ($A' = Sr$, Ca) and $Bi_2CaNaTa_3O_{12}$, were employed. Since acid treatment of $Bi_2CaNaTa_3O_{12}$ has not been reported, the characteristics of acid-treated $Bi_2CaNaTa_3O_{12}$ are presented. The photocatalytic activities and UV–Vis diffuse reflectance spectra of both these Aurivillius phases and the protonated forms derived from them are reported. The UV–Vis diffuse reflectance spectra of $Bi_2SrTa_2O_9$ and its acid-treated product, $H_{1.8}[Sr_{0.8}Bi_{0.2}Ta_2O_7]$, [8] are also demonstrated, furthermore, to discuss the effect of selective leaching on the electronic structures of the Aurivillius phases.

2. Experimental

The Aurivillius phases were prepared by solid-state reactions. The preparation procedure for $Bi_2SrNaNb_3O_{12}$ was slightly modified from that described in our previous report [7]. $Bi_2SrNaNb_3O_{12}$ was prepared from $Bi_2SrNb_2O_9$ and $NaNbO_3$ at 1100 °C for 12 h with intermittent grinding conducted every 3 h. $Bi_2CaNaNb_3O_{12}$ was prepared as described elsewhere [7]. $Bi_2CaNaTa_3O_{12}$, a tantalate analogue of $Bi_2CaNaNb_3O_{12}$, [7] was prepared from a stoichiometric mixture of $Bi_2CaTa_2O_9$ and $NaTaO_3$ at 1000 °C for 24 h with intermittent grinding. $Bi_2CaNaTa_3O_{12}$ crystallized as an orthorhombic phase, and the lattice parameters refined by Rietveld refinement (space group: *B2cb* (No. 41)) [23] were $a = 0.5475(3)$, $b = 0.5449(3)$, and $c = 3.273(2)$ nm, which are very close to the lattice parameters of $Bi_2CaNaNb_3O_{12}$ ($a = 0.54836(3)$, $b = 0.54585(4)$ and $c = 3.2731(1)$ nm) [7]. The composition of the metals (determined by inductively coupled plasma emission spectrometry, ICP) was consistent with the nominal composition.

$Bi_2A'NaNb_3O_{12}$ ($A' = Sr$, Ca) was converted into the corresponding protonated forms by treatment with 6 M HCl for 72 h, as described elsewhere [7]. ICP and thermogravimetry (TG) analyses revealed that the protonated phases obtained in the present conversion were $H_{1.7}[Sr_{0.7}Bi_{0.3}NaNb_3O_{10}]$ and $H_{1.8}[Ca_{0.8}Bi_{0.2}NaNb_3O_{10}]$. The slight compositional deviation of $H_{1.7}[Sr_{0.7}Bi_{0.3}NaNb_3O_{10}]$ from the reported value ($H_{1.8}[Sr_{0.8}Bi_{0.2}NaNb_3O_{10}]$) [7] might be ascribed to the difference in firing conditions for $Bi_2SrNaNb_3O_{12}$. $Bi_2CaNaTa_3O_{12}$ was treated with 6 M HCl for 24 h.

The XRD patterns of the products were obtained using a Rigaku RINT-2500 diffractometer with monochromated Cu Kα radiation. ICP analysis was conducted with a Nippon Jarrell-Ash ICAP575 Mark II, a Thermo Jarrell-Ash IRIS/AP, or a Seiko Instruments SPS7000A spectrometer. Samples were dissolved in mixed acid (5 mL of HNO_3, 10 mL of HCl, and 5 mL of HF) at 200 °C for 2 h. TG analysis was performed with a MacScience TG-DTA2000S thermobalance operated under an air flow (heating rate: 10 °C/min). UV–Vis diffuse reflectance spectra were recorded on a Shimadzu UV-2500PC spectrometer.

The behavior of photocatalytic H_2 evolution from an aqueous ethanol solution was investigated using a closed gas-circulation system. One gram of an Aurivillius phase or air-dried protonated form was dispersed in 700 mL of 20 vol% of the aqueous ethanol solution in a glass cell under an Ar atmosphere. The dispersion was irradiated by an ultra-high-pressure Hg lamp (500 W), and the amount of H_2 was determined by gas chromatography (Shimadzu, GC-8A).

3. Results and discussion

Fig. 1 shows the XRD patterns of $Bi_2CaNaTa_3O_{12}$ (Fig. 1a), air-dried acid-treated $Bi_2CaNaTa_3O_{12}$ (Fig. 1b), and acid-treated $Bi_2CaNaTa_3O_{12}$ dried at 120 °C (Fig. 1c). The XRD pattern of acid-treated $Bi_2CaNaTa_3O_{12}$ dried at 120 °C is similar to those of the protonated forms derived from $Bi_2A'NaNb_3O_{12}$ ($A' = Sr$, Ca) [7]. All the XRD reflections can be indexed

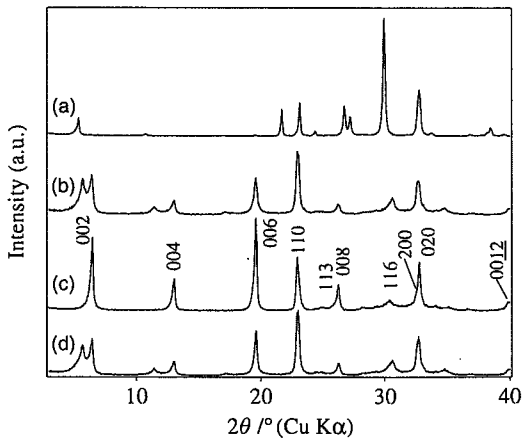

Fig. 1. XRD patterns of: (a) $Bi_2CaNaTa_3O_{12}$; (b) acid-treated $Bi_2CaNaTa_3O_{12}$; (c) the sample obtained by heating (b) at 120 °C; (d) acid-treated $Bi_2CaNaTa_3O_{12}$ after photocatalytic H_2 evolution.

based on an orthorhombic cell with $a = 0.5496(2)$, $b = 0.5465(3)$, and $c = 2.72(1)$ nm. These values appear to be consistent with those of a closely-related protonated Ruddlesden–Popper phase, $H_2CaNaTa_3O_{12}$ ($a = 0.38851(7)$, $c = 2.698(1)$ nm; the a parameter corresponds approximately to $1/\sqrt{2}$ of the a and b parameters of acid-treated $Bi_2CaNaTa_3O_{12}$) [24]. The XRD profile of the air-dried product (Fig. 1b) shows a similar characteristic in the high-angle region (at $2\theta > 20°$), but another set of $0\,0\,l$ reflections (the interlayer distance estimated from the low-angle reflection is 1.58 nm) appears in the low-angle region. According to the findings of an earlier report on the hydrated phases of protonated triple-layered Ruddlesden–Popper phases, [24] these reflections are ascribable to a hydrated phase, $H_{1.8}[Ca_{0.8}Bi_{0.2}NaTa_3O_{10}] \cdot xH_2O$, which should be converted into $H_{1.8}[Ca_{0.8}Bi_{0.2}NaTa_3O_{10}]$ upon drying at 120 °C via deintercalation of water.

The composition was determined to be $H_{1.8}[Ca_{0.8}Bi_{0.2}NaTa_3O_{10}]$ by ICP and TG analyses. The presence of a small amount of bismuth and a decrease in the Ca/Ta molar ratio can be ascribed to a cation disorder ($Bi \leftrightarrow Ca$), as reported for another protonated form, $H_{1.8}[Ca_{0.8}Bi_{0.2}NaNb_3O_{10}]$, derived from the niobate analogue of $Bi_2CaNaTa_3O_{12}$, $Bi_2CaNaNb_3O_{12}$ [7]. These results clearly indicate the successful conversion of $Bi_2CaNaTa_3O_{12}$ into a protonated form of a layered perovskite tantalate, $H_{1.8}[Ca_{0.8}Bi_{0.2}NaTa_3O_{10}]$.

Fig. 2 shows the UV–Vis diffuse reflectance spectra of $Bi_2CaNaTa_3O_{12}$ and its acid-treated product, $H_{1.8}[Ca_{0.8}Bi_{0.2}NaTa_3O_{10}]$. Upon acid treatment, a clear blue shift is shown, and the adsorption edge energy increases correspondingly from 3.7 to 4.1 eV. Similar blue shifts were observed for the other two Aurivillius-type niobates (from $Bi_2SrNaNb_3O_{12}$ to $H_{1.7}[Sr_{0.7}Bi_{0.3}NaNb_3O_{10}]$, $3.2 \rightarrow 3.3$ eV; from $Bi_2CaNaNb_3O_{12}$ to $H_{1.8}[Ca_{0.8}Bi_{0.2}NaNb_3O_{10}]$, $3.1 \rightarrow 3.4$ eV).

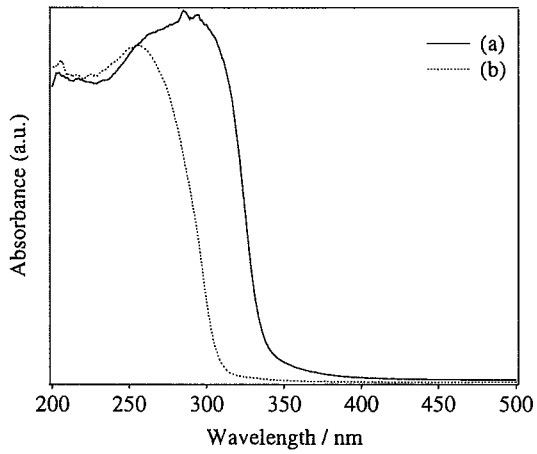

Fig. 2. UV–Vis diffuse reflectance spectra of: (a) $Bi_2CaNaTa_3O_{12}$; (b) $H_{1.8}[Ca_{0.8}Bi_{0.2}NaTa_3O_{10}]$.

The photocatalytic H_2 evolution behavior of these three Aurivillius phases and the corresponding protonated forms is shown in Fig. 3. None of the results for the Aurivillius phases show evidence of photocatalytic H_2 evolution. All the protonated forms, on the contrary, show photocatalytic activity for H_2 evolution. $H_{1.8}[Ca_{0.8}Bi_{0.2}NaTa_3O_{10}]$ shows the highest degree of activity among the protonated forms. The XRD patterns of all the protonated forms after H_2 evolution showed the presence of additional $0\,0\,l$ reflections due to the hydrated phases (estimated interlayer distances: $H_{1.8}[Ca_{0.8}Bi_{0.2}NaTa_3O_{10}]$, $d = 1.58$ nm (Fig. 1d); $H_{1.7}[Sr_{0.7}Bi_{0.3}NaNb_3O_{10}]$, $d = 1.70$ nm; $H_{1.8}[Ca_{0.8}Bi_{0.2}NaNb_3O_{10}]$, $d = 1.65$ nm).

A possible reason why H_2 evolution was observed only for the protonated forms is the change in electronic structures upon selective leaching of bismuth oxide sheets, since the blue shifts of the adsorption edges are clearly shown. Although the electronic structures of these three triple-layered Aurivillius phases have not been studied, the electronic structure of a double-layered Aurivillius phase, $Bi_2SrTa_2O_9$, has been discussed [25–29]. Since we have converted $Bi_2SrTa_2O_9$ into a protonated form, $H_{1.8}[Sr_{0.8}Bi_{0.2}Ta_2O_7]$, [8] the UV–Vis diffuse reflectance spectra of $Bi_2SrTa_2O_9$ and $H_{1.8}[Sr_{0.8}Bi_{0.2}Ta_2O_7]$ have been measured, and a similar blue shift upon acid treatment has been observed ($3.6 \rightarrow 3.7$ eV).

All of proposed band structures of $Bi_2SrTa_2O_9$ agree with the presence of a significant contribution of orbitals of bismuth in the bismuth oxide sheets to the valence and/or conduction bands [25,27–29]. It is therefore, natural to observe a significant change in electronic structure upon selective leaching of bismuth oxide sheets. The adsorption edge energy of $Bi_2SrTa_2O_9$

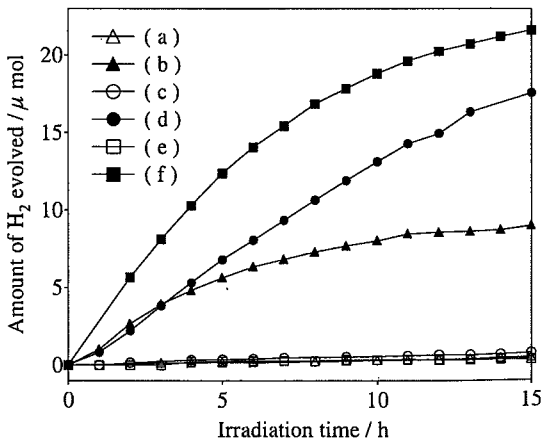

Fig. 3. Photocatalytic H_2 evolution from aqueous ethanol solutions on: (a) $Bi_2SrNaNb_3O_{12}$; (b) $H_{1.7}[Sr_{0.7}Bi_{0.3}NaNb_3O_{10}]$; (c) $Bi_2CaNaNb_3O_{12}$; (d) $H_{1.8}[Ca_{0.8}Bi_{0.2}NaNb_3O_{10}]$; (e) $Bi_2CaNaTa_3O_{12}$; (f) $H_{1.8}[Ca_{0.8}Bi_{0.2}NaTa_3O_{10}]$.

(3.6 eV) is not consistent with the calculated bandgaps (≈5 eV [25] and ≈2 eV [28,29]), however, presumably because the bandgap of $Bi_2SrTa_2O_9$ is indirect [28].

Similar blue shifts upon selective leaching of the bismuth oxide sheets are observed (0.1–0.4 eV) for the triple-layered Aurivillius phases. Based on the above discussion of $Bi_2SrTa_2O_9$ and $H_{1.8}[Sr_{0.8}Bi_{0.2}Ta_2O_7]$, it is thus very likely that the transitions for the adsorptions of these Aurivillius phases also involve orbitals of bismuth in the bismuth oxide sheets and that the electronic structures of these Aurivillius phases change upon selective leaching of the bismuth oxide sheets. The bottoms of the new conduction bands seem to be more negative than the redox potential of H^+/H_2, leading to photocatalytic H_2 evolution.

Since the Aurivillius phases possess no interlayer space, the creation of an interlayer surface through selective leaching of the bismuth oxide sheets leads to a drastic increase in surface area. The presence of hydrates after photocatalytic activity measurement clearly indicates the presence of water in the interlayer space during photocatalytic H_2 evolution. In addition, the intercalation of ethanol can also be expected, since the intercalation of alcohol molecules in the presence of water was observed for protonated forms of double- and triple-layered Dion–Jacobson phases in the course of alkoxy group formation on the interlayer surface [30,31]. Thus, it is reasonable to assume that the large interlayer surface created by selective leaching of the bismuth oxide sheets contributed to photocatalytic H_2 evolution in the present study. Similar enhancement of photocatalytic activities by migration of reactants (water, alcohols) in the interlayer space was reported for other ion-exchangeable layered perovskites [13,15,16]. Machida et al., on the contrary, reported a negative effect of hydration on the photocatalytic activities of double-layered protonated forms, $M'LnTa_2O_7$ ($M' = Cs$, Rb, Na, H; $Ln = La$, Pr, Nd, Sm). Since they ascribed this observation mainly to the deformation of $[LnTa_2O_7]$ slabs upon hydration, it is reasonable to assume that the rigid triple-layered protonated forms employed in the present study demonstrate a positive effect of the intercalation of water on photocatalytic activity.

4. Conclusions

We have demonstrated that photocatalytic activity appears upon selective leaching of the bismuth oxide sheets in three triple-layered Aurivillius phases, $Bi_2SrNaNb_3O_{12}$, $Bi_2CaNaNb_3O_{12}$, and $Bi_2CaNaTa_3O_{12}$. The adsorption edges in the UV–Vis diffuse reflectance spectra show blue shifts upon selective leaching of the bismuth oxide sheets, and in light of the similar blue shift of the adsorption edge for double-layered $Bi_2SrTa_2O_9$, electrical structure changes upon selective leaching of the bismuth oxide sheets can be considered a possible reason for the appearance of the photocatalytic activities. The creation of interlayer space is also likely to contribute to the photocatalytic activities. Since this process can provide various protonated forms with novel compositions, the present study offers a new route to acquiring layered perovskite photocatalysts with novel compositions.

Acknowledgements

The authors express their gratitude to Prof. Kazuyuki Kuroda, Department of Applied Chemistry, Waseda University, Prof. Kiyoshi Okada, Department of Metallurgy and Ceramics Science, Tokyo Institute of Technology, and Dr. Shigeo Satokawa, Tokyo Gas Co., Ltd., for their valuable suggestion. We thank Mr. Shinsuke Tani for his assistance in the experiments. This work was supported in part by the Grant-in-Aid for Scientific Research (No. 14350462) from the Ministry of Education, Science, Sports, and Culture, Japan.

References

[1] R.E. Schaak, T.E. Mallouk, Chem. Mater. 14 (2002) 1455.
[2] B. Aurivillius, Ark. Kemi. 1 (1949) 463.
[3] B. Aurivillius, Ark. Kemi. 1 (1949) 499.
[4] B. Aurivillius, Ark. Kemi. 2 (1950) 519.
[5] W. Sugimoto, M. Shirata, Y. Sugahara, K. Kuroda, J. Am. Chem. Soc. 121 (1999) 11601.
[6] M. Shirata, Y. Tsunoda, W. Sugimoto, Y. Sugahara, Mater. Res. Soc. Symp. Proc. 658 (2001) GG6.24.1.
[7] W. Sugimoto, M. Shirata, K. Kuroda, Y. Sugahara, Chem. Mater. 14 (2002) 2946.
[8] Y. Tsunoda, M. Shirata, W. Sugimoto, Z. Liu, O. Terasaki, K. Kuroda, Y. Sugahara, Inorg. Chem. 40 (2001) 5768.
[9] R.E. Schaak, T.E. Mallouk, Chem. Commun. (2002) 706.
[10] M. Kudo, H. Ohkawa, W. Sugimoto, N. Kumada, Z. Liu, O. Terasaki, Y. Sugahara, Inorg. Chem. 42 (2003) 4479.
[11] K. Domen, J.N. Kondo, M. Hara, T. Takata, Bull. Chem. Soc. Jpn. 73 (2000) 1307.
[12] A. Kudo, J. Ceram. Soc. Jpn. 109 (2001) S81.
[13] K. Domen, J. Yoshimura, T. Sekine, A. Tanaka, T. Onishi, Catal. Lett. 4 (1990) 339.
[14] T. Takata, A. Tanaka, M. Hara, J.N. Kondo, K. Domen, Catal. Today 44 (1998) 17.
[15] J. Yoshimura, Y. Ebina, J. Kondo, K. Domen, J. Phys. Chem. 97 (1993) 1970.
[16] T. Takata, Y. Furumi, K. Shinohara, A. Tanaka, M. Hara, J.N. Kondo, K. Domen, Chem. Mater. 9 (1997) 1063.
[17] Y. Ebina, A. Tanaka, J.N. Kondo, K. Domen, Chem. Mater. 8 (1996) 2534.
[18] Y. Ebina, T. Sasaki, M. Harada, M. Watanabe, Chem. Mater. 14 (2002) 4390.
[19] M. Machida, J. Yabunaka, T. Kijima, Chem. Mater. 12 (2000) 812.
[20] M. Machida, J. Yabunaka, T. Kijima, S. Matsushima, M. Arai, Int. J. Inorg. Mater. 3 (2001) 545.
[21] M. Machida, K. Miyazaki, S. Matsushima, M. Arai, J. Mater. Chem. 13 (2003) 1433.

[22] A. Kudo, S. Hijii, Chem. Lett. (1999) 1103.
[23] F. Izumi, in: R.A. Young (Ed.), Rietveld Analysis, Oxford University Press, Oxford, 1993, p. 236.
[24] R.E. Schaak, T.E. Mallouk, J. Solid State Chem. 155 (2000) 46.
[25] J. Robertson, C.W. Chen, W.L. Warren, C.D. Gutleben, Appl. Phys. Lett. 69 (1996) 1704.
[26] A.J. Hartmann, R.N. Lamb, J.F. Scott, C.D. Gutleben, Integr. Ferroelectr. 18 (1997) 101.
[27] M.-H. Tsai, S.K. Day, IEEE Trans. Ultrason. Ferroelectr. 47 (2000) 929.
[28] M.G. Stachiotti, C.O. Rodriguez, C. Ambrosch-Draxl, N.E. Christensen, Phys. Rev. B 61 (2000) 14434.
[29] A. Shimizu, S. Takada, H. Shimooka, S. Takahashi, S. Kohiki, M. Arai, M. Oku, Chem. Mater. 14 (2002) 3971.
[30] S. Takahashi, T. Nakato, S. Hayashi, Y. Sugahara, K. Kuroda, Inorg. Chem. 34 (1995) 5065.
[31] S. Tahara, Y. Sugahara, Langmuir 19 (2003) 9473.

Inorg. Chem. **2003**, *42*, 4479–4484

A Layered Tungstic Acid $H_2W_2O_7 \cdot nH_2O$ with a Double-Octahedral Sheet Structure: Conversion Process from an Aurivillius Phase $Bi_2W_2O_9$ and Structural Characterization

Manabu Kudo,[†] Hajime Ohkawa,[†] Wataru Sugimoto,[‡] Nobuhiro Kumada,[§] Zheng Liu,[∥] Osamu Terasaki,[⊥] and Yoshiyuki Sugahara*[,†]

Department of Applied Chemistry, School of Science and Engineering, Waseda University, Shinjuku-ku, Tokyo 169-8555, Japan, Department of Fine Materials Engineering, Faculty of Textile Science and Technology, Shinshu University, Ueda, Nagano 386-8567, Japan, Faculty of Engineering, Yamanashi University, Miyamae, Kofu, Yamanashi 400-8511, Japan, Institute of Multidisciplinary Research for Advanced Materials, Tohoku University, Aoba-ku, Sendai, Miyagi 980-8577, Japan, and Department of Physics, Graduate School of Science and CIR, Tohoku University, Aoba-ku, Sendai, Miyagi 980-8578, Japan

Received November 18, 2002

The conversion process of an Aurivillius phase, $Bi_2W_2O_9$, into a layered tungstic acid by hydrochloric acid treatment has been investigated, and resultant $H_2W_2O_7 \cdot nH_2O$ has been fully characterized. The *c* parameter of $Bi_2W_2O_9$ [2.37063(5) nm] decreases to 2.21(1) nm in an acid-treated product dried at ambient temperature. The *a* and *b* parameters of $Bi_2W_2O_9$ [$a = 0.54377(1)$ nm and $b = 0.54166(1)$ nm] also decrease slightly to $a = 0.524(1)$ nm and $b = 0.513(1)$ nm in the acid-treated product dried at ambient temperature, indicating structural changes in the ReO_3-like slabs in $Bi_2W_2O_9$ upon acid treatment. Drying at 120 °C leads to a further decrease in the *c* parameter [1.86(1) nm] with no notable change in the *a* and *b* parameters [$a = 0.5249(2)$ nm and $b = 0.513(2)$ nm]. The formation of an expandable layered structure is demonstrated by the successful intercalation of *n*-octylamine [interlayer distance 2.597(9) nm] and *n*-dodecylamine [interlayer distance 3.56(2) nm]. The compositions of the acid-treated products are determined to be $H_2W_2O_7 \cdot nH_2O$ typically with $n = 0.58$ for the air-dried product and $n = 0$ for the product dried at 120 °C. As a consequence, the composition of the layer is $H_2W_2O_7$, and the decrease in the *c* parameter upon drying is ascribable to the loss of interlayer water. Scanning electron microscopy reveals no morphological change during acid treatment, which strongly suggests a selective leaching of the bismuth oxide sheets as a reaction mechanism. High-resolution transmission electron microscopy (HREM) observation of the acid-treated product shows consistency with a structural model for $H_2W_2O_7$, derived from $Bi_2W_2O_9$ through removal of the bismuth oxide sheets and contraction along the *c* axis. HREM observation also reveals that the WO_6 octahedra arrangement changes slightly with acid treatment. A one-dimensional electron density map projected on the *c* axis for the product dried at 120 °C, $H_2W_2O_7$, shows good consistency with that calculated for the structural model.

Introduction

Several tungstic acids (alternatively referred to as tungsten trioxide hydrates) with different compositions and structures have been identified. One of these, $WO_3 \cdot 2H_2O$,[1–3] which is isostructural with $MoO_3 \cdot 2H_2O$, consists of single sheets of corner-sharing $WO_5(OH_2)$ octahedra and interlayer water.[4] $WO_3 \cdot H_2O$[1,2] can be obtained through the removal of interlayer water from $WO_3 \cdot 2H_2O$.[5] Water molecules are directly bound to tungsten atoms in $WO_3 \cdot H_2O$.[6] A colloidal tungstic acid prepared by acidification of sodium tungstate was also reported and identified as $WO_3 \cdot nH_2O$, which possesses a

* To whom correspondence should be addressed. E-mail: ys6546@waseda.jp.
[†] School of Science and Engineering, Waseda University.
[‡] Faculty of Textile Science and Technology, Shinshu University.
[§] Faculty of Engineering, Yamanashi University.
[∥] Institute of Multidisciplinary Research for Advanced Materials, Tohoku University. Current address: Bio Nanotec Research Institute Inc., Sumitomofudosan-Hamacho Bldg., 3-42-3 Nihonbashi Hamacho, Chuo-ku, Tokyo 103-0007, Japan.
[⊥] Department of Physics, Tohoku University. Current address: Structural Chemistry, Arrhenius Laboratory, Stockholm University S-10691, Stockholm Sweden.

(1) Freedman, M. L. *J. Am. Chem. Soc.* **1959**, *81*, 3834–3839.
(2) Freedman, M. L.; Leber, S. *J. Less-Common Met.* **1964**, *7*, 427–432.
(3) Furusawa, K.; Hachisu, S. *Sci. Light (Tokyo)* **1966**, *15*, 115–130.
(4) Gopalakrishnan, J.; Bhuvanesh, N. S. P.; Raju, A. R. *Chem. Mater.* **1994**, *6*, 373–379.

10.1021/ic0206746 CCC: $25.00
Published on Web 06/17/2003

layered structure.[5] The hemihydrate $WO_3 \cdot 1/2H_2O$ by contrast possesses a cubic pyrochlore-type structure consisting of six-membered rings of corner-sharing WO_6 octahedra.[7–9] Water molecules are present in the tunnels consisting of WO_6 octahedra. In the structure of $WO_3 \cdot 1/3H_2O$, single-octahedral infinite sheets consisting of six-membered rings are stratified along the c axis with a displacement by $a/2$.[10,11] Water molecules are directly coordinated to tungsten atoms.

A variety of protonated layered oxides have been prepared from oxides through acid treatment (the so-called "*chimie douce*" approach), typically involving exchange of interlayer metal cations in the interlayer space of layered oxides with protons.[12] Ion-exchangeable layered perovskites ($M_m[A_{n-1}B_nO_{3n+1}]$; M = Rb, K, etc.; A = Sr, Ca, La, etc.; B = Ti, Nb, Ta; m = 1, Dion–Jacobson phases;[13,14] m = 2, Ruddlesden–Popper phases)[15,16] consist of interlayer cations (M) and perovskite-like slabs ($[A_{n-1}B_nO_{3n+1}]$) and can be easily converted into their protonated forms through acid treatment.[17] Aurivillius phases,[18–20] $Bi_2A_{n-1}B_nO_{3n+3}$, resulting from alternative stacking of the same type of perovskite-like slabs ($[A_{n-1}B_nO_{3n+1}]$) and bismuth oxide sheets, are known as related phases. We first reported a novel conversion of an Aurivillius phase, $Bi_2ANaNb_3O_{12}$, into a protonated form of a layered perovskite, $H_{1.8}[Sr_{0.8}Bi_{0.2}NaNb_3O_{10}]$, through selective leaching of the bismuth oxide sheets.[21–23] Subsequent reports on the conversion of other Aurivillius phases ($Bi_2CaNaNb_3O_{12}$,[23] $Bi_2SrTa_2O_9$,[24] and $Bi_2Sr_2Nb_2MnO_{12}$[17]) into corresponding protonated forms demonstrated that this route can be applied to various Aurivillius phases to prepare new protonated forms.

The preparation of tungsten-containing oxides and tungstic acids through acid treatment has also been investigated extensively. A typical example is $WO_3 \cdot 1/2H_2O$ preparation, which was achieved by acid treatment of the pyrochlore-type oxide $(A_2O)_xW_2O_6$ (A = Rb, Cs, NH_4; $0.3 < x < 0.5$).[7] Additionally, acid treatment of $LiMWO_6$ (M = Nb, Ta) resulted in the formation of $HMWO_6$ with layered structures.[25–27] Acid treatment of $LiVWO_6$[4] and $LiM'W_2O_8$[28] (M' = Al, Fe) led, moreover, to the formation of $H_xV_xW_{1-x}O_3 \cdot yH_2O$ phases (x = 0.125 and 0.33), $WO_3 \cdot 2H_2O$ or $WO_3 \cdot 1/3H_2O$, but the reactions were not reported to be topotactic. Very recently, Schaak et al. have briefly reported the conversion of an Aurivillius phase, $Bi_2W_2O_9$, into $H_2W_2O_7$.[29] Since their aim was to prepare nanoscaled colloids through exfoliation, they did not establish experimental conditions for single-phase synthesis. Consequently, only XRD results were provided. In terms of the reaction mechanism, they reported that this process proceeded through selective leaching of bismuth oxide sheets.

Here, we report the conversion process of $Bi_2W_2O_9$ into single-phase $H_2W_2O_7 \cdot nH_2O$ by hydrochloric acid treatment. In the course of this study, we noted a slight contraction along the a and b axes upon acid treatment in addition to a contraction along the c axis, suggesting that the structure of the layers in $H_2W_2O_7 \cdot nH_2O$ is not identical to that of the ReO_3-like slabs in $Bi_2W_2O_9$. Since the structures of the perovskite-like slabs were completely retained during the conversion of the other Aurivillius phases ($Bi_2A_{n-1}B_nO_{3n+3}$; B = Nb, Ta, and Mn),[17,21–24] this observation may raise doubts about the reaction mechanism of this conversion. Thus, besides full characterization of the resulting $H_2W_2O_7 \cdot nH_2O$, we present structural considerations of $H_2W_2O_7$ (a phase obtainable by drying at 120 °C) on the basis of high-resolution transmission electron microscopy (HREM) to demonstrate that the structure of $H_2W_2O_7$ can be derived from $Bi_2W_2O_9$ through selective leaching of bismuth oxide sheets, even with a slight structural change in the ReO_3-like slab.

Experimental Section

Preparation of $Bi_2W_2O_9$. $Bi_2W_2O_9$ was prepared by calcining a stoichiometric mixture of Bi_2O_3 and WO_3 at 800 °C for 48 h with intermittent grinding, under conditions similar to those described in the previous report.[30] The phase purity was confirmed by X-ray powder diffraction (XRD) analysis. The lattice parameters were determined to be a = 0.54377(1) nm, b = 0.54166(1) nm, and c = 2.37063(5) nm, results consistent with those of the previous report [a = 0.5440(1) nm, b = 0.5413(1) nm, and c = 2.3740(5) nm].[31] Inductively coupled emission spectroscopy (ICP) analysis demonstrated that the Bi:W molar ratio was 1.0. These analytical results indicate the successful formation of $Bi_2W_2O_9$.

Acid Treatment of $Bi_2W_2O_9$. About 1 g of $Bi_2W_2O_9$ was added to 200 mL of 6 M HCl, and the mixture was stirred at ambient temperature for 72 h. The resultant product was a yellow powder. The same reaction was performed on a much larger scale (10 g of

(5) Chemseddine, A.; Babonneau, F.; Livage, J. *J. Non-Cryst. Solids* **1987**, *91*, 271–278.
(6) Szymański, J. T.; Roberts, A. C. *Can. Mineral.* **1984**, *22*, 681–688.
(7) Coucou, A.; Figlarz, M. *Solid State Ionics* **1988**, *28–30*, 1762–1765.
(8) Nedjar, R.; Borel, M. M.; Hervieu, M.; Raveau, B. *Mater. Res. Bull.* **1988**, *23*, 91–97.
(9) Günter, J. R.; Amberg, M.; Schmalle, H. *Mater. Res. Bull.* **1989**, *24*, 289–292.
(10) Gerand, B.; Nowogrocki, G.; Guenot, J.; Figlarz, M. *J. Solid State Chem.* **1979**, *29*, 429–434.
(11) Gerand, B.; Nowogrocki, G.; Figlarz, M. *J. Solid State Chem.* **1981**, *38*, 312–320.
(12) Gopalakrishnan, J. *Chem. Mater.* **1995**, *7*, 1265–1275.
(13) Dion, M.; Ganne, M.; Tournoux, M. *Mater. Res. Bull.* **1981**, *16*, 1429–1435.
(14) Jacobson, A. J.; Johnson, J. W.; Lewandowski, J. T. *Inorg. Chem.* **1985**, *24*, 3727–3729.
(15) Ruddlesden, S. N.; Popper, P. *Acta Crystallogr.* **1957**, *10*, 538–539.
(16) Ruddlesden, S. N.; Popper, P. *Acta Crystallogr.* **1958**, *11*, 54–55.
(17) Schaak, R. E.; Mallouk, T. E. *Chem. Mater.* **2002**, *14*, 1455–1471.
(18) Aurivillius, B. *Ark. Kemi* **1949**, *1*, 463.
(19) Aurivillius, B. *Ark. Kemi* **1949**, *1*, 499.
(20) Aurivillius, B. *Ark. Kemi* **1950**, *2*, 519.
(21) Sugimoto, W.; Shirata, M.; Sugahara, Y.; Kuroda, K. *J. Am. Chem. Soc.* **1999**, *121*, 11601–11602.
(22) Shirata, M.; Tsunoda, Y.; Sugimoto, W.; Sugahara, Y. *Mater. Res. Soc. Symp. Proc.* **2001**, *658*, GG6.24.1–5.
(23) Sugimoto, W.; Shirata, M.; Kuroda, K.; Sugahara, Y. *Chem. Mater.* **2002**, *14*, 2946–2952.
(24) Tsunoda, Y.; Shirata, M.; Sugimoto, W.; Liu, Z.; Terasaki, O.; Kuroda, K.; Sugahara, Y. *Inorg. Chem.* **2001**, *40*, 5768–5771.
(25) Kumada, N.; Horiuchi, O.; Muto, F.; Kinomura, N. *Mater. Res. Bull.* **1988**, *23*, 209–216.
(26) Bhat, V.; Gopalakrishnan, J. *Solid State Ionics* **1988**, *26*, 25–32.
(27) Bhuvanesh, N. S. P.; Gopalakrishnan, J. *Inorg. Chem.* **1995**, *34*, 3760–3764.
(28) Bhuvanesh, N. S. P.; Uma, S.; Subbanna, G. N.; Gopalakrishnan, J. *J. Mater. Chem.* **1995**, *5*, 927–930.
(29) Schaak, R. E.; Mallouk, T. E. *Chem. Commun.* **2002**, 706–707.
(30) Watanabe, A.; Goto, M. *J. Less-Common Met.* **1978**, *61*, 265–272.
(31) Champarnaud-Mesjard, J.-C.; Frit, B.; Watanabe, A. *J. Mater. Chem.* **1999**, *9*, 1319–1322.

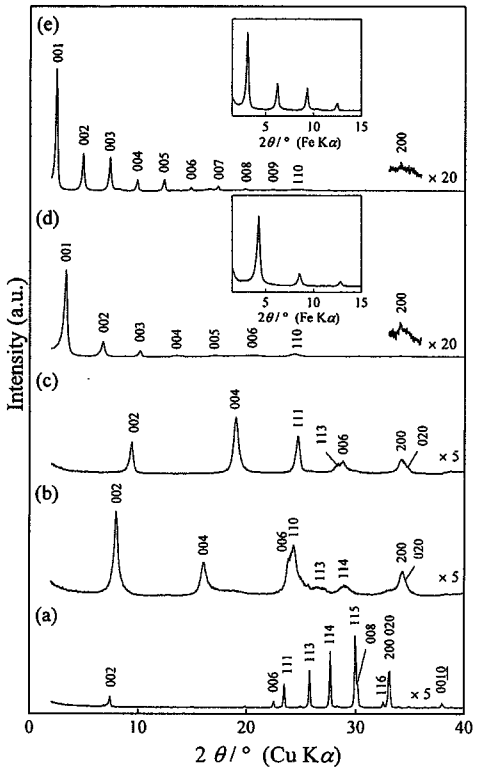

Figure 1. XRD patterns of (a) $Bi_2W_2O_9$, (b) air-dried acid-treated $Bi_2W_2O_9$, and (c) acid-treated $Bi_2W_2O_9$ dried at 120 °C, (d) (b) treated with the *n*-octylamine-heptane 1:1 mixture, and (e) (b) treated with the 1:1 *n*-dodecylamine–heptane mixture.

$Bi_2W_2O_9$ in 2.0 L of 6 M HCl), and 20 mL of a supernatant liquid were collected after 0.5, 1, 3, 6, 12, 24, and 72 h.

Intercalation of *n*-Alkylamines into the Acid-Treated $Bi_2W_2O_9$. About 2 g of air-dried acid-treated $Bi_2W_2O_9$ were reacted with 20 mL of *n*-octylamine (C8A)–heptane or *n*-dodecylamine (C12A)–heptane 1:1 mixture (as volume) at ambient temperature for 7 days. The product was separated by centrifugation, washed with heptane, and air-dried.

Analyses. XRD patterns were obtained with a Rigaku RINT-2500 diffractometer (monochromated Cu Kα radiation) or a MacScience M0^{3}XHF^{22} diffractometer (Mn-filtered Fe Kα radiation). The amounts of metals were determined by ICP analysis (Nippon Jarrell Ash, ICAP575 MarkII). The samples were dissolved by heating in a mixture of HCl (5 mL), HNO_3 (5 mL), and HF (5 mL) at 200 °C for 2 h. A thermogravimetry (TG) curve of the acid-treated product was obtained on a thermobalance (MacScience, TG-DTA2000S, 10 °C/min). HREM images and electron diffraction (ED) patterns were obtained using a transmission electron microscope (JEOL JEM-4000EX) operated at 400 kV. The morphology was studied with scanning electron microscopy (SEM, Hitachi S-2500).

Results and Discussion

Acid-Treatment Process of $Bi_2W_2O_9$. Figure 1 demonstrates the XRD patterns of $Bi_2W_2O_9$ and its acid-treated products. $Bi_2W_2O_9$, which consists of bismuth oxide sheets and double-octahedral ReO_3-like slabs, shows intense (00*l*) reflections,[30] which are characteristic of layered structures. The *c* parameter [2.37063(5) nm] is doubled, because two successive ReO_3-type slabs show the relative displacement by $(a + b)/2$. Thus, the *c* parameter corresponds to the thickness of two bismuth oxide sheets and two ReO_3-like slabs.[31]

In the XRD pattern of the acid-treated product after air-drying (Figure 1b), all the reflections can be indexed on the basis of an orthorhombic cell. Upon acid treatment, the (00*l*) reflections of $Bi_2W_2O_9$ disappear and new (00*l*) reflections appear at higher angles, suggesting the formation of a layered structure with a smaller repeating distance through acid treatment. Corresponding to these shifts in the (00*l*) reflections, the *c* parameter of $Bi_2W_2O_9$ [2.37063(5) nm] decreases to 2.21(1) nm in the air-dried product. The (200) and (020) reflections of $Bi_2W_2O_9$ ($2\theta \approx 33.1°$)[30] should be observed in the same positions if no structural change in the ReO_3-like slabs occurs during acid treatment. In the XRD pattern of the air-dried product, however, no corresponding reflection is observed at $2\theta \approx 33.1°$, and reflections assignable to (200) and (020) are present at $2\theta = 34.2$ and 35.0°, respectively. Thus, the structure of the ReO_3-like slabs in $Bi_2W_2O_9$ is modified through acid treatment. The *a* and *b* parameters correspondingly decrease from those of $Bi_2W_2O_9$ [a = 0.54377(1) nm and b = 0.54166(1) nm] to a = 0.524(1) nm and b = 0.513(1) nm in the air-dried product.

The effect of drying on the air-dried product was also studied. When the variations in an XRD pattern profile upon drying at 50 °C were investigated, it was found that the (00*l*) reflections gradually shifted to higher angles. When the air-dried product was dried at 120 °C, the observed XRD pattern (Figure 1c) was identical to that of the product dried at 50 °C overnight. Thus, we analyzed the XRD pattern of the product dried at 120 °C further and indexed all the reflections on the basis of an orthorhombic cell. This analysis showed that the *c* parameter decreases with respect to that of the air-dried product [2.21(1) nm] to 1.86(1) nm in the product dried at 120 °C. The *a* and *b* parameters of the product dried at 120 °C are a = 0.5249(2) nm and b = 0.513(2) nm, which are closely similar to those of the air-dried product [a = 0.524(1) nm and b = 0.513(1) nm]. The reported lattice parameters for $H_2W_2O_7$ [a = 0.5441(2) nm, b = 0.5415(2) nm, and c = 1.881(1) nm][29] do not show complete consistency with the observed values of the air-dried product and the product dried at 120 °C.

The suggestion of a layered structure for the acid-treated product is further supported by its intercalation behavior (Figure 1d,e). Upon treatment with *n*-alkylamines (C8A, C12A), the interlayer distances calculated from the (00*l*) reflections increase to 2.597(9) nm (C8A) and 3.56(2) nm (C12A). The (110) reflection (at 24.3°) and the (200) reflection, on the contrary, are present at the same 2θ angles after the intercalation reactions. These results indicate an expansion along the *c* axis with no structural change along the *a* and *b* axes and provide additional clear evidence for a layered structure of the acid-treated product. The mechanism appears to be an acid–base reaction of the type which is involved in the intercalation of organic bases into various protonated forms of layered oxides.[17,32] The exchange of protons with tetramethylammonium ions in the exfoliation

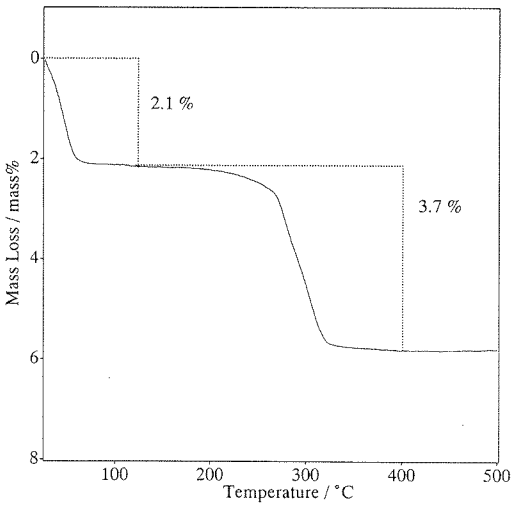

Figure 2. TG curve of air-dried acid-treated $Bi_2W_2O_9$.

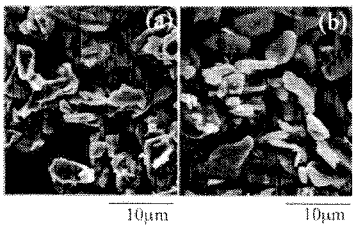

Figure 3. Scanning electron micrographs of (a) $Bi_2W_2O_9$ and (b) acid-treated $Bi_2W_2O_9$.

process of $H_2W_2O_7$[29] should also involve an intercalation process in the initial stage.

The composition of the acid-treated product is estimated on the basis of ICP and TG results. The Bi:W molar ratio in the acid-treated product was 0.01, indicating that essentially all of bismuth was leached by acid treatment. The TG curve of the air-dried product is shown in Figure 2. The mass loss (≤400 °C) is clearly divided into two parts with an intermediate plateau. The first mass loss (≤120 °C) can be ascribed to the loss of interlayer water, since the *c* parameter decreases without a collapse of the layers upon drying at 120 °C (Figure 1). The second mass loss (>180 °C) can then be ascribed to dehydration of the layers in the acid-treated product. With the second mass loss assigned to water and the remaining mass to WO_3, the WO_3:H_2O molar ratio is calculated as 2.0. Taking the first mass loss into account, we conclude that the compositions of the air-dried product is $H_2W_2O_7 \cdot nH_2O$ with a typical *n* value of 0.58 and that the product dried at 120 °C is $H_2W_2O_7$ (with $n = 0$).

The conversion could proceed either through dissolution of $Bi_2W_2O_9$ and subsequent crystallization of tungstic acid or through selective leaching of the bismuth oxide sheets in $Bi_2W_2O_9$ without dissolution. Thus, the change in morphology during acid treatment should provide critical information concerning the reaction mechanism (SEM; Figure 3). Both $Bi_2W_2O_9$ and its acid-treated product possess very similar platelike morphologies, and no notable change in particle size is observed. The concentrations of tungsten in the supernatant liquids (determined by ICP during the large-scale synthesis) were, moreover, always less than 1% of tungsten originally contained in $Bi_2W_2O_9$. These results clearly indicate that the present conversion reaction does not proceed through a dissolution−crystallization mechanism: a selective leaching process is highly likely.

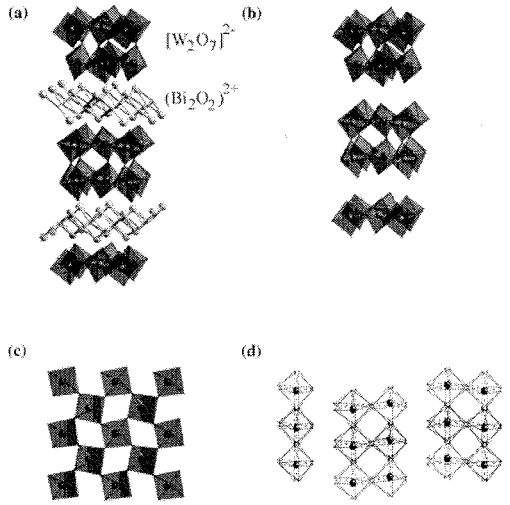

Figure 4. (a) Structure of $Bi_2W_2O_9$ and (b−d) proposed structural model of acid-treated $Bi_2W_2O_9$ ($H_2W_2O_7$): (b) overview; (c) [001] view; (d) [110] view.

Structural Characterization of the Acid-Treated Product, $H_2W_2O_7 \cdot nH_2O$. All the characterization results presented above suggest that bismuth oxide sheets are selectively leached and that protons ($2\ H^+/[W_2O_7]^{2-}$) and water molecules are introduced to form a new layered compound, $H_2W_2O_7 \cdot nH_2O$, which shows essential consistency with the previous report for $H_2W_2O_7$ formation.[29] The XRD results also clearly indicate that a slight structural change in the ReO_3-like slabs in $Bi_2W_2O_9$ occurs upon acid treatment, although SEM observation suggests selective leaching of the bismuth oxide sheets as a reaction mechanism. To demonstrate that the structure of $H_2W_2O_7 \cdot nH_2O$ can be reasonably derived from that of $Bi_2W_2O_9$, a preliminary structural model of $H_2W_2O_7$ is proposed. Since the changes in the *a* and *b* parameters are relatively small (96% along the *a* axis and 95% along the *b* axis), only a limited structural modification of the ReO_3-like slabs in $Bi_2W_2O_9$ appears necessary to simulate the structures of the layers in $H_2W_2O_7$. As a consequence, a preliminary structural model is derived from the reported structure of $Bi_2W_2O_9$[31] through removal of the bismuth oxide sheets from the structure of $Bi_2W_2O_9$, and thus, the space group of $Bi_2W_2O_9$ ($Pna2_1$)[31] is applied to the proposed model. The positions of the protons are not determined in the proposed model. The lattice parameters of the acid-treated product dried at 120 °C (corresponding to $H_2W_2O_7$) are employed for the proposed model. The arrangement of atoms in the *ab* plane is therefore essentially unchanged through this modification. The resultant structural model is shown in Figure 4b along with the structure of $Bi_2W_2O_9$ (Figure 4a). On the basis of this proposed prelimi-

(32) Lagaly, G. *Solid State Ionics* **1986**, *22*, 43−51.

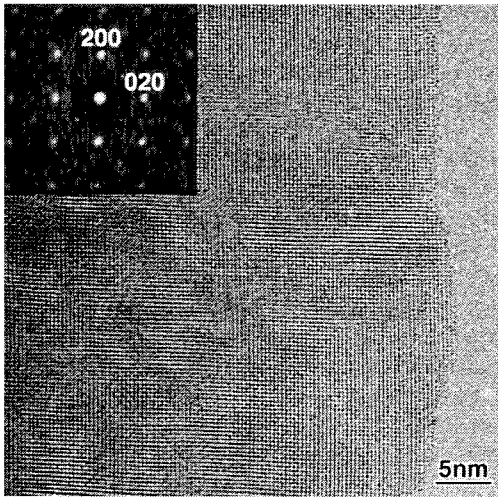

Figure 5. HREM image of acid-treated $Bi_2W_2O_9$ along [001]. A corresponding ED pattern is shown in the inset.

nary model, we shall proceed to interpret the HREM images of $H_2W_2O_7 \cdot nH_2O$. It should be noted that the HREM images should correspond to $H_2W_2O_7$, since interlayer water molecules are removed during HREM observation conducted under vacuum.

The ED pattern of $H_2W_2O_7$ along the [001] zone axis and the corresponding HREM image are shown in Figure 5. The ED pattern corresponds to the *ab* plane of the orthorhombic cell, which is consistent with the indexing of the XRD pattern. The HREM image shows a regular dot array, which exhibits excellent consistency with the arrangement of tungsten atoms in the *ab* plane in the proposed model (Figure 4c).

The HREM image of $H_2W_2O_7$ along the [110] zone axis is shown in Figure 6. The HREM image was recorded at a value close to Scherzer's defocus, and the black dots therefore correspond to the tungsten atoms in Figure 6a. A layered structure with two sheets of tungsten atoms present in one layer is clearly revealed. A simulated image is calculated to verify the proposed model. An enlarged image and a corresponding simulated [110] image are demonstrated in the insets. A clear similarity is evident between these two images, indicating that the layers consist of two WO_6 octahedral sheets in a manner similar to the ReO_3-like slabs in $Bi_2W_2O_9$. In the ED pattern, diffusing streaks are clearly observed, and are ascribed to the presence of stacking faults (as shown by the HREM image). To analyze the structure, we performed Fourier transformation of the HREM image in a thin perfect region. The resulting Fourier diffractogram (FD) is also shown in the inset, and is consistent with the orthorhombic cell.

Figure 6b exhibits the HREM image recorded with overfocus aberration along the [110] zone axis. It should be noted that tungsten atoms are present as white dots in Figure 6b. An enlarged image and a corresponding simulated [110] image, shown as insets, exhibit excellent similarity, especially for the arrangement of W atoms, a result further supporting the validity of the proposed model (Figure 4d). The arrangement of the proposed model suggests that the *c* axis should be doubled, which is consistent with the observed *c* parameter of $H_2W_2O_7$ [1.86(1) nm]. This interpretation is supported by the observed repeating distance in the HREM image (~0.9 nm), which is in excellent agreement with *c*/2 (0.93 nm).

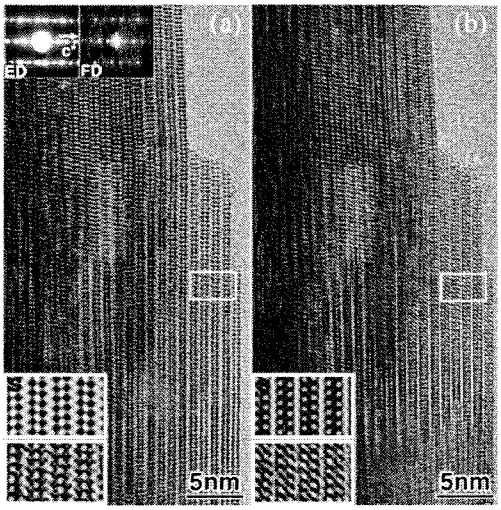

Figure 6. HREM images of acid-treated $Bi_2W_2O_9$ along [110]: (a) image recorded at a value close to Scherzer's defocus; (b) image recorded with an overfocus aberration. An enlarged image and corresponding simulated image are also shown in the insets for both HREM images. Corresponding Fourier diffractogram (FD) and ED are shown in the insets in the image (a). FD was obtained from a thin region including the area enclosed with a white rectangle.

These HREM observations and simulated images based on the proposed model suggest that the structure of the double-octahedral layers in $H_2W_2O_7$ resembles that of the ReO_3-like slabs in the original $Bi_2W_2O_9$. Closer inspection of the observed [110] images and the proposed model, however, reveals a deviation of the actual structure of $H_2W_2O_7$ from the proposed model. To demonstrate this deviation, the angle between the (001) plane and the tie line connecting two dots (corresponding approximately to the tungsten atom positions) in the same layer (projected on the [110] direction) is employed. The angle in the simulated image based on the proposed preliminary model is $97 \pm 1°$, while that in the observed image is $91 \pm 2°$. This discrepancy could be ascribed to tungsten atom displacement, which is frequently observed in phase transition of WO_3,[33,34] but the variations in the *a* and *b* parameters upon acid treatment cannot be explained only by this displacement. In the structure of $Bi_2W_2O_9$, one apical oxygen in the WO_6 octahedron is weakly bound to bismuth atoms in the bismuth oxide sheet.[31] It is therefore reasonable to assume that the oxygen arrangement is also affected by selective leaching of the bismuth oxide sheets by acid treatment, leading to the shrinkage along the *a* and *b* axes. This change in oxygen arrangement can also be regarded as a change in the WO_6 octahedra arrangement. The WO_6 octahedra arrangement in $Bi_2W_2O_9$ is reported to be distorted, and the distortion is

(33) Woodward, P. M.; Sleight, A. W.; Vogt, T. *J. Phys. Chem. Solids* **1995**, *56*, 1305−1315.
(34) Woodward, P. M.; Sleight, A. W.; Vogt, T. *J. Solid State Chem.* **1997**, *131*, 9−17.

partly ascribed to the attraction of apical oxygen by bismuth atoms.[31] It appears, therefore, that the observed change in oxygen arrangement can be regarded as relaxation of the WO_6 octahedra arrangement upon the removal of the bismuth oxide sheets.

When the structures of $H_2W_2O_7{\cdot}nH_2O$ and $H_2W_2O_7$ are compared with that of $WO_3{\cdot}H_2O$, a single-octahedral layered compound with an orthorhombic cell, the a and b parameters of $H_2W_2O_7{\cdot}nH_2O$ and $H_2W_2O_7$ (a = ~0.525 nm and b = ~0.513 nm) are found to be closely similar to the corresponding lattice parameters of $WO_3{\cdot}H_2O$ (a = 0.5249 nm and c = 0.5133 nm; the b axis is perpendicular to the layers in a $WO_3{\cdot}H_2O$ structure).[6] These similarities strongly suggest that these three compounds possess a similar arrangement of the WO_6 octahedra: the observed a and b parameters of $H_2W_2O_7{\cdot}nH_2O$ and $H_2W_2O_7$ are reasonable for two-dimensionally linked WO_6 octahedra.

This conversion is unique among similar conversions,[17,21-24] because of the structural modification of the ReO_3-like slabs involved. The distortion of the WO_6 octahedra arrangement in $Bi_2W_2O_9$ is larger than that of other Aurivillius phases with a $Bi_2A_{n-1}B_nO_{3n+3}$ composition, indicating that the A-site cations regularize the perovskite-like slab structures.[31] The flexibility of the WO_6 octahedra network therefore also appears to be caused by the lack of A-site cations and to allow the structural change upon selective leaching of the bismuth oxide sheets. It should be noted that the WO_6 octahedra arrangement remains distorted even after the selective leaching of the bismuth oxide sheets. This appears to be ascribable to the cooperative antiparallel displacement of tungsten atoms, as observed in $Bi_2W_2O_9$,[31] Bi_2WO_6,[35] and WO_3.[34]

To examine the structure of $H_2W_2O_7{\cdot}nH_2O$ further, a one-dimensional electron density map projected on the c axis was calculated using five (00l) reflections of $H_2W_2O_7$ (dried at 120 °C). A one-dimensional electron density map was also calculated from the proposed model. These two profiles, shown in Figure 7, match with only a small discrepancy in intensity, a result adding strong support for the proposed structure of $H_2W_2O_7$. Two intense peaks are assignable as a contribution of tungsten atoms, and the W−W distance along the c axis is therefore estimated to be 0.39 nm. Since the W−W tie line deviates from the c axis only slightly, the distance along the c axis (0.39 nm) should be close to the actual W−W distance. The reported W−W distances in $Bi_2W_2O_9$,[31] $WO_3{\cdot}H_2O$,[6] and monoclinic and triclinic WO_3[33,34] are in the range of 0.365−0.392 nm and, thus, show reasonable consistency with the value observed in this study.

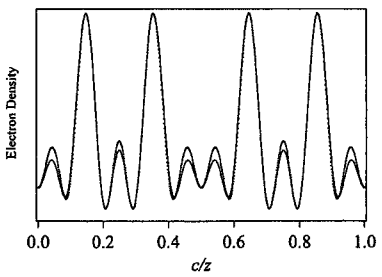

Figure 7. One-dimensional electron density maps projected on the c axis. The solid line is from experimental data for acid-treated $Bi_2W_2O_9$ (dried at 120 °C), and the dotted line is from the proposed model.

Conclusions

We have reported the conversion process of $Bi_2W_2O_9$ into a tungstic acid, $H_2W_2O_7{\cdot}nH_2O$, with a double-octahedral layered structure as well as its full characterization. The air-dried product is $H_2W_2O_7{\cdot}nH_2O$ (typically n = 0.58) with interlayer water [a = 0.524(1) nm, b = 0.513(1) nm, and c = 2.21(1) nm]. The product dried at 120 °C is $H_2W_2O_7$ with similar a and b parameters and a smaller c parameter [a = 0.5249(2) nm, b = 0.513(2) nm, and c = 1.86(1) nm]. The proposal of a layered structure is strongly supported by successful intercalation of n-alkylamines (n-octylamine and n-dodecylamine). No evidence for the dissolution−recrystallization mechanism was provided by SEM observations, a result suggesting selective leaching of bismuth oxide sheets as a reaction mechanism. The HREM observations clearly indicate that the arrangement of tungsten atoms in the double-octahedral layers in $H_2W_2O_7{\cdot}nH_2O$ is similar to those in the ReO_3-like slabs in original $Bi_2W_2O_9$. Closer inspection of the [110] image, moreover, indicates a change in the WO_6 octahedra arrangement. Since one apical oxygen in each WO_6 octahedron is attracted by bismuth atoms in $Bi_2W_2O_9$ [a = 0.54377(1) nm and b = 0.54166(1) nm], the slight decrease in the a and b parameters upon acid treatment appears to be ascribable to a change in the WO_6 octahedra arrangement through the selective leaching of bismuth oxide sheets. Thus, all the results presented clearly show that this conversion proceeds through a "*chimie douce*"-type process involving selective leaching of bismuth oxide sheets. Besides the uniqueness of the conversion process, resultant $H_2W_2O_7{\cdot}nH_2O$ could be interesting because of its possible properties originating from a double-octahedral layered structure.

Acknowledgment. The authors gratefully thank Prof. Kazuyuki Kuroda, Department of Applied Chemistry at Waseda University, for his valuable discussions and Ms. Fumi Nakasone for her assistance. This work was financially supported in part by the Grant-in-Aid for Scientific Research (No. 14350462) from the Ministry of Education, Science, Sports, and Culture of Japan.

IC0206746

(35) Knight, K. S. *Mineral. Mag.* **1992**, *56*, 399−409.

Interlayer Surface Modification of the Protonated Triple-Layered Perovskite $HCa_2Nb_3O_{10}\cdot xH_2O$ with *n*-Alcohols

Seiichi Tahara and Yoshiyuki Sugahara*

Department of Applied Chemistry, School of Science and Engineering, Waseda University, Shinjuku-ku, Tokyo 169-8555, Japan

Received March 5, 2003. In Final Form: July 10, 2003

Organic derivatives of the protonated triple-layered perovskite $HCa_2Nb_3O_{10}\cdot xH_2O$ with *n*-alkoxyl groups on the interlayer surface have been prepared by grafting *n*-alcohols. Interlayer surface modification of $HCa_2Nb_3O_{10}\cdot xH_2O$ is achieved by a direct reaction of $HCa_2Nb_3O_{10}\cdot xH_2O$ with methanol or ethanol, and single-phase *n*-alkoxyl derivatives of $HCa_2Nb_3O_{10}\cdot xH_2O$ ($n \geq 3$ in n-$C_nH_{2n+1}O-$ groups) can be formed by reacting *n*-alkoxyl derivatives (methoxyl and *n*-propoxyl derivatives) with *n*-alcohols in an autoclave at 150 °C. X-ray diffraction analysis shows the changes in interlayer distances upon treatment of $HCa_2Nb_3O_{10}\cdot xH_2O$ or intermediate *n*-alkoxyl derivatives with *n*-alcohols. Solid-state ^{13}C CP/MAS (cross polarization and magic-angle spinning) NMR spectroscopy demonstrates the presence of signals due to *n*-alkoxyl groups originating from the reactant *n*-alcohol molecules. Differential thermal analysis curves of the products exhibit exothermic peaks at temperatures higher than 200 °C. These results indicate successful preparation of $HCa_2Nb_3O_{10}\cdot xH_2O$ derivatives possessing various *n*-alkoxyl groups (n-$C_nH_{2n+1}O-$, $n = 1-4, 6, 8, 10, 12, 14, 16$, and 18) on the interlayer surface. Although a reaction between an *n*-propoxyl derivative and *n*-decanol does not proceed at 80 °C, a single-phase *n*-decoxyl derivative can be obtained at 80 °C by adding a small amount of water (1 mass %), which strongly suggests a hydrolysis–esterification mechanism. IR and solid-state ^{13}C CP/MAS NMR spectroscopies indicate that the *n*-alkyl chains in *n*-alkoxyl derivatives ($n \geq 10$ in n-$C_nH_{2n+1}O-$ groups) possess an *all-trans* conformation. A linear relationship with a slope of 0.166 nm/carbon atom is observed between the interlayer distance and the number of carbon atoms in the *n*-alkyl chains, suggesting that the *n*-alkyl chains of *n*-alkoxyl groups are present as bilayers with a tilt angle of 41° in the interlayer space.

Introduction

Ion-exchangeable layered perovskites, $M[A_{m-1}B_mO_{3m+1}]$ (the "Dion–Jacobson phases") and $M_2[A_{m-1}B_mO_{3m+1}]$ (the "Ruddlesden–Popper phases"), consist of two-dimensional perovskite-like slabs characterized by a sliced ABO_3 perovskite structure (with the A-site cation coordinated by 12 oxygen atoms and the B-site cation placed at the center of the BO_6 octahedron, *m* expressing the thickness of the perovskite-like slabs) and exchangeable interlayer cations.[1] When the layered perovskites are treated with mineral acids, the corresponding protonated forms ($H[A_{m-1}B_mO_{3m+1}]$ and $H_2[A_{m-1}B_mO_{3m+1}]$) are easily obtained. The protonated forms of layered perovskites are reported to exhibit photocatalytic activity,[2] ion conductivity,[3] and intercalation behavior.[1,4,5] With regard to the intercalation reaction, *n*-alkylamines were intercalated in the interlayer space by an acid–base mechanism.[1,4] A protonated form of a Dion–Jacobson-type layered perovskite, $HLaNb_2O_7\cdot xH_2O$ (A = La, B = Nb, and $n = 2$), can react with *n*-alcohols as well as with *n*-alkylamines and pyridine.[1,4] The reactions with *n*-alcohols were once reported to be simple intercalation,[6] but it has been found that the reactions lead to the formation of alkoxyl groups on the interlayer surface.[7] The resultant perovskite-like slabs with alkoxyl groups bound on the interlayer surface via Nb–O–C bonds can be regarded as macromolecular heterometallic oxoalkoxides.

Because metal alkoxides react with various organic species bearing hydroxyl groups, alkoxyl groups can be replaced with other groups.[8] The reactions with alcohols can be expressed as follows:

$$Nb(OR)_y + zR'OH \rightarrow Nb(OR)_{y-z}(OR')_z + zROH$$

Similar reactions have been reported for alkoxyl derivatives of $HLaNb_2O_7\cdot xH_2O$, though these reactions proceeded via a hydrolysis-esterification mechanism.[9] In this type of reaction, 2-propanol, which does not react with $HLaNb_2O_7\cdot xH_2O$, can react with an *n*-propoxyl derivative of $HLaNb_2O_7\cdot xH_2O$ to form an isopropoxyl derivative. To date, however, reactions of this type have been reported only for $HLaNb_2O_7\cdot xH_2O$.

We report here the preparation of *n*-alkoxyl derivatives of $HCa_2Nb_3O_{10}\cdot xH_2O$, a protonated form of a triple-layered Dion–Jacobson-type layered perovskite. In addition to direct reactions with *n*-alcohols, we report the aforementioned alcohol-exchange-type reactions for n-$C_nH_{2n+1}OH$ with $n \geq 3$. Characterization of the resulting products by X-ray diffraction (XRD), infrared (IR) adsorption spectroscopy, solid-state nuclear magnetic resonance (NMR)

* Author to whom correspondence should be addressed.

(1) Schaak, R. E.; Mallouk, T. E. *Chem. Mater.* **2002**, *14*, 1455.
(2) Yoshimura, J.; Ebina, Y.; Kondo, J.; Domen, K.; Tanaka, A. *J. Phys. Chem.* **1993**, *97*, 1970.
(3) Sato, M.; Abo, J.; Jin, T.; Ohta, M. *J. Alloys Compd.* **1993**, *192*, 81.
(4) Gopalakrishnan, J.; Bhat, V.; Raveau, B. *Mater. Res. Bull.* **1987**, *22*, 413.
(5) Jacobson, A. J.; Johnson, J. W.; Lewandowski, J. T. *Inorg. Chem.* **1985**, *24*, 3727.
(6) Matsuda, T.; Miyamae, N.; Takeuchi, M. *Bull. Chem. Soc. Jpn.* **1993**, *66*, 1551.
(7) Takahashi, S.; Nakato, T.; Hayashi, S.; Sugahara, Y.; Kuroda, K. *Inorg. Chem.* **1995**, *34*, 5065.
(8) Bradley, D. C.; Mehrotra, R. C.; Rothwell, I. P.; Singh, A. *Alkoxo and Aryloxo Derivatives of Metals*; Academic Press: San Diego, 2001.
(9) Suzuki, H.; Notsu, K.; Takeda, Y.; Sugimoto, W.; Sugahara, Y. *Chem. Mater.* **2003**, *15*, 636.

10.1021/la0343876 CCC: $25.00
Published on Web 10/03/2003

spectroscopy, thermogravimetry (TG), and differential thermal analysis (DTA) is presented.

Experimental Section

Instrumentation. The XRD patterns of the products were recorded on a Mac Science M0^{3}XHF^{22} diffractometer with Mn-filtered Fe Kα radiation. The lattice parameters were determined using (00*l*), (10*l*), and (110) reflections by the least-squares method. Reflections with $2\theta < 10°$ were excluded for the lattice parameter calculation. Solid-state ^{13}C NMR spectra were obtained with a JEOL CMX-400 spectrometer at 100.54 MHz with cross polarization and magic-angle spinning (CP/MAS) techniques. The contact time was 2 ms, and the pulse delay was 5 s. The sample spinning rate was about 5 kHz. The TG and DTA curves were recorded on a Mac Science TG-DTA 2010S under air flow. The heating rate was 10 °C/min, and α-Al_2O_3 was used as a standard. IR analysis was performed with a Perkin-Elmer Spectrum One instrument using the KBr disk technique.

Preparation of $KCa_2Nb_3O_{10}$ and $HCa_2Nb_3O_{10}\cdot xH_2O$. $KCa_2Nb_3O_{10}$ was prepared according to the method described elsewhere.[10] A mixture of K_2CO_3, $CaCO_3$, and Nb_2O_5 was calcined at 1200 °C for 48 h with intermittent grinding after 24 h. An excess amount of K_2CO_3 (30 mol %) was added to compensate for the loss of potassium due to volatilization. After calcination, excess K_2CO_3 was removed by washing the product with distilled water. $KCa_2Nb_3O_{10}$ was obtained by drying the washed product at 120 °C. $HCa_2Nb_3O_{10}\cdot xH_2O$ was obtained from $KCa_2Nb_3O_{10}$ as reported previously:[11] $KCa_2Nb_3O_{10}$ was treated with 6 M HCl for 72 h at 60 °C. After acid treatment, the product was centrifuged and washed with distilled water. A hydrated phase ($HCa_2Nb_3O_{10}\cdot xH_2O$: HCaNb) was obtained by drying at room temperature, and its anhydrous phase ($HCa_2Nb_3O_{10}$) was formed upon drying at 120 °C. The XRD pattern of the anhydrous phase corresponded to a tetragonal structure with $a = 0.3851(1)$ nm and $c = 1.4377(4)$ nm, a result consistent with those in the previous reports.[11,12] Inductively coupled plasma emission spectrometry confirmed that essentially all of the potassium ions had been removed. TG analysis showed that the amount of proton in the interlayer space was 1.0 per perovskite unit [$Ca_2Nb_3O_{10}$].

Reaction of $HCa_2Nb_3O_{10}\cdot xH_2O$ (HCaNb) with Methanol and Ethanol. For the reaction with methanol, 0.5 g of HCaNb, 13.8 mL of methanol, and 1.2 mL of water (corresponding to 10 mass % methanol) were allowed to react in an autoclave at 100 °C for 3 days. The resultant product was then centrifuged, washed with acetone, and dried at room temperature to obtain a white powder (C1/HCaNb). For the reaction with ethanol, 0.3 g of HCaNb, 13.8 mL of ethanol, and 1.2 mL of water were reacted in an autoclave at 150 °C for 7 days. The resultant product was then centrifuged, washed with acetone, and dried at room temperature to obtain a white powder (C2/HCaNb).

Reaction of C1/HCaNb with *n*-Propanol. For the reaction with *n*-propanol, 0.3 g of C1/HCaNb and 15 mL of *n*-propanol were allowed to react in an autoclave at 150 °C for 7 days. After centrifugation, the product was washed with acetone and dried at room temperature to obtain a white powder (C3/HCaNb).

Reaction of C3/HCaNb with *n*-Alcohols. Typically, 0.1 g of C3/HCaNb was reacted with 15 mL of *n*-$C_nH_{2n+1}OH$ ($n = 4$, 6, 8, 10, 12, 14, 16, and 18) in an autoclave at 150 °C for 7 days. After centrifugation, the product was washed with acetone or tetrahydrofuran and dried at room temperature to obtain a white powder (C*n*/HCaNb, $n = 4$, 6, 8, 10, 12, 14, 16, and 18).

Influence of the Addition of Water. C3/HCaNb was reacted with *n*-decanol or a mixture of *n*-decanol and distilled water (water content 1, 2, or 3 mass %) in an autoclave at 80 °C for 7 days to investigate the influence of water on this system. After reaction, the product was obtained by centrifuging, washing with acetone, and drying at room temperature. To investigate the hydrolytic deintercalation behavior, C3/HCaNb and a mixture of 2-pentanone and distilled water (water content 3 mass %) were reacted in an autoclave at 80 or 150 °C, and the product was subsequently centrifuged.

Results and Discussion

Preparation of the *n*-Alkoxyl Derivatives of HCaNb. To prepare single-phase products, it was necessary to employ appropriate starting compounds and reaction conditions, which depended on reactant *n*-alcohols. Upon reaction of HCaNb with methanol (100 °C) or ethanol (150 °C) in the autoclave, the (00*l*) reflections of HCaNb disappear and new low-angle reflections with higher orders appear (methanol, C1/HCaNb; ethanol, C2/HCaNb), indicating the formation of new layered compounds with different interlayer distances. The interlayer distance of C1/HCaNb is 1.547(2) nm, which is different from those of the hydrated phase (1.6249(3) nm, HCaNb) and the anhydrous phase (1.4377(4) nm) of HCaNb. The material, C2/HCaNb, exhibits a slightly larger interlayer distance of 1.7681(7) nm, which exceeds those of the hydrated and the anhydrous phases. We also attempted to achieve direct reactions of HCaNb with *n*-$C_nH_{2n+1}OH$ ($n \geq 3$). Although these experiments resulted in the presence of reflections with yet larger interlayer distances (≥1.93 nm), reflections due to the hydrated phase (HCaNb) were also present, indicating that single-phase products were not obtained.

For the reactions with *n*-$C_nH_{2n+1}OH$ ($n \geq 3$), we consequently employed the alcohol-exchange-type reactions that were reported for $HLaNb_2O_7\cdot xH_2O$.[9] When C1/HCaNb was reacted with *n*-propanol in a sealed glass ampule at 80 °C, the XRD pattern of the resultant product showed the presence of unreacted C1/HCaNb only. Upon heating in the autoclave at 150 °C, in contrast, C1/HCaNb reacted with *n*-propanol to form a compound (C3/HCaNb) with new reflections corresponding to a larger interlayer distance (1.930(2) nm), and no reflections due to C1/HCaNb were observed.

We also attempted reactions between C1/HCaNb and *n*-$C_nH_{2n+1}OH$ ($n \geq 4$) using the autoclave in a similar fashion at 150 °C. The interlayer distances calculated from the newly appearing reflections (2.12−4.40 nm) were larger than that of C1/HCaNb (1.547(2) nm). All the XRD patterns of the reaction products demonstrate the additional presence of unreacted C1/HCaNb, however. When C3/HCaNb was used as an intermediate instead of C1/HCaNb, essentially the same interlayer distances were observed. Moreover, the reactions were completed because no reflections due to C3/HCaNb were present in the XRD patterns of C*n*/HCaNb with $4 \leq n \leq 18$.

Figure 1 shows the XRD patterns of C1/HCaNb, C3/HCaNb, C10/HCaNb, and C18/HCaNb. All the XRD patterns of C*n*/HCaNb can be indexed on the basis of a tetragonal cell. Besides the low-angle reflections described previously, reflections of C*n*/HCaNb at higher angles provide further information on the structures of the products. The reflection at $2\theta = 41.6°$, the (110) reflection of HCaNb, reflects the perovskite-like slab structure along the *ab* plane, and its presence in the same position in all the C*n*/HCaNb products indicates that the structure of the perovskite-like slab is preserved after the reactions. The XRD patterns of C3/HCaNb, C10/HCaNb, and C18/HCaNb show the (100) reflection at 29.1°, suggesting that these products possess a simple stacking sequence without displacement (a tetragonal cell with primitive symmetry: P-type cell).[13] Other C*n*/HCaNb ($2 \leq n \leq 18$) products also

(10) Hamada, D.; Machida, M.; Sugahara, Y.; Kuroda, K. *J. Mater. Chem.* **1996**, *6*, 69.
(11) Jacobson, A. J.; Lewandowski, J. T.; Johnson, J. W. *J. Less-Common Met.* **1986**, *116*, 137.
(12) Dion, M.; Ganne, M.; Tournoux, M. *Rev. Chim. Miner.* **1986**, *23*, 61.
(13) Tsunoda, Y.; Shirata, M.; Sugimoto, W.; Liu, Z.; Terasaki, O.; Kuroda, K.; Sugahara, Y. *Inorg. Chem.* **2001**, *40*, 5768.

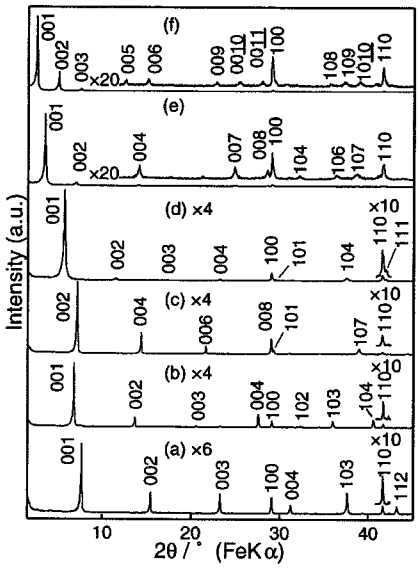

Figure 1. XRD patterns of (a) the anhydrous phase of HCaNb, (b) the hydrated phase (HCaNb), (c) C1/HCaNb (HCaNb after reaction with methanol), (d) C3/HCaNb (C1/HCaNb after reaction with *n*-propanol), (e) C10/HCaNb (C3/HCaNb after reaction with *n*-decanol), and (f) C18/HCaNb (C3/HCaNb after reaction with *n*-octadecanol).

Table 1. Lattice Parameters of HCaNb and Its Reaction Products with *n*-Alcohols

sample	*a*, nm	*c*,[a] nm
anhydrous HCaNb	0.3851(1)	1.4377(4)
hydrated HCaNb	0.3851(1)	1.6249(3)
C1/HCaNb[b]	0.3860(2)	3.093(3)
C2/HCaNb[b]	0.3858(2)	1.7681(7)
C3/HCaNb[c]	0.3860(8)	1.930(2)
C4/HCaNb[d]	0.3857(7)	2.123(1)
C6/HCaNb[d]	0.3864(9)	2.473(7)
C8/HCaNb[d]	0.3858(1)	2.828(1)
C10/HCaNb[d]	0.3859(3)	3.150(1)
C12/HCaNb[d]	0.3858(2)	3.477(1)
C14/HCaNb[d]	0.3859(8)	3.809(5)
C16/HCaNb[d]	0.3861(6)	4.111(7)
C18/HCaNb[d]	0.3846(4)	4.403(3)

[a] The *c* parameter of C1/HCaNb is doubled, indicating that *c*/2 (1.547(2) nm) corresponds to the interlayer distance. The *c* parameters of the other samples correspond to their interlayer distances. [b] Prepared by direct reaction with hydrated HCaNb. [c] Prepared from C1/HCaNb. [d] Prepared from C3/HCaNb.

show the (100) reflection in a similar fashion. Thus, the *c* parameters of C*n*/HCaNb ($2 \le n \le 18$) correspond to repeating distances. The XRD pattern of C1/HCaNb, on the contrary, does not show the (100) reflection (the reflections at 29.0 and 29.3° are assigned as (008) and (101)). Because the reported protonated forms of layered perovskites exhibit either a P-type cell[3,11] or an I-type cell[14-16] (a tetragonal cell with body-centered symmetry), it is likely that C1/HCaNb possesses an I-type cell exhibiting a stacking sequence with a relative displacement by $(a + b)/2$ and a doubled *c* parameter. Table 1 summarizes the lattice parameters of HCaNb and C*n*/HCaNb.

Figure 2 shows the solid-state ^{13}C CP/MAS NMR spectra of C1/HCaNb, C3/HCaNb, C10/HCaNb, and C18/HCaNb.

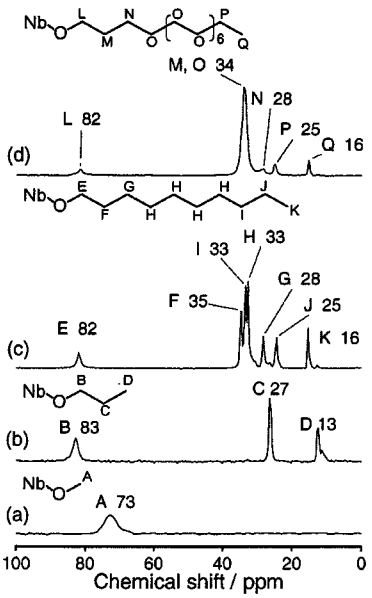

Figure 2. Solid-state ^{13}C CP/MAS NMR spectra of (a) C1/HCaNb (HCaNb after reaction with methanol), (b) C3/HCaNb (C1/HCaNb after reaction with *n*-propanol), (c) C10/HCaNb (C3/HCaNb after reaction with *n*-decanol), and (d) C18/HCaNb (C3/HCaNb after reaction with *n*-octadecanol).

The chemical shifts of the α-carbon (−*C*−O−) signals of C1/HCaNb, C3/HCaNb, C10/HCaNb, and C18/HCaNb are 73, 83, 82, and 82 ppm, respectively. Because the chemical shifts of the α-carbon signals of methanol, *n*-propanol, *n*-decanol, and *n*-octadecanol in the liquid-state NMR spectra were 50.0, 64.1, 62.4, and 63.0 ppm, respectively, these α-carbon signals of *n*-alcohols show downfield shifts by about 20 ppm after the reactions. Similar shifts of the α-carbon signals were observed in previous reports[7,9] for the alkoxyl derivatives of $HLaNb_2O_7\cdot xH_2O$, and such downfield shifts were reported to be indicative of the formation of an Nb−O−C bond. After the reactions between C1/HCaNb and *n*-propanol and between C3/HCaNb and *n*-decanol (or *n*-octadecanol), the signals assignable to *n*-alkoxyl groups of the intermediates are not observed, indicating that all the *n*-alkoxyl groups in the intermediates have been removed.

The TG and DTA curves of HCaNb, C1/HCaNb, C3/HCaNb, C10/HCaNb, and C18/HCaNb are shown in Figure 3. The DTA curves of the products exhibit exothermic peaks at >200 °C, which are not observed in the DTA curve of HCaNb. These exothermic peaks are consequently ascribable to the oxidative decomposition of the *n*-alkoxyl groups. With the XRD results taken into account, the ^{13}C CP/MAS NMR and DTA results provide sufficient evidence for the formation of HCaNb possessing *n*-alkoxyl groups on the interlayer surface: C*n*/HCaNb (*n* = 1, 2, 3, 4, 6, 8, 10, 12, 14, 16, and 18) samples are *n*-alkoxyl derivatives of HCaNb.

The TG curves of C10/HCaNb and C18/HCaNb show abrupt mass losses at around 300 °C (where intense exothermic DTA peaks are present), while those of C1/HCaNb and C3/HCaNb exhibit gradual mass changes (Figure 3). Slight mass gains are observed in the TG curves of C1/HCaNb and C3/HCaNb from ~500 to ~600 °C, and these might be ascribed to oxidation of carbonaceous substances. Thus, the oxidative decomposition processes of the derivatives with smaller alkoxyl groups are different from those of the other derivatives. The amounts of *n*-alkoxyl groups on the interlayer surface are estimated

(14) Schaak, R. E.; Mallouk, T. E. *J. Solid State Chem.* **2000**, *155*, 46.
(15) Uma, S.; Raju, A. R.; Gopalakrishnan, J. *J. Mater. Chem.* **1993**, *3*, 709.
(16) Gopalakrishnan, J.; Bhat, V. *Inorg. Chem.* **1987**, *26*, 4299.

Table 2. Amounts of *n*-Alkoxyl Groups in the Interlayer Space[a]

	mass loss, mass %	amount of *n*-alkoxyl groups[b]		mass loss, mass %	amount of *n*-alkoxyl groups[b]
C1/HCaNb	3.7	0.76	C10/HCaNb	19.3	0.81
C2/HCaNb	6.0	0.84	C12/HCaNb	22.0	0.80
C3/HCaNb	8.4	0.89	C14/HCaNb	24.4	0.79
C4/HCaNb	10.3	0.88	C16/HCaNb	26.9	0.80
C6/HCaNb	13.5	0.84	C18/HCaNb	30.5	0.85
C8/HCaNb	16.1	0.79			

[a] Estimated from the mass loss in TG analysis. [b] The values are per perovskite unit [$Ca_2Nb_3O_{10}$]. The values are calculated on the basis of the assumed compositions of $(RO)_x(HO)_{1-x}[Ca_2Nb_3O_9]$.

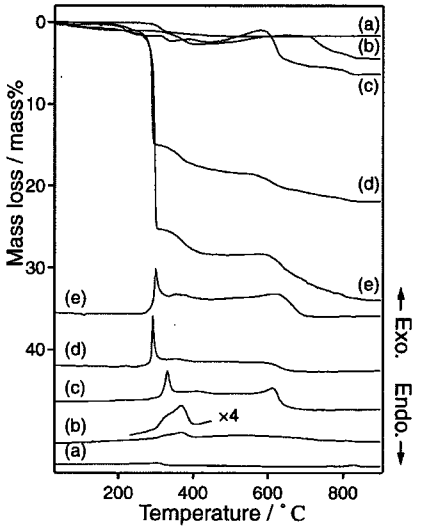

Figure 3. TG and DTA curves of (a) the anhydrous phase of HCaNb, (b) C1/HCaNb (HCaNb after reaction with methanol), (c) C3/HCaNb (C1/HCaNb after reaction with *n*-propanol), (d) C10/HCaNb (C3/HCaNb after reaction with *n*-decanol), and (e) C18/HCaNb (C3/HCaNb after reaction with *n*-octadecanol).

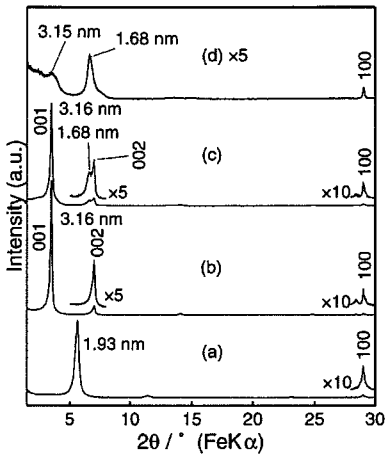

Figure 4. XRD patterns of the reaction products of C3/HCaNb with (a) *n*-decanol and (b–d) *n*-decanol–water mixtures, as follows: (b) 1, (c) 2, and (d) 3 mass % water. The reactions were conducted at 80 °C for 7 days.

from the mass losses between 200 and 900 °C by assuming that all the alkoxyl groups were completely decomposed up to 900 °C. The estimated amounts of the alkoxyl groups on the interlayer surface are in the range from 0.76 to 0.89 per perovskite unit [$Ca_2Nb_3O_{10}$] (Table 2). The amounts of alkoxyl groups are, therefore, slightly smaller than that required for their presence at every other NbO_6 octahedron on the interlayer surface. These values are similar to the reported values for *n*-alkoxyl derivatives of $HLaNb_2O_7 \cdot xH_2O$.[9]

Effect of Water on the Reaction Process. In the previous study,[9] the reaction of the *n*-propoxyl derivative of $HLaNb_2O_7 \cdot xH_2O$ with *n*-decanol proceeded only in the presence of water. We, therefore, added small amounts of water (1–3 mass %) for the reaction at 80 °C, where a reaction between C1/HCaNb and *n*-propanol did not occur. The XRD patterns of the reaction products of C3/HCaNb with mixtures of *n*-decanol and distilled water after 7 days are shown in Figure 4. The XRD pattern of the reaction product with the mixture containing 3 mass % water (Figure 4d) shows an intense reflection of the hydrated phase at 1.68 nm and a weak reflection of the *n*-decoxyl derivative at 3.15 nm. With a decrease in the amount of water to 2 mass %, the (001) and (002) reflections of the *n*-decoxyl derivative increase drastically (Figure 4c). Reaction of *n*-decanol and C3/HCaNb in the presence of 1 mass % water resulted in a single-phase *n*-decoxyl derivative (Figure 4b). Because no reaction between C3/HCaNb and *n*-decanol occurs without the addition of water (Figure 4a), the addition of water is clearly required for the formation of the *n*-decoxyl derivative at 80 °C. The reactions of C3/HCaNb with various *n*-alcohols ($C_nH_{2n+1}OH$, $n \geq 3$) consequently seem to proceed according to the hydrolysis–esterification mechanism, which is identical to the mechanism concluded for the same type of reactions of $HLaNb_2O_7 \cdot xH_2O$.[9]

We also studied the hydrolytic deintercalation behavior of C3/HCaNb at high temperatures using a mixture of 2-pentanone and distilled water (3 mass % water). The XRD pattern of the product treated at 80 °C showed reflections of the *n*-propoxyl derivative and the hydrated phase (HCaNb), and the product treated at 150 °C contained the *n*-propoxyl derivative and the anhydrous phase of HCaNb. These results indicate that the type of protonated phases formed via hydrolysis depends on the reaction temperature (the hydrated phase, HCaNb, occurring after reaction at 80 °C, and the anhydrous phase of HCaNb after reaction at 150 °C). Thus, the same phases could form during reactions with *n*-alcohols in the presence of water.

On the basis of the reactions between the *n*-alkoxyl derivatives of $HLaNb_2O_7 \cdot xH_2O$ with alcohols,[9] water, present as an impurity, is anticipated to play a key role in the hydrolysis–esterification mechanism during the reaction of C*n*/HCaNb with another *n*-alcohol; water hydrolyzes the $(RO)NbO_5$ site and is regenerated by subsequent esterification. During reactions at 80 °C, the hydrated phase (or hydrated-phase-type interlayer environment) is expected to form on the basis of the hydrolysis behavior demonstrated with the mixture of 2-pentanone and distilled water. Because the amount of water is small, water molecules appear to be captured in the interlayer space of the generated protonated form to produce the hydrated phase. The amount of free water can, therefore, be expected to decrease drastically when

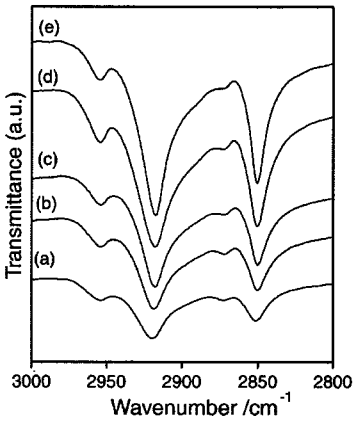

Figure 5. IR spectra of (a) C10/HCaNb, (b) C12/HCaNb, (c) C14/HCaNb, (d) C16/HCaNb, and (e) C18/HCaNb.

a small amount of the hydrated phase forms in the initial stage of the reaction at 80 °C. Because no similar reactions occurred in a water-free system with $HLaNb_2O_7$·xH_2O,[9] the hydrated-phase formation accounts for the lack of a reaction between C3/HCaNb and *n*-decanol at 80 °C without the addition of water. The hydrated phase does not appear to be observed in the XRD pattern because of its small amount. This interpretation is further supported by the fact that the addition of 1 mass % water leads to the formation of a single-phase *n*-decoxyl derivative at 80 °C. The formation of the hydrated phase with the addition of an excess amount of water (2 or 3 mass %) is also consistent with the assumed mechanism; when the hydrolysis reaction is dominant, the hydrated phase (not the anhydrous phase) is formed. During reactions at 150 °C, on the other hand, water cannot be present in the interlayer space of the protonated form, and it is, therefore, present as free water; the reaction can proceed at 150 °C as a consequence. This interpretation is consistent with the proceeding of the substitution reactions of the *n*-alkoxyl derivatives of $HLaNb_2O_7$·xH_2O with other alcohols at 80 °C; because the anhydrous phase of $HLaNb_2O_7$ was formed via hydrolysis with a mixture of 2-pentanone and distilled water at 80 °C,[9] water did not seem to be present in the interlayer space during reactions at 80 °C.

Arrangement of *n*-Alkyl Chains in the Interlayer Space. IR spectroscopy was applied to investigate the arrangement of *n*-alkyl chains in the interlayer space because C−H stretching band positions are sensitive to the conformation of the *n*-alkyl chains.[17-19] The IR spectra of C*n*/HCaNb (n = 10, 12, 14, 16, and 18) are shown in Figure 5. In all the spectra, absorption bands due to CH_2 and CH_3 stretching vibrations are observed at the same wavenumbers (2953 cm^{-1}, $\nu_{as(CH_3)}$; 2918 cm^{-1}, $\nu_{as(CH_2)}$; 2872 cm^{-1}, $\nu_{s(CH_3)}$; 2850 cm^{-1}, $\nu_{s(CH_2)}$),[20] suggesting that the *n*-alkyl chains in the interlayer space exhibit very similar conformations. The wavenumbers of the CH_2 stretching vibration ($\nu_{as(CH_2)}$ = 2918 cm^{-1} and $\nu_{s(CH_2)}$ = 2850 cm^{-1}) indicate that the conformation of the alkyl chains in the interlayer space is an *all-trans* ordered state.[19] In the ^{13}C CP/MAS NMR spectra of C10/HCaNb and C18/HCaNb,

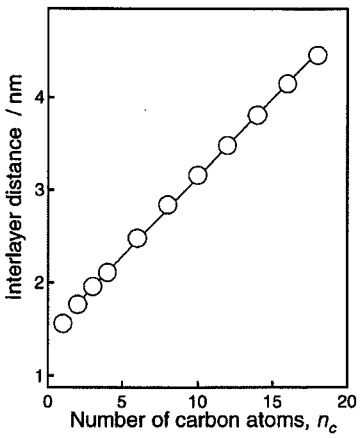

Figure 6. Variation in the interlayer distance of the *n*-alkoxyl derivatives of HCaNb as a function of the number of carbon atoms in the *n*-alkyl chains, n_c.

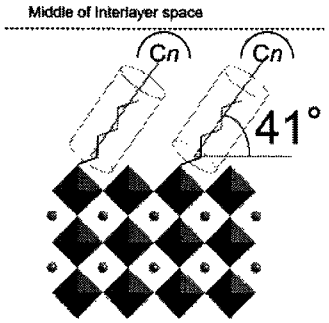

Figure 7. Proposed schematic model for the arrangement of the *n*-alkoxyl groups in the interlayer space of HCaNb for the *n*-alkoxyl derivatives of HCaNb with $n \geq 2$.

moreover, the CH_2 signals were observed only at 33−34 ppm, which is ascribed to the *all-trans* alkyl chain,[21] a result consistent with the IR results.

The relationship between the number of carbon atoms in *n*-alkyl chains and the interlayer distance is shown in Figure 6. A linear relationship is clearly observed for C*n*/HCaNb with $n \geq 2$. Because only the space group for the XRD pattern of C1/HCaNb appears to be I-type, the interlayer distance of C1/HCaNb must be excluded in the following discussion. The slope (the increase in interlayer distance per one carbon atom) was calculated from the interlayer distance of C*n*/HCaNb ($n \geq 2$) to be 0.166 nm/carbon atom. The IR and ^{13}C CP/MAS NMR results demonstrate that C*n*/HCaNb with $n \geq 10$ possesses *n*-alkyl chains in the interlayer space with the *all-trans* conformation, and the same *all-trans* conformation is expected for the *n*-alkoxyl groups with $3 \leq n \leq 8$. The observed slope is larger than the increase in the *all-trans n*-alkyl chain (0.127 nm/carbon atom), indicating that the *n*-alkyl chains in the interlayer space form a bilayer arrangement. The tilt angle of the *n*-alkyl chains estimated from the slope in Figure 6 is 41°. Figure 7 demonstrates a proposed model of the arrangement of *n*-alkoxyl groups bound on the interlayer surface of HCaNb .

Conclusions

We have demonstrated that various *n*-alkoxyl derivatives of $HCa_2Nb_3O_{10}$·xH_2O (HCaNb) can be prepared by

(17) Snyder, R. G.; Strauss, H. L.; Elliger, C. A. *J. Phys. Chem.* **1982**, *86*, 5145.
(18) MacPhail, R. A.; Strauss, H. L.; Snyder, R. G.; Elliger, C. A. *J. Phys. Chem.* **1984**, *88*, 334.
(19) Vaia, R. A.; Teukolsky, R. K.; Giannelis, E. P. *Chem. Mater.* **1994**, *6*, 1017.
(20) Nakamoto, K. *Infrared and Raman Spectra of Inorganic and Coordination Compounds*, 5th ed.; Wiley-Interscience: New York, 1997, Part B.
(21) Pursch, M.; Brindle, R.; Ellwanger, A.; Sander, L. C.; Bell, C. M.; Handel, H.; Albert, K. *Solid State Nucl. Magn. Reson.* **1997**, *9*, 191.

employing different starting compounds and reaction conditions. Single-phase *n*-alkoxyl derivatives are obtained by a direct reaction of HCaNb only with methanol and ethanol. The single-phase *n*-propoxyl derivative of HCaNb is formed by a reaction between the methoxyl derivative of HCaNb and *n*-propanol at 150 °C. Reactions between the *n*-propoxyl derivative and *n*-$C_nH_{2n+1}OH$ (n = 4−18) at 150 °C lead to the formation of various single-phase *n*-alkoxyl derivatives of HCaNb. Because water is essential for the reaction between the *n*-propoxyl derivative and *n*-decanol to proceed at 80 °C, the hydrolysis−esterification mechanism is strongly suggested. The hydrate formation behavior of HCaNb and $HLaNb_2O_7 \cdot xH_2O$ can account for the differences in the reaction temperatures for these two Dion−Jacobson phases without the addition of water. The *n*-alkyl chains ($n \geq 10$ in the *n*-$C_nH_{2n+1}O-$ groups) in the interlayer space are in the *all-trans* conformation, and the linear relationship between the number of carbon atoms in the *n*-alkyl chains and the interlayer distance demonstrates that the *n*-alkyl chains form bilayers with a tilt angle of 41°. The present study exhibits the factors (reaction temperature, use of intermediates, water content) for the single-phase formation of the *n*-alkoxyl derivatives of HCaNb and suggests that the alkoxyl modification of the interlayer surface could extend to various protonated forms of ion-exchangeable layered perovskites.

Acknowledgment. The authors gratefully thank Prof. Kazuyuki Kuroda of Waseda University, Department of Applied Chemistry, for his valuable suggestions. This work was financially supported in part by the Grant-in-Aid for Scientific Research (No. 14350462) from the Ministry of Education, Science, Sports, and Culture, Japan, and by 21COE "Practical Nano-Chemistry" from MEXT, Japan.

LA0343876

Available online at www.sciencedirect.com
SCIENCE DIRECT
Journal of Organometallic Chemistry 686 (2003) 145–150
Journal of Organometallic Chemistry
www.elsevier.com/locate/jorganchem

Hydrosilylation in the 2D interlayer space between inorganic layers: reaction between immobilized C=C groups on the interlayer surface of layered perovskite $HLaNb_2O_7 \cdot xH_2O$ and chlorohydrosilanes

Satoru Yoshioka [a], Yosuke Takeda [a], Yuko Uchimaru [b], Yoshiyuki Sugahara [a,*]

[a] *Department of Applied Chemistry, School of Science and Engineering, Waseda University, Ohkubo-3 Shinjuku-ku, Tokyo 169-8555, Japan*
[b] *National Institute of Advanced Science and Technology, AIST Tsukuba Central 5-2, Tsukuba, Ibaraki 305-8565, Japan*

Received 1 April 2003; accepted 18 June 2003

Abstract

The C=C bonds immobilized in the interlayer space of layered perovskite, $HLaNb_2O_7 \cdot xH_2O$, have undergone hydrosilylation reactions with chlorohydrosilanes. The C=C bonds are immobilized by the reaction between an *n*-propoxyl derivative of $HLaNb_2O_7 \cdot xH_2O$ and 4-penten-1-ol to form a $CH_2=CH(CH_2)_3O-$ derivative of $HLaNb_2O_7 \cdot xH_2O$, and a corresponding increase in the interlayer distance from 1.54 to 1.85 nm is observed. The $CH_2=CH(CH_2)_3O-$ derivative is further treated with dichloromethylsilane or trichlorosilane, and the interlayer distance increases to 2.41 (dichloromethylsilane) or 2.07 (trichlorosilane) nm. Solid-state ^{13}C-CP/MAS-NMR spectroscopy and infra-red (IR) spectroscopy reveal that the C=C groups disappear after the treatment with dichloromethylsilane or trichlorosilane, and ^{13}C-NMR signals assignable to the hydrosilylated products are clearly observed. Besides hydrosilylation reactions, siloxane formation involving hydrolysis of the Si–Cl groups also proceeds. The structure of the perovskite-like slabs in $HLaNb_2O_7 \cdot xH_2O$ is preserved throughout the process, indicating the successful modification of immobilized C=C groups via hydrosilylation with no structural change in the inorganic host layers.

Keywords: Layered perovskite; Dion–Jacobson phase; Hydrosilylation; Chlorosilane; Grafting reaction; Interlayer surface modification

1. Introduction

It is well known that some layered compounds can accommodate ions and molecules in the interlayer space to form intercalation compounds [1–3]. These intercalation reactions are generally considered to be reversible; guest species can be deintercalated under appropriate conditions. It is also possible to immobilize organic or organometallic groups on the interlayer surface. These reactions, called 'grafting reactions,' have been applied for layered compounds possessing reactive groups on the interlayer surface. Typical host compounds are layered polysilicates, whose interlayer surface bears silanol (SiOH) groups [4]. The silanol groups can react with organochlorosilanes (such as R_3SiCl) [5] and alcohols [6] to form covalent Si–O–Si and Si–O–C bonds, respectively. Other typical examples are kaolinite, [7,8] FeOCl, [9] and zirconium phosphate [10]. Interlayer space environments can therefore be modified through these reactions. Zirconium phosphate [11] and layered polysilicate [12] with grafted long alkyl chains can selectively adsorb molecules, for example. Another example is zirconium phosphate with grafted polyether chains which can solvate $LiClO_4$, and resulting $LiClO_4$-intercalated zirconium phosphate exhibited ionic conductivity [13].

Ion-exchangeable layered perovskites consist of perovskite-like slabs $[A_{n-1}B_nO_{3n+1}]$ and interlayer cations (M) [14]. Based on the layer charge, ion-exchangeable layered perovskites can be classified into the Dion–Jacobson phases ($M[A_{n-1}B_nO_{3n+1}]$) [15,16] and the Ruddlesden–Popper phases ($M_2[A_{n-1}B_nO_{3n+1}]$) [17,18]. These phases can be converted into their protonated forms by acid treatment [14,19]. $HLaNb_2O_7 \cdot xH_2O$ (HLN), one of the protonated

* Corresponding author. Tel./fax: +81-3-5286-3204.
E-mail address: ys6546@waseda.jp (Y. Sugahara).

0022-328X/03/$ - see front matter © 2003 Elsevier B.V. All rights reserved.
doi:10.1016/S0022-328X(03)00618-1

Dion–Jacobson-type layered perovskites, can react with *n*-alcohols to form *n*-alkoxyl groups, which are directly bound to niobium [20]. Direct reactions have been reported only for *n*-alcohols, and additional types of alcohols can be dissociatively immobilized via a hydrolysis-esterification mechanism using *n*-alkoxyl derivatives as intermediates [21]. Even with the use of appropriate intermediates, however, the reaction is affected by a steric factor: when an *n*-propoxyl derivative was treated with bulky *tert*-butanol, the substitution reaction was not completed. A more versatile method of designing interlayer space environments is therefore required.

Hydrosilylation has been known for decades in silicon chemistry [22–25]. The use of this type of reaction is not limited to molecular chemistry, and it has also been applied extensively to the surface modification of solids possessing SiH and C=C groups on their surfaces [26–30]. It is therefore expected that a hydrosilylation reaction can be employed to immobilize desirable functional groups in the interlayer space if appropriate groups (such as C=C, C≡C, and SiH groups) can be bound covalently on the interlayer surface. To date, the use of such approaches has been very limited, however. To the best of our knowledge, only one research group has reported the hydrosilylation on the surface of layered compounds: 2D silicate frameworks possessing alkenyl and alkynyl groups were prepared via reactions of a silicate mineral, apophyllite, with alkenylchlorosilanes and alkynylchlorosilanes and resulting organically-modified 2D silicates subsequently underwent hydrosilylation reactions with pentamethyldisiloxane [31,32].

We report here hydrosilylation of C=C groups immobilized on the interlayer surface of HLN with chlorohydrosilanes [$Cl_x(H)SiMe_{3-x}$] (Scheme 1). We first report the immobilization of CH_2=$CH(CH_2)_3O$– groups on the interlayer surface of HLN, after which we present the results for hydrosilylation reactions between the C=C groups in the CH_2=$CH(CH_2)_3O$– groups and chlorohydrosilanes, $Cl_x(H)SiMe_{3-x}$ (mainly $x = 2$, 3). Since the purpose of this study is modification of the interlayer space of HLN via hydrosilylation, attention has been paid to providing evidence for the preservation of the perovskite-like slab structures of HLN during the grafting and hydrosilylation reactions.

2. Experimental

2.1. Immobilization of 4-penten-1-ol on the interlayer space of $HLaNb_2O_7 \cdot xH_2O$ (HLN)

The preparation of $HLaNb_2O_7 \cdot xH_2O$ (HLN) and its conversion into the *n*-propoxyl derivative (*n*-propoxyl-HLN) were described elsewhere [21]. About 1.3 g of *n*-propoxyl-HLN and 40 ml of 4-penten-1-ol were sealed in a glass ampoule and heated at 80 °C for 7 d. After centrifugation, the resultant product was washed with acetone and air-dried to give a CH_2=$CH(CH_2)_3O$– derivative (CH_2=$CH(CH_2)_3O$–HLN).

2.2. Reaction between chlorohydrosilanes ($Cl_x(H)SiMe_{3-x}$) and CH_2=$CH(CH_2)_3O$–HLN

All the procedures were performed based on the standard Schlenk technique under protective nitrogen atmosphere [33] or in a glove box filled with nitrogen. About 0.3 g of CH_2=$CH(CH_2)_3O$–HLN and 20 ml of $Cl_x(H)SiMe_{3-x}$ ($x = 1$, 2, 3) were heated at reflux for 3 d. As a catalyst, $H_2PtCl_6 \cdot 6H_2O$ (as an acetonitrile solution) was employed with a Pt/Si ratio of 5×10^{-4}. The resultant product was washed with hexane and dried under reduced pressure.

2.3. Analyses

X-ray diffraction (XRD) patterns were obtained using a MacScience M03XHF^{22} with Fe–K_α radiation. Infrared (IR) spectra were recorded on a Perkin–Elmer Spectrometer One. Solid-state ^{13}C- and ^{29}Si-NMR with magic angle spinning and a cross polarization technique (^{13}C- and ^{29}Si-CP/MAS-NMR) were obtained using a JEOL CMX-400 spectrometer operated at 100.52 (^{13}C) and 79.42 (^{29}Si) MHz with a spinning rate of ~5 kHz. The carbon content was determined by internal service at the Waseda Material Characterization Center.

3. Results and discussion

3.1. Immobilization of 4-penten-1-ol on the interlayer space of $HLaNb_2O_7 \cdot xH_2O$ (HLN)

Fig. 1 shows the XRD patterns of *n*-propoxyl-HLN and *n*-propoxyl-HLN treated with 4-penten-1-ol. The low-angle reflection expressing its interlayer distance shifts to a lower angle upon treatment with 4-penten-1-ol, indicating that the interlayer distance increases from 1.54 to 1.85 nm. The reflection at $2\theta = 28.8°$, a (1 0 0) reflection of HLN, can be observed in the same position only when the structure of the perovskite-like slabs does not change. The observation of the reflection at $2\theta = 28.8°$ therefore indicates that treatment with 4-penten-1-ol affects the interlayer distance only.

The ^{13}C-CP/MAS-NMR spectra of *n*-propoxyl-HLN and its reaction product with 4-penten-1-ol are demonstrated in Fig. 2. Signals A, B and C observed in the spectrum of *n*-propoxyl-HLN are assigned to *n*-propoxyl groups [21]. In the spectrum of the reaction

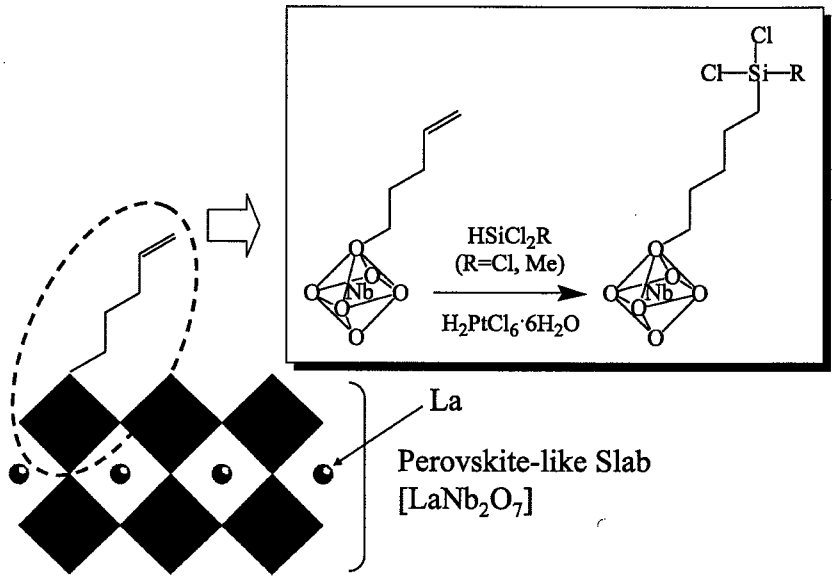

Scheme 1. Schematic representation of hydrosilylation in the interlayer space of the organic derivative of layered perovskite $HLaNb_2O_7 \cdot xH_2O$.

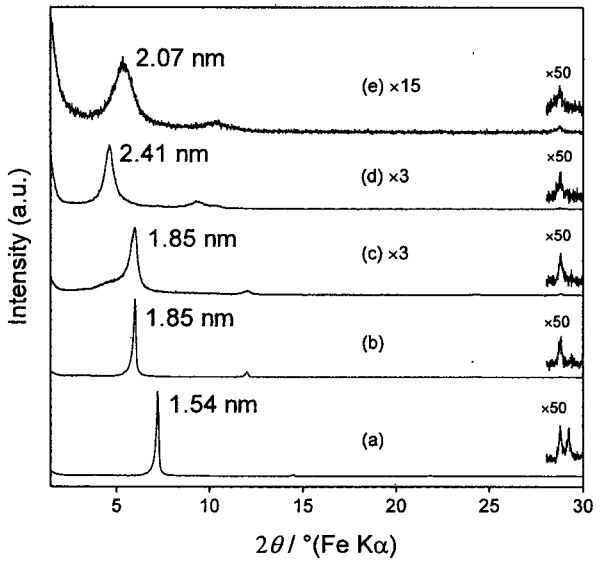

Fig. 1. XRD patterns of (a) *n*-propoxyl-HLN; (b) CH_2=$CH(CH_2)_3O$-HLN; (c) CH_2=$CH(CH_2)_3O$–HLN treated with chlorodimethylsilane; (d) CH_2=$CH(CH_2)_3O$–HLN treated with dichloromethylsilane and (e) CH_2=$CH(CH_2)_3O$–HLN treated with trichlorosilane.

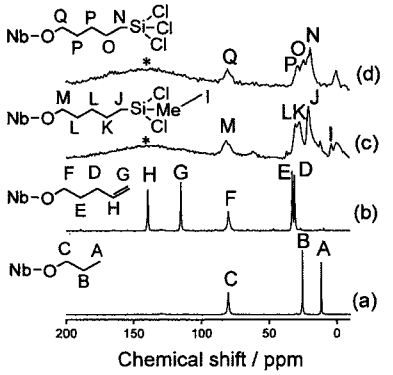

Fig. 2. Solid-state ^{13}C-CP/MAS-NMR spectra of (a) *n*-propoxyl-HLN; (b) CH_2=$CH(CH_2)_3O$–HLN; (c) CH_2=$CH(CH_2)_3O$–HLN treated with dichloromethylsilane and (d) CH_2=$CH(CH_2)_3O$–HLN treated with trichlorosilane. Broad signals masked by asterrisks are backgrounds.

product with 4-penten-1-ol, these three signals disappear and new signals D–H appear (signal D at 31 ppm, signal E at 33 ppm, signal F at 80 ppm, signal G at 115 ppm and signal H at 139 ppm). These signals are assignable to the CH_2=$CH(CH_2)_3O$– groups, as shown in Fig. 2b. The large downfield shift of the carbon atom attached to oxygen (signal F) from 62 ppm (a typical value in liquid-state ^{13}C-NMR of molecular CH_2=$CH(CH_2)_3OH$) to 80 ppm indicates that the CH_2=$CH(CH_2)_3O$– groups are present in the form of CH_2=$CH(CH_2)_3O$–Nb, since similar downfield shifts have been observed for other alkoxyl-derivatives of HLN, [20,21] for example, signal C of *n*-propoxyl-HLN at 81 ppm in Fig. 2a.

The IR spectra of *n*-propoxyl-HLN and *n*-propoxyl-HLN treated with 4-penten-1-ol are shown in Fig. 3. In the spectra of *n*-propoxyl-HLN and its reaction product with 4-penten-1-ol, $\nu_{(CH)}$ bands of CH_3 and $-CH_2-$ groups are observed in the range of 2800–3000 cm^{-1} [34]. In the spectrum of the reaction product with 4-penten-1-ol, additional bands assignable to CH_2=$CH(CH_2)_3O$– groups ($\nu_{(CH)}$, 3074 cm^{-1}; $\nu_{(C=C)}$, 1640 cm^{-1}) are clearly observed besides the $\nu_{(CH)}$ bands of the $-CH_2-$ groups. These results show good consistency with the solid-state ^{13}C-NMR results.

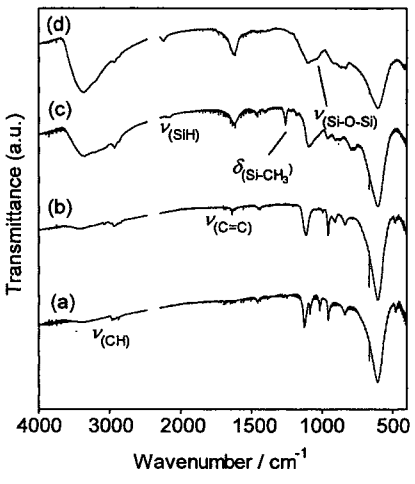

Fig. 3. IR spectra of (a) *n*-propoxyl-HLN; (b) CH_2=$CH(CH_2)_3O$–HLN; (c) CH_2=$CH(CH_2)_3O$–HLN treated with dichloromethylsilane and (d) CH_2=$CH(CH_2)_3O$–HLN treated with trichlorosilane.

These results indicate that 4-penten-1-ol is dissociatively immobilized on the interlayer surface of HLN in a way similar to the reaction between *n*-alkoxyl derivatives of HLN and alcohols [21]. The amount of CH_2=$CH(CH_2)_3O$– groups is estimated from the carbon content (9.96%) to be 0.81 group per [$LaNb_2O_7$] unit, indicating that 81% of the protonated site [(HO)NbO_5] in $HLaNb_2O_7 \cdot xH_2O$ is converted into a [CH_2=$CH(CH_2)_3O$]NbO_5 site.

3.2. Hydrosilylation in the interlayer space of HLN

The XRD patterns of the products after treatment of the CH_2=$CH(CH_2)_3O$– derivative of HLN (CH_2=$CH(CH_2)_3O$–HLN) with chlorohydrosilanes are shown in Fig. 1. After the treatment with chlorodimethylsilane [Cl(H)$SiMe_2$], no clear variation in the XRD pattern is observed; only a weak shoulder reflection appears at $2\theta = \sim 4.56°$ ($d = 2.43$ nm). After the treatments with dichloromethylsilane [Cl_2(H)SiMe] and trichlorosilane ($HSiCl_3$), on the contrary, the XRD patterns change drastically; the reflection corresponding to the interlayer distance of CH_2=$CH(CH_2)_3O$–HLN ($d = 1.85$ nm) disappears, and new low-angle reflections appear (dichloromethylsilane-treated product, $d = 2.41$ nm; trichlorosilane-treated product, $d = 2.07$ nm). It should be also noted that the reflection at $2\theta = 28.8°$, the (1 0 0) reflection of HLN, is observed in these two XRD patterns. Thus, the treatments with dichloromethylsilane and trichlorosilane lead to expansion of the interlayer distance without changing the perovskite-like slab structure. The lower reactivity of chlorodimethylsilane in comparison with those of dichloromethylsilane and trichlorosilane is ascribed to the electronic effect of chlorine substituent on the reactivity of hydrosilanes toward Pt-catalyzed hydrosilylation reactions [22,35,36]. Hereafter, further characterization results are presented for these two products only.

The solid-state ^{13}C-CP/MAS-NMR spectra of the products treated with chlorohydrosilanes are demonstrated in Fig. 2. After the treatments with dichloromethylsilane and trichlorosilane, the signals due to C=C groups (signals G and H) disappear, and new signals appear. It is known that hydrosilylation of 1-alkenes with hydrosilanes readily proceeds in the presence of various transition metal catalysts including Pt(0) complexes to give 1-silylalkanes (β-adduct) [37]. It seems that a similar addition reaction also proceeds in our system, and thus, major signals in the ^{13}C-CP/MAS-NMR spectra can be assigned to the structures assumed based on hydrosilylation reactions. For the product treated with dichloromethylsilane, signal I (4 ppm), signal J (21 ppm), signal K (27 ppm), signal L (30 ppm) and signal M (82 ppm) are assigned to carbon atoms in a [$CH_3(Cl)_2Si(CH_2)_5O$]NbO_5 site, as shown in Fig. 2c [38]. In the spectrum of trichlorosilane-treated product, signals assignable to a [$Cl_3Si(CH_2)_5O$]NbO_5 site appear at 22 (signal N), 27 (signal O), 31 (signal P with a shoulder at 32 ppm) and 83 (signal Q) ppm (Fig. 2d) [39]. Thus, taking the observed expansion of the interlayer distances into account, we conclude that hydrosilylation proceeds successfully in the interlayer space of HLN.

The IR spectra of the products treated with chlorohydrosilanes are shown in Fig. 3. Compared with the spectrum of CH_2=$CH(CH_2)_3O$–HLN, the $\nu_{(CH)}$ band of the CH_2=CH– groups at 3074 cm^{-1} disappears in the spectrum of the product treated with dichloromethylsilane. A new band appears at 1259 cm^{-1} and can be ascribed to the $\delta_{(Si-CH_3)}$ mode [34]. These observations show good consistency with the ^{13}C-CP/MAS-NMR results, which indicate the occurrence of hydrosilylation. The occurrence of hydrosilylation is also shown clearly by the disappearance of the $\nu_{(CH)}$ band of the CH_2=CH– groups in the spectrum of the product treated with trichlorosilane. In both the spectra, $\nu_{(SiH)}$ bands are detected at 2160 cm^{-1} for the product treated with dichloromethylsilane and at 2238 and 2248 cm^{-1} for the product treated with trichlorosilane [34]. In addition, a weak shoulder at 1039 cm^{-1}, which could be assigned to the $\nu_{(Si-O-Si)}$ mode, appears in the spectrum of the product treated with trichlorosilane. The appearance of the $\nu_{(SiH)}$ band and the $\nu_{(Si-O-Si)}$ band will be discussed below.

Fig. 4 shows solid-state ^{29}Si-CP/MAS-NMR spectra of the products treated with chlorohydrosilanes [40]. In the spectrum of the product treated with dichloromethylsilane, a intense signal that can be assigned to a $Cl_2(CH_3)SiCH_2$– environment is observed at 33 ppm. Similarly, an intense signal assignable to the Cl_3SiCH_2– environment is present at 14 ppm for the product treated with trichlorosilane. The presence of these two signals

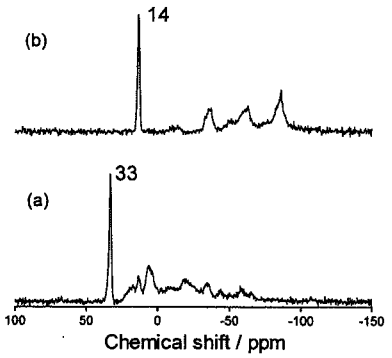

Fig. 4. Solid-state ^{29}Si-CP/MAS-NMR spectra of (a) CH_2=$CH(CH_2)_3O$–HLN treated with dichloromethylsilane and (b) CH_2=$CH(CH_2)_3O$–HLN treated with trichlorosilane.

shows good consistency with the occurrence of hydrosilylation in the interlayer space. Besides these signals, weak signals are present in an upfield region. In the spectrum of the product treated with dichloromethylsilane, the signals at −20 and −35 ppm are ascribable to the $Cl(CH_3)Si(O–)CH_2$– and $H(CH_3)Si(O–)_2$ environments, respectively. In addition, the signal at 6 ppm appears to be due to the $(CH_3)Si(O–)_2CH_2$– environment. In the spectrum of the product treated with trichlorosilane, the signals at −35, −62 and −86 ppm can be ascribed to the $HSiCl_2(O–)$, $HSiCl(O–)_2$ and $HSi(O–)_3$ environments, respectively. These environments can be formed by the formation of siloxane bonds via the hydrolysis of Si–Cl groups and subsequent condensation. When siloxane formation occurs without hydrosilylation, SiH groups remain (as an $H(CH_3)Si(O–)_2$ environment for the product treated with dichloromethylsilane and as $HSiCl_2(O–)$, $HSiCl(O–)_2$ and $HSi(O–)_3$ environments for the product treated with trichlorosilane), which is consistent with the IR results. Hydrolysis could proceed during the synthesis process because of the presence of a trace of impurity water and/or during the washing procedures, since Si–Cl groups are highly reactive to water.

4. Conclusions

We have demonstrated that hydrosilylation involving the C=C bonds immobilized on the interlayer surface of a layered perovskite $HLaNb_2O_7 \cdot xH_2O$ (HLN) occurs if dichloromethylsilane and trichlorosilane are employed as hydrosilylation reagents. The CH_2=$CH(CH_2)_3O$– groups are successfully bound to the interlayer surface of HLN via the reaction between *n*-propoxyl-HLN and 4-penten-1-ol, as clearly shown by spectroscopic analyses, and the interlayer distance increases correspondingly from 1.54 to 1.85 nm. The C=C bonds in the CH_2=$CH(CH_2)_3O$– groups can be further reacted with the chlorohydrosilanes (dichloromethylsilane and trichlorosilane) by hydrosilylation. The interlayer distance of the CH_2=$CH(CH_2)_3O$– derivative (1.85 nm) increases further to 2.41 nm (dichloromethylsilane) and 2.07 nm (trichlorosilane). Besides hydrosilylation reactions, siloxane formation involving hydrolysis of the Si–Cl groups also proceeds. It should be noted that the reflection at $2\theta = 28.8°$, which is the (1 0 0) reflection of HLN and which indicates the ordering of the perovskite-like slabs along the *ab* plane, remains in the same position during the modifications with 4-penten-1-ol and hydrosilylation, indicating that the perovskite-like slab structure is preserved throughout the whole process. The present results offer a versatile approach for grafting functional groups on the interlayer surface of layered perovskites, and this approach may be applicable to other layered compounds undergoing grafting reactions.

Acknowledgements

The authors gratefully thank Prof. Kazuyuki Kuroda, Department of Applied Chemistry at Waseda University, for his valuable suggestions. This work was financially supported in part by the Grant-in-Aid for Scientific Research (No. 14350462) from the Ministry of Education, Science, Sports, and Culture, Japan and by 21COE "Practical Nano-Chemistry" from MEXT, Japan.

References

[1] M.S. Whittingham, A.J. Jacobson (Eds.), Intercalation Chemistry, Academic Press, New York, 1982.
[2] A.J. Jacobson, in: A.K. Cheetham, P. Day (Eds.), Solid State Chemistry: Compounds, Clarendon Press, Oxford, 1992, p. 182.
[3] D. O'Hare, in: D.W. Bruce, D. O'Hare (Eds.), Inorganic Materials, second ed., Wiley, Chichester, 1996, p. 171.
[4] E. Ruiz-Hitzky, J.M. Rojo, Nature 287 (1980) 28.
[5] T. Yanagisawa, K. Kuroda, C. Kato, Bull. Chem. Soc. Jpn 61 (1988) 3743.
[6] Y. Mitamura, Y. Komori, S. Hayashi, Y. Sugahara, K. Kuroda, Chem. Mater. 13 (2001) 3747.
[7] J.J. Tunney, C. Detellier, Chem. Mater. 5 (1993) 747.
[8] Y. Komori, H. Enoto, R. Takenawa, S. Hayashi, Y. Sugahara, K. Kuroda, Langmuir 16 (2000) 5506.
[9] S. Kikkawa, F. Kanamaru, M. Koizumi, Inorg. Chem. 15 (1976) 2195.
[10] S. Yamanaka, Inorg. Chem. 15 (1976) 2811.
[11] J.W. Johnson, A.J. Jacobson, W.M. Butler, S.E. Rosenthal, J.F. Brody, J.T. Lewandowski, J. Am. Chem. Soc. 111 (1989) 381.
[12] M. Ogawa, S. Okutomo, K. Kuroda, J. Am. Chem. Soc. 120 (1998) 7361.
[13] S. Yamanaka, M. Sarubo, K. Tadanobu, M. Hattori, Solid State Ionics 57 (1992) 271.
[14] R.E. Schaak, T.E. Mallouk, Chem. Mater. 14 (2002) 1455.
[15] M. Dion, M. Ganne, M. Tournoux, Mater. Res. Bull. 16 (1981) 1429.

[16] A.J. Jacobson, J.W. Johnson, J.T. Lewandowski, Inorg. Chem. 24 (1985) 3727.
[17] S.N. Ruddlesden, P. Popper, Acta Crystallogr. 10 (1957) 538.
[18] S.N. Ruddlesden, P. Popper, Acta Crystallogr. 11 (1958) 54.
[19] A.J. Jacobson, J.T. Lewandowski, J.W. Johnson, J. Less-Common Met. 116 (1986) 137.
[20] S. Takahashi, T. Nakato, S. Hayashi, Y. Sugahara, K. Kuroda, Inorg. Chem. 34 (1995) 5065.
[21] H. Suzuki, K. Notsu, Y. Takeda, W. Sugimoto, Y. Sugahara, Chem. Mater. 15 (2003) 636.
[22] J.L. Speier, Adv. Organometal. Chem. 17 (1979) 407.
[23] I. Ojima, in: S. Patai, Z. Rappoport (Eds.), The Chemistry of Organic Silicon Compounds (Chaper 25), Wiley, Chichester, 1989 (Chaper 25).
[24] T. Hiyama, T. Kusumoto, in: B.M. Trost, I. Fleming (Eds.), Comprehensive Organic Synthesis (Chapter 3.12), Pergamon Press, Oxford, 1991 (Chapter 3.12).
[25] B. Marciniec, J. Gulinski, W. Urbaniak, Z.W. Kornetka, in: B. Marciniec (Ed.), Comprehensive Handbook on Hydrosilylation, Pergamon Press, Oxford, 1992.
[26] J.M. Buriak, Chem. Commun. (1999) 1051.
[27] R. Boukherroub, S. Morin, F. Bensebaa, D.D.M. Wayner, Langmuir 15 (1999) 3831.
[28] J.M. Buriak, M.P. Stewart, T.W. Geders, M.J. Allen, H.C. Choi, J. Smith, D. Raftery, L.T. Canham, J. Am. Chem. Soc. 121 (1999) 11491.
[29] H.A. Ketelson, M.A. Brook, R.H. Pelton, Polym. Adv. Technol. 6 (1995) 335.
[30] C.A. Fyfe, J. Niu, Macromolecules 28 (1995) 3894.
[31] D.E. Katsoulis, T.C.-S. Chao, E.A. McQuiston, C. Chen, M.E. Kenney, Mater. Res. Soc. Symp. Proc. 519 (1998) 321.
[32] T.C. Chao, D.E. Katsoulis, M.E. Kenney, Chem. Mater. 13 (2001) 4269.
[33] D.F. Shriver, M.A. Drezdzon, The Manipulation of Air-Sensitive Compounds, second ed., Wiley-Interscience, New York, 1986.
[34] H.F. Shurvell, in: J.M. Chalmers, P.R. Griffiths (Eds.), Handbook of Vibrational Spectroscopy. Sample Characterization and Spectral Data Processing, vol. 3, Wiley, Chichester, 2002, p. 1783.
[35] C. Eaborn, B.W. Bott, in: A.G. MacDiarmid (Ed.), Organometallic Compounds of the Group IV Elements Part 2, vol. 1, Marcel Dekker, New York, 1986, p. 1968.
[36] Chapter 4 in Ref. [25].
[37] Chapter 3 in Ref. [25].
[38] If an α-addition occurs to form a $[CH_3(Cl)_2Si(CH_3)CH(CH_2)_3O]NbO_5$ site, signals with similar chemical shifts are expected. The presence of unidentified weak signals at 0, 12 and 62 ppm indicates the presence of an unidentified side reaction (or unidentified side reactions).
[39] The occurrence of an α-addition is not suggested by the ^{13}C-CP/MAS-NMR spectrum. The presence of an unidentified weak signal at 3 ppm indicates the presence of an unidentified side reaction.
[40] H. Marsmann, in: P. Diehl, E. Fluck, R. Kosfeld (Eds.), NMR Basic Principles and Progress 17 Oxygen-17 and Silicon-29, Springer-Verlag, Berlin, 1981, p. 65.

Transworld Research Network
37/661 (2), Fort P.O., Trivandrum-695 023, Kerala, India

Recent Res. Devel. Inorganic Chem., 4(2004): ISBN: 81-7895-122-3

Novel materials derived from layered perovskites using a *Chimie Douce* approach

Seiichi Tahara and Yoshiyuki Sugahara
Department of Applied Chemistry, School of Science and Engineering, Waseda University, Shinjuku-ku, Tokyo 169-8555, Japan

Abstract

This review describes the application of a Chimie Douce approach to layered perovskites to achieve a preparation of protonated forms with novel compositions and inorganic-organic hybrids. The Aurivillius phases can be converted into the protonated forms of layered perovskites and layered tungstic acid by acid treatment at room temperature. The structures, photocatalytic activities and intercalation behavior of these compounds are discussed here. We also describe inorganic-organic hybrids derived from protonated forms of Dion-Jacobson-type layered perovskites. The reactions of the protonated forms of ion-exchangeable layered perovskites, $HLaNb_2O_7 \cdot xH_2O$ and $HCa_2Nb_3O_{10} \cdot xH_2O$,

Correspondence/Reprint request: Dr. Yoshiyuki Sugahara, Department of Applied Chemistry, Waseda University, Ohkubo 3-4-1, Shinjuku-ku, Tokyo 169-8555, Japan. E-mail: ys6546@waseda.jp

with n-alcohols lead to the formation of n-alkoxy derivatives possessing Nb-O-C covalent bonds. Various organic derivatives of ion-exchangeable layered perovskites can be prepared from n-alkoxy derivatives and organic compounds via an alcohol-exchange-type reaction or hydrosilylation.

Introduction

The *Chimie Douce* (soft chemistry) approach has been attracting increasing interest for the design of materials possessing novel compositions and nano-scaled structures.[1-5] The *Chimie Douce* approach enables us to prepare the materials at temperatures that are much lower than those employed by traditional methods (solid-state reaction, *etc.*). The *Chimie Douce* approach may potentially lead, moreover, to successful preparation of novel materials that can not be prepared with traditional methods.[1-5] The *Chimie Douce* approach includes various processes, such as topotactic reactions and sol-gel processes, and various inorganic compounds and inorganic-organic hybrids have been prepared using the *Chimie Douce* approach.

Solid-state reactions have been employed extensively to synthesize complex oxides (ceramic method). Generally, starting powders possessing a stoichiometric composition (occasionally with an excess amount of a volatile element, such as lead, added or carbonates employed instead of oxides) are mixed and then calcined to form a single-phase target compound.[6] It is worth noting that metastable phases can not be prepared through solid-state reactions, since any metastable phase is expected to be converted into a thermodynamically-stable phase at high temperatures.[3] The *Chimie Douce* approach, on the contrary, could lead to the formation of these metastable phases. The *Chimie Douce* approach is also capable of use for the preparation of inorganic-organic hybrids, which exhibit not only the individual properties of organic or inorganic components but also tunable or improved properties through the combination of organic and inorganic components.[5,7-10] For the preparation of inorganic-organic hybrids, low temperatures are generally required to preserve the structures of the inorganic components and to avoid decomposition of the organic groups. To meet the aforementioned requirements, the *Chimie Douce* approach is an excellent selection as a preparation method for inorganic-organic hybrids. When an inorganic-organic hybrid is prepared by polymerization of organic functional groups bound on an inorganic oxo-cluster, for example, a low temperature is required to avoid both decomposition of the polymerizable organic groups and structural change of the inorganic oxo-clusters.[5,11,12]

Extensive research has been devoted to the application of the *Chimie Douce* approach to layered transition metal oxides, which contain two-dimensional inorganic nano-sheets.[1-4,13] Ion-exchange reactions and acid-base reactions have typically been employed in the *Chimie Douce* approach.

Layered titanate $K_2Ti_4O_9$ and layered titanoniobate $KTiNbO_5$ can be easily converted into their protonated forms, $H_2Ti_4O_9$[14] and $HTiNbO_5$,[15] by acid-treatment, for example. In addition, interlayer cations can also be exchanged with organic cations. A typical example is the ion-exchange reaction between the potassium ions of $K_4Nb_6O_{17}$ and *n*-alkylammonium ions to form intercalation compounds.[16] The intercalation of *n*-alkylamine into $HTiNbO_5$ is a well-known example of an acid-base reaction.[17,18] Thus, application of the *Chimie Douce* approach to the layered transition metal oxides leads to the formation of novel materials with no structural change in the inorganic nano-sheets.

Compounds with the perovskite structure or perovskite-related structures are interesting materials, since some of these compounds exhibit excellent electrical,[19,20] magnetic,[21] and/or optical properties.[22] Various perovskite and perovskite-related compounds with a wide range of compositions have therefore been prepared through solid-state reactions.[23] Among these, ion-exchangeable layered perovskites have been attracting increasing interest.[4] Ion-exchangeable layered perovskites consist of perovskite-like slabs and interlayer cations. Perovskite-like slabs are denoted by $[A_{m-1}B_mO_{3m+1}]$ and are considered to be nano-sheets, ABO_3 perovskite structures sliced along the (100) axis. The thickness of the perovskite-like slabs is expressed by *m*. Interlayer cations, expressed as M, are typically monovalent alkali metal ions. Ion-exchangeable layered perovskites can be classified into two kinds of phases based on the interlayer cation density per $[A_{m-1}B_mO_{3m+1}]$: Dion-Jacobson phases, $M[A_{m-1}B_mO_{3m+1}]$, and Ruddlesden-Popper phases, $M_2[A_{m-1}B_mO_{3m+1}]$.[4] Figure 1 shows typical structures of ion-exchangeable layered perovskites ($m = 3$). Protonated forms of ion-exchangeable layered perovskites can be obtained easily through acid treatment and are reported to exhibit photocatalytic activities,[24,25] proton conductivities[26] and intercalation behavior.[4,27-35] As concerns intercalation behavior, various organic amines have been intercalated in the interlayer space *via* acid-base reactions.[4,27-35] It is also known that a protonated form of the Dion-Jacobson phase, $HLaNb_2O_7 \cdot xH_2O$, can react with *n*-alcohol to form *n*-alkoxy derivatives possessing Nb-O-C covalent bonds.[36]

Aurivillius phases have been attracting increasing attention as fatigue-free ferroelectric materials.[20,37-39] Aurivillius phases possess both perovskite-like slabs $[A_{m-1}B_mO_{3m+1}]$ and bismuth oxide sheets Bi_2O_2.[40-42] Their structures are shown in Figure 1 along with those of the Dion-Jacobson and Ruddlesden-Popper phases. Although bismuth oxide sheets are present between the perovskite-like slabs, it is worth noting that the structures of perovskite-like slabs in Aurivillius phases are closely similar to those of ion-exchangeable layered perovskites.

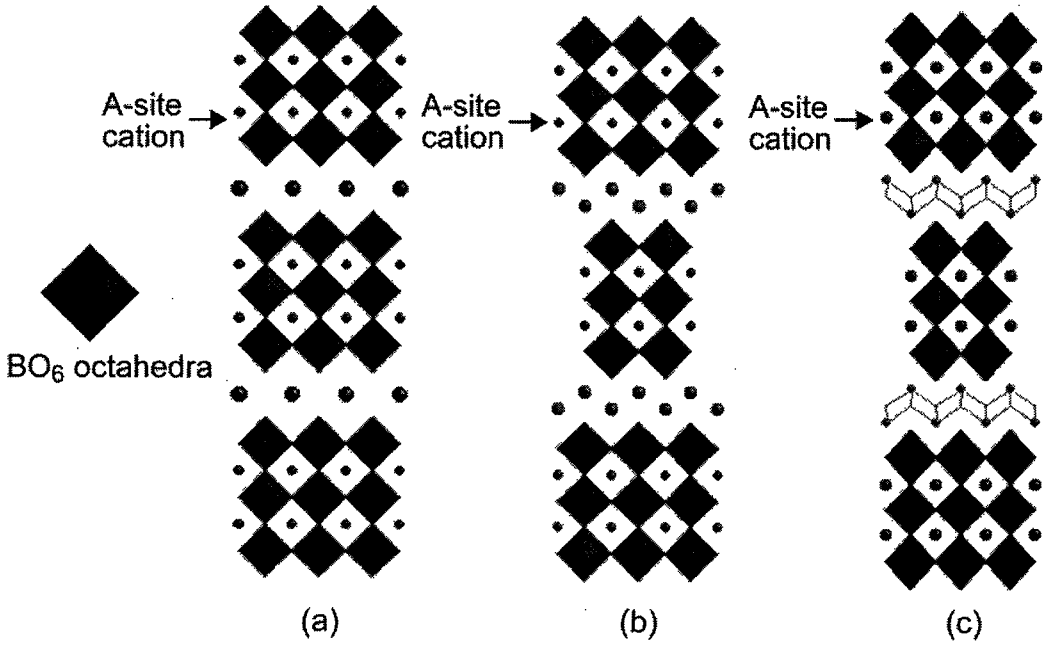

Figure 1. Structures of layered perovskites (m = 3); (a) Dion-Jacobson phase $M[A_{m-1}B_mO_{3m+1}]$, (b) Ruddlesden-Popper phase $M_2[A_{m-1}B_mO_{3m+1}]$, and (c) Aurivillius phase $Bi_2O_2[A_{m-1}B_mO_{3m+1}]$. The gray balls and lines in (c) represent the bismuth oxides sheets.

In this review, we describe the preparation of layered perovskites possessing novel interlayer environments employing the *Chimie Douce* approach. Protonated forms of layered perovskites[43-46] and layered tungstic acid[47] have been prepared by acid-treatment of the Aurivillius phases. We present here the structures, compositions[43,45-47] and properties[43,45-49] of novel protonated forms of layered perovskites and layered tungstic acid. In addition, we describe the preparation of inorganic-organic hybrids from protonated forms of the Dion-Jacobson phases through grafting reactions. [50-52]

Selective leaching of bismuth oxide sheets

Various protonated forms derived from the Dion-Jacobson and the Ruddlesden-Popper phases have been prepared by acid treatment of layered perovskites containing alkali metal ions.[4,26,27,29,53-58] One proton per $[A_{m-1}B_mO_{3m+1}]$ is present in protonated forms of the Dion-Jacobson phases and two protons per $[A_{m-1}B_mO_{3m+1}]$ are present in protonated forms of the Ruddlesden-Popper phases. Based on these reports, perovskite-like slabs are generally expected to be stable with respect to acid treatment. It is well known that bismuth oxide (Bi_2O_3), on the other hand, can be easily dissolved in acid.[59,60] If perovskite-like slabs and bismuth oxide sheets in the Aurivillius phase show different dissolution behavior in acids, protonated forms of layered

perovskites are expected to be prepared. We therefore investigated acid treatment of the Aurivillius phases, $Bi_2ANaB_3O_{12}$ (A = Sr or Ca, B = Nb; A = Ca, B = Ta) and $Bi_2SrTa_2O_9$. $Bi_2ANaB_3O_{12}$ (A = Sr or Ca, B = Nb; A = Ca, B = Ta) were treated with 6 M HCl to obtained protonated forms of layered perovskites by selective leaching of bismuth oxide sheets.[43-45] Acid treatment of $Bi_2SrTa_2O_9$ with 3 M HCl led to formation of a protonated form of a layered perovskite.[46]

The X-ray diffraction (XRD) patterns of $Bi_2SrTa_2O_9$ and its acid-treated product are shown in Figure 2. The shifts of (00*l*) reflections demonstrate the contraction along the *c* axis (stacking direction), and the presence of reflections at 32.6° (overlapped (020) and (200) reflections of $Bi_2SrTa_2O_9$ and a (110) reflection of acid-treated product, with the different indexing resulting from the change in space group) in the XRD pattern of acid-treated product provides evidence for the preservation of perovskite-like slabs. Protons are present in the interlayer space instead of the bismuth oxide sheets after acid treatment, as revealed by thermogravimetry (TG). Before our studies, Suzuki *et. al.* reported that the XRD pattern of the acid-treated single crystal of an Aurivillius phase, $Bi_2SrTa_2O_9$, showed the new reflections, whose appearance was ascribed to the decomposition of perovskite-like slabs.[61] The reported XRD pattern of the acid-treated product is closely similar to the XRD pattern in our study, indicating that the change in the XRD profile is also ascribable to the selective leaching of the bismuth oxide sheets.

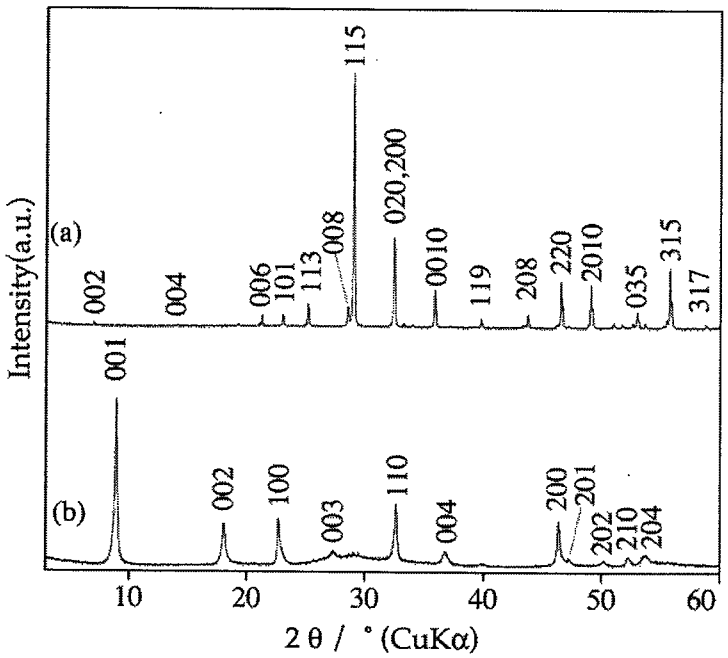

Figure 2. The XRD patterns of (a) $Bi_2SrTa_2O_9$ and (b) the acid-treated product of $Bi_2SrTa_2O_9$.

Based on the previous reports for an m = 2 member of the Aurivillius phases, $Bi_2AB_2O_9$ (A = Sr, Ca, Ba or Pb, and B = Nb or Ta), bismuth ions, which are originally believed to be present in the bismuth oxide sheets, and A-site cations, which are expected to be present in perovskite-like slabs, are actually partially disordered.[62-66] It is therefore reasonable to assume the presence of a similar disorder in an m = 3 member of the Aurivillius phases, $Bi_2ANaB_3O_{12}$ (A = Sr or Ca, B = Nb; A = Ca, B = Ta). The numbers of protons per $[A_{m-1}B_mO_{3m+1}]$ (1.8) are slightly lower than expected for ideal perovskite-like slabs (2.0), supporting the assumption of similar disordering between the bismuth ions and A-site cations. With the compositional analyses taken into account, the selective leaching of bismuth oxide sheets in $Bi_2ANaB_3O_{12}$ (A = Sr or Ca, B = Nb; A = Ca, B = Ta) and $Bi_2SrTa_2O_9$ is, therefore, expressed as follows;

$$(Bi_{1.8}A_{0.2}O_2)^{1.8+}[Bi_{0.2}A_{0.8}NaB_3O_{10}]^{1.8-} \rightarrow H_{1.8}Bi_{0.2}A_{0.8}NaB_3O_{10} \quad (1)$$
(A = Sr or Ca, B = Nb; A = Ca, B = Ta)

$$(Bi_{1.8}Sr_{0.2}O_2)^{1.8+}[Bi_{0.2}Sr_{0.8}Ta_2O_7]^{1.8-} \rightarrow H_{1.8}Bi_{0.2}Sr_{0.8}Ta_2O_7 \quad (2)$$

It is apparent from the previous reports that A-site cations affect the dielectric properties[67] and the disordering between A-site cations in the perovskite-like slabs and bismuth ions in the bismuth oxides sheets affects the *Curries* temperature T_c.[63] The structures of Aurivillius phases have, therefore, been investigated to predict dielectric properties by Rietveld refinement of XRD and Neutron diffraction patterns.[62-66] The compositions of the acid-treated products of these Aurivillius phases, $H_{1.8}Bi_{0.2}A_{0.8}NaB_3O_{10}$ (A = Sr or Ca, B = Nb; A = Ca, B = Ta) and $H_{1.8}Bi_{0.2}Sr_{0.8}Ta_2O_7$, provide the first direct evidence for the presence of disordering between A-site cations and bismuth ions in the Aurivillius phases.

High-resolution electron microscopic (HREM) observation provides the information for structure of $H_{1.8}Bi_{0.2}Sr_{0.8}Ta_2O_7$[46]. The HREM images show the presence of two types of stacking sequences, a *P*-type stacking sequence and an *I*-type stacking sequence with relative displacement $(a + b)/2$, as shown in Figure 3. Reported protonated forms of the ion-exchangeable layered perovskites, on the contrary, possess either the *P*-type stacking sequence or the *I*-type stacking sequence: protonated forms of the Dion-Jacobson phases possess the *P*-type stacking sequence[26-28,58,68] and those of the Ruddlesden-Popper phases, such as $H_2La_2Ti_3O_{10}$, $H_2SrNb_2O_7$ and $H_2SrTa_2O_7$, exhibit the *I*-type stacking sequence.[29,53,54,56,69] The presence of this type of stacking disorder is also demonstrated by the streaking of electron diffraction (ED) pattern along the c^* axis. The presence of a broad reflection in an XRD pattern of $H_{1.8}Bi_{0.2}Sr_{0.8}Ta_2O_7$ at the 2θ range of 20 – 40° (Figure 2) also appears to be attributed to the stacking disorder.

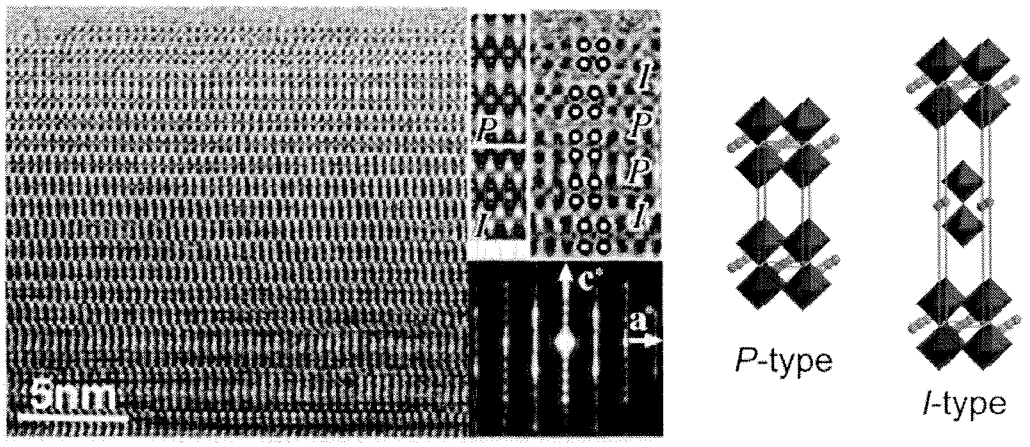

Figure 3. The HREM images of $H_{1.8}Bi_{0.2}Sr_{0.8}Ta_2O_7$, and the structural models of *P*-type and *I*-type stacking sequences. In the HREM images, two simulated images for *P*-type and *I*-type stacking sequences (middle), enlarged images (right), and the ED pattern along *c** axis (bottom) are shown.

We have reported the effect of mineral acid types on the conversion of $Bi_2SrNaNb_3O_{12}$ into the corresponding protonated form.[44] For acid treatment with HX (X = Cl, Br or I), conversion into the protonated form proceeded, while acid treatment with HNO_3 or H_2SO_4 led to no conversion. These results suggest that anions significantly influence the selective leaching of bismuth oxide sheets.

There is another series of the Aurivillius phases possessing ReO_3-like tungstate slabs.[70] The structures of the ReO_3-like slabs are considered to be sliced A-site-deficient perovskites. These compounds, which can be expressed as $Bi_2W_mO_{3m+3}$ in a general formula, consist of bismuth oxide sheets and ReO_3-like slabs.[71] We have reported the conversion of an m = 2 member of this type of the Aurivillius phase, $Bi_2W_2O_9$, into $H_2W_2O_7{\cdot}xH_2O$ through treatment with 6M HCl.[47] Schaak *et. al.* also briefly reported the selective leaching of bismuth oxide sheets in $Bi_2W_2O_9$.[72]

The lattice parameters of the Aurivillius phase and its protonated phases calculated by XRD patterns are listed in Table 1. The decrease from the *c* parameter of $Bi_2W_2O_9$ to the *c* parameter of acid-treated product, combined with the TG and ICP results, indicates that the novel layered tungstic acid, $H_2W_2O_7{\cdot}xH_2O$, is prepared by selective leaching of bismuth oxide sheets. Interestingly, the *a* and *b* parameters changed after acid treatment of $Bi_2W_2O_9$. The HREM images showed that the changes in the *a* and *b* parameters can be attributed to change in the distortion of the WO_6 octahedra arrangement. In the structure of $Bi_2W_2O_9$, Bi atoms in bismuth oxide sheets are weakly bound to the apical oxygen atoms of WO_6 octahedra. [71] Selective leaching of

Table 1. The lattice parameters of Aurivillius phases and converted protonated forms and tungstic acid.

Compound	Cell	*a* / nm	*b* / nm	*c* / nm
$Bi_2SrNaNb_3O_{12}$	tetragonal	0.39007(1)	-	1.6463(1)
$H_{1.8}Bi_{0.2}Sr_{0.8}NaNb_3O_{10}$ [1]	tetragonal	0.391(2)	-	1.39(2)
$Bi_2CaNaNb_3O_{12}$	tetragonal	0.38686(3)	-	1.6365(1)
$H_{1.8}Bi_{0.2}Ca_{0.8}NaNb_3O_{10}$ [1]	tetragonal	0.390(3)	-	1.41(1)
$Bi_2SrTa_2O_9$ [2]	orthorhombic	0.55520(4)	0.55521(2)	2.505(2)
$H_{1.8}Bi_{0.2}Sr_{0.8}Ta_2O_7$ [1]	tetragonal	0.391(4)	-	0.98(1)
$Bi_2W_2O_9$	orthorhombic	0.54377(1)	0.54166(1)	2.37063(5)
$H_2W_2O_7 \cdot xH_2O$ [3]	orthorhombic	0.524(1)	0.513(1)	2.21(1)
$H_2W_2O_7$ [1]	orthorhombic	0.5249(2)	0.513(2)	1.86(1)

[1] The anhydrous phases were obtained by drying at 120 °C.
[2] The lattice parameter of cubic perovskite oxides is 0.39 nm (= $a/\sqrt{2}$) and the interlayer distance is 1.25 nm ($c/2$).
[3] The hydrated phases were obtained by drying at ambient temperature.

bismuth oxide sheets appears, therefore, to lead to relaxation of the WO_6 octahedra arrangement.

The successful conversions conducted while preserving the BO_6 octahedra arrangement at ambient temperature clearly show that conversions involving selective leaching of bismuth oxide sheets can be classified as a *Chimie Douce* approach. The B-site cations in the reported ion-exchangeable layered

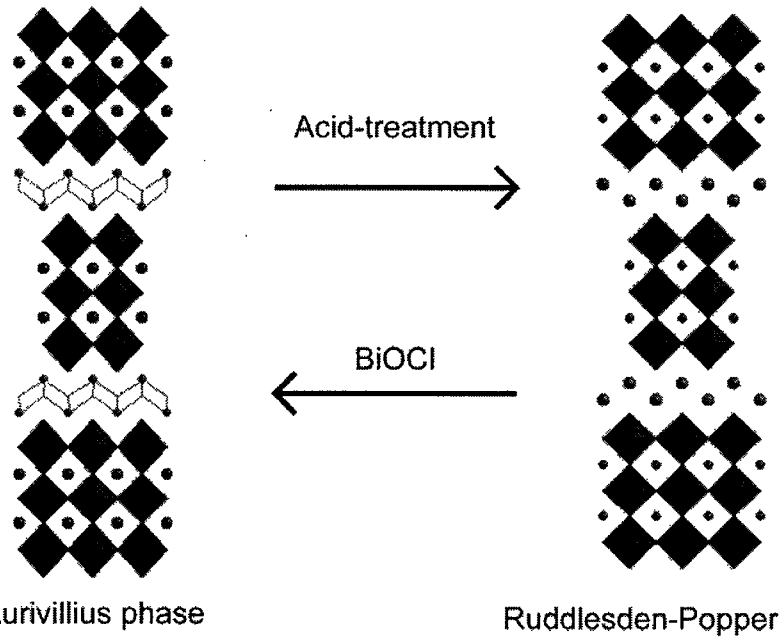

Figure 4. Reversible conversion reactions between the Ruddlesden-Popper phases and the Aurivillius phases.

perovskites are limited to only Ti, Nb and Ta.[73,74] The B-site cations of the Aurivillius phases, to the contrary, can be any of various metals, including Ti, Mn, Fe, Nb, Ta, W and Mo. The acid-treated products are, therefore, the novel protonated forms of layered perovskites or novel layered tungstic acid in terms of composition. Recently, Gopalakrishnan *et. al.* prepared the Aurivillius phases through a reaction between the Ruddlesden-Popper phases and BiOCl.[75] These conversions can be considered to be the reverse of our conversion reactions. The new convertible relationship between the Ruddlesden-Popper phases and the Aurivillius phases is, therefore, likely to be established, as shown in Figure 4.

Properties of protonated layered perovskites

Photocatalytic activities

Photocatalysts have been attracting considerable attention as solar energy conversion materials.[76-78] For photocatalytic semiconductors, H_2 evolution is caused by holes at the valence bands, and electrons at the conduction bands generate O_2 from water. If a sacrificial regent is employed, either hydrogen or oxygen is generated. Photocatalytic activity is, therefore, partially dependent on the band gap energy and positions of conduction and/or valence bands, indicating that the compositions of photocatalysts influence the photocatalytic activities. Some ion-exchangeable layered perovskites, both the Dion-Jacobson phases and the Ruddlesden-Popper phases, have been reported to exhibit photocatalytic reactions using sacrificial reagents.[25,78-82] Protonation,[24,25] loading of Ni or Pt,[79,83] and increasing the surface area by pillaring[84] or exfoliation[85] are known to enhance the photocatalytic activities of ion-exchangeable layered perovskites. As concerns the protonated forms of the Dion-Jacobson-type niobates and tantalates, $HPbNb_2O_7$ was reported to exhibit photocatalytic activity under visible light irradiation,[24] and double-layered tantalates are also known to exhibit photocatalytic activities with no sacrificial reagents.[80-82] We therefore investigated the photocatalytic activities of the m = 3 members of the Aurivillius phases, $Bi_2ANaNb_3O_{12}$ (A = Ca or Sr) and $Bi_2CaNaTa_3O_{12}$, and those of the protonated forms of layered perovskites, $H_{1.7}Bi_{0.3}Sr_{0.7}NaNb_3O_{10}$, $H_{1.8}Bi_{0.2}Ca_{0.8}NaNb_3O_{10}$ and $H_{1.8}Bi_{0.2}Ca_{0.8}NaTa_3O_{10}$.[48] Photocatalytic activity was estimated based on H_2 evolution from water containing ethanol as a sacrificial reagent.

Figure 5 shows the photocatalytic H_2 evolution behavior of the Aurivillius phases and their acid-treated products. Although photocatalytic activities of the Aurivillius phases, Bi_2WO_6, $Bi_2W_2O_9$ and Bi_3TiNbO_9, were reported,[86] the Aurivillius phases explored in this study show no activities for photocatalytic H_2 evolution. The acid-treated products, on the contrary, exhibit the

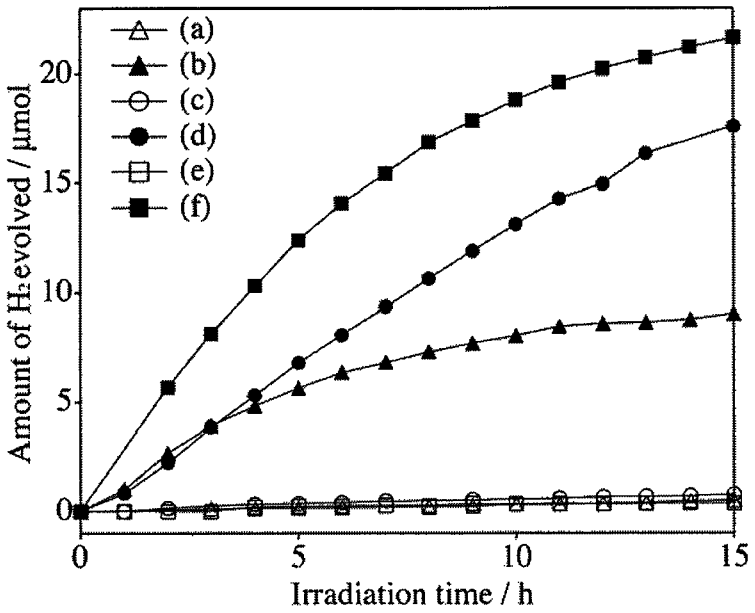

Figure 5. The photocatalytic H_2 evolution behavior from aqueous ethanol solutions on: (a) $Bi_2SrNaNb_3O_{12}$, (b) $H_{1.7}Bi_{0.3}Sr_{0.7}NaNb_3O_{10}$, (c) $Bi_2CaNaNb_3O_{12}$, (d) $H_{1.8}Bi_{0.2}Sr_{0.8}NaNb_3O_{10}$, (e) $Bi_2CaNaTa_3O_{12}$, (f) $H_{1.8}Bi_{0.2}Sr_{0.8}NaTa_3O_{10}$.

photocatalytic activity. The appearance of photocatalytic activities of the protonated forms is attributable to two factors. The first of these is the change in the positions of the bottom of conduction bands. The conduction bands and valence bands of some Aurivillius phases were reported to involve orbitals of bismuth in the bismuth oxide sheets,[87-90] indicating that selective leaching of the bismuth oxide sheets is likely to lead to changes in the electric structures. Selective leaching of bismuth oxide sheets leads to the formation of new conduction bands that are more negative than redox potential H^+/H_2, generating H_2. The second factor is the increase in the surface areas after selective leaching of bismuth oxide sheets. The XRD patterns of all the protonated forms after H_2 evolution showed the presence of hydrated phases, indicating effective use of the interlayer space during the photocatalytic H_2 evolution. These results suggest that selective leaching of bismuth oxide sheets in the Aurivillius phase is a promising method for preparation of new photocatalysts.

Intercalation behavior of protonated layered perovskites with organic bases

It is well known that some layered compounds can incorporate organic ions and molecules in the interlayer space to obtain intercalation compounds where inorganic nano-sheets and organic ions/molecules are stacked

alternatively.[91-93] The reaction mechanisms can be ion-exchange, acid-base or redox reactions. In recent decades, protonated forms of the Dion-Jacobson phases were reported to accommodate various organic molecules such as *n*-alkylamine,[27,30] diamine,[94] pyridine[27] and aniline.[95] Intercalation reaction of the Ruddlesden-Popper phases generally did not occur, however, which was once attributed to the fact that the Ruddlesden-Popper phases possess the *I*-type stacking sequence, $(a + b)/2$.[33] Only Schaak *et. al.* reported intercalation of an organic compound into a Ruddlesden-Popper phase: *n*-decylamine was intercalated into $H_2CaNaTa_3O_{10}$.[96]

We have reported that *n*-alkylamines could be intercalated in the protonated forms of layered perovskites and layered tungstic acid derived from Aurivillius phases by acid treatment.[43,45,47] The amounts of *n*-alkylamine in the intercalation compounds of the protonated forms of layered perovskites were about 1.0 per $[A_{m-1}B_mO_{3m+1}]$, indicating that approximately half of the interlayer protons ($1.8H^+$ per $[A_{m-1}B_mO_{3m+1}]$) were reacted with *n*-alkylamine.[49]

These observations can be reasonably explained based on interlayer surface geometry. A cross-section area of *n*-alkylamine is 0.186 nm^2 (diameter: 0.486 nm). The distance (center to center) between the nearest cavities was 0.39 nm (equal to the *a* parameter) and the distance between the second-nearest cavities was 0.55 nm ($= \sqrt{2}a$).[97] When one *n*-alkylamine molecule occupies a cavity, another *n*-alkylamine molecule cannot occupy the nearest cavities. The *n*-alkylamine molecules occupy the second nearest cavities, therefore, yielding an interlayer surface on which every other cavity is occupied by the *n*-alkylamine molecule. Since the number of protons (1.8) corresponds to ~90% of the number of cavities, about 1.0 of interlayer protons per $[Bi_{0.2}Sr_{0.8}Ta_2O_7]$ can be reacted with *n*-alkyamine. Figure 6 shows the proposed structure of these intercalation compounds based on limitation of the amount of *n*-alkylamine in the interlayer space.

We have succeeded in the intercalation of *n*-alkylamine in $H_{1.8}Bi_{0.2}Sr_{0.8}Ta_2O_7$ and $H_{1.8}Bi_{0.2}Sr_{0.8}NaNb_3O_{10}$, whose proton contents per $[A_{m-1}B_mO_{3m+1}]$ are close to those in the Ruddlesden-Popper phases. Although the Ruddlesden-Popper phases have been believed to exhibit no intercalation capability due to their *I*-type stacking sequence,[33] the single-phase products of *n*-alkylamine-intercalation compounds of $H_{1.8}[A_{m-1}B_mO_{3m+1}]$ can be obtained. Since the protonated forms of layered perovskites, $H_{1.8}Bi_{0.2}Sr_{0.8}Ta_2O_7$, possess two types of stacking sequences (as discussed in the previous section), these results indicate that *n*-alkylamine can be intercalated into both *P*-type and *I*-type interlayer environments in $H_{1.8}Bi_{0.2}Sr_{0.8}Ta_2O_7$. The discrepancy with the previous observation of a Ruddlesden-Popper phase, $H_2La_2Ti_3O_{10}$, can be ascribed to differences in the B-site cations: tantalates and niobates exhibit stronger acidity than titanates

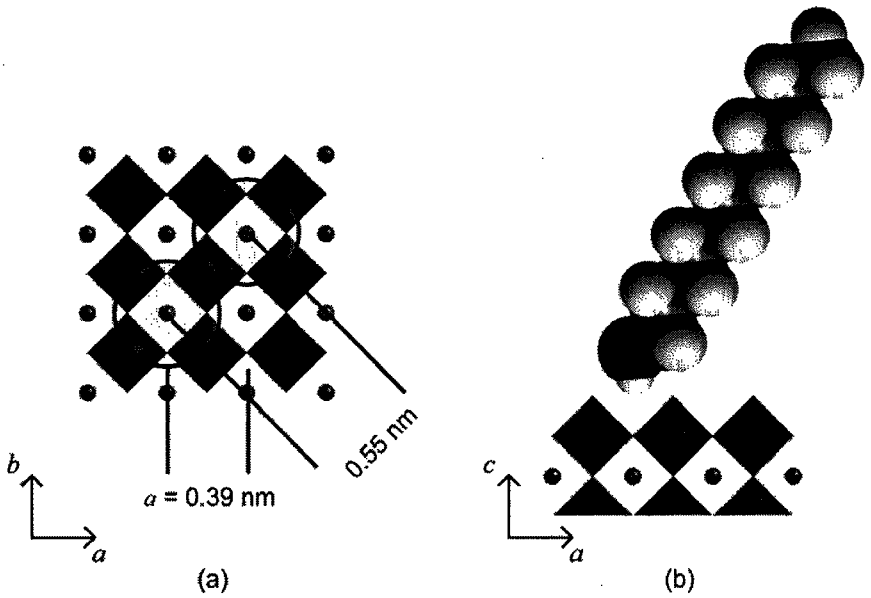

Figure 6. The proposed structure of an intercalation compound of $H_{1.8}Bi_{0.2}Sr_{0.8}Ta_2O_7$ with *n*-alkylamine: along (a) [001] and (b) [010]. The area of gray circle in (a) shows the cross-section area of *n*-alkylamine.

[17,27,30,32,98,99]. Thus, although Ruddlesden-Popper-type $H_2La_2Ti_3O_{10}$ did not accommodate *n*-alkylamine, *n*-alkylamine can be intercalated in the interlayer space of $H_{1.8}Bi_{0.2}Sr_{0.8}Ta_2O_7$ and $H_{1.8}Bi_{0.2}Sr_{0.8}NaNb_3O_{10}$ despite the similarity of their compositions to those of the Ruddlesden-Popper phases. This interpretation is consistent with the fact that Schaak *et. al.* reported the intercalation capability of the Ruddlesden-Popper-type tantalate, $H_2CaNaTa_3O_{10}$.[96]

Surface modification of Dion-Jacobson-type layered perovskites

Some layered materials have been reported to form not only intercalation compounds but also organic derivatives, which possess covalent bonds between the organic moiety and the interlayer surface of inorganic nano-sheets through grafting reaction. For example, layered polysilicates can react with chlorosilane or alkoxysilane[100,101] and kaolinite can reacted with alcohols.[102] In addition, FeOCl[103] and $Zr(HPO_4)_22H_2O$[104] have also been reported to form various organic derivatives. As concerns ion-exchangeable layered perovskites, Takahashi *et. al.* first reported reactions between a Dion-Jacobson phase, $HLaNb_2O_7{\cdot}xH_2O$, and *n*-alcohols and proved the formation of *n*-alkoxy derivatives possessing Nb-O-C covalent bonds, which bound alkoxy groups on the surface of perovskite-like slabs [$LaNbO_7$].[36]

It is well known in sol-gel chemistry that metal alkoxides can react with alcohol (so-called alcohol-exchange or alcoholysis reactions).[105] This type of reaction can be generally expressed as follows:

$$M(OR)_y + zR'OH \rightarrow M(OR')_z(OR)_{y-z} + zROH$$

These reactions have also been known to occur with Nb alkoxides.[106-109] If these reactions proceed on the interlayer surface, reactions with various alcohols, which are unable to react with the interlayer surface of the ion-exchangeable layered perovskites, are expected to lead to the preparation of various alkoxy derivatives.

We therefore investigated the alcohol-exchange-type reactions on the interlayer surface of *n*-alkoxy derivatives of a Dion-Jacobson phase, $HLaNb_2O_7 \cdot xH_2O$.[50] We investigated a reaction between the *n*-alkoxy derivative of $HLaNb_2O_7 \cdot xH_2O$ and *n*-decanol, 2-propanol, *tert*-butanol or ethylene glycol in a sealed ampoule at 80°C. The reaction of the *n*-propoxy derivative with *n*-decanol led to the formation of an *n*-decoxy derivative possessing Nb-O-C covalent bonds. The reaction of the *n*-decoxy derivative with 2-propanol also led to the formation of a 2-propoxy derivative. When the *n*-decoxy derivative was reacted with bulky *tert*-butanol, the XRD pattern of the resultant product showed only one type of interlayer distance. Solid-state ^{13}C CP/MAS NMR, however, showed that both *n*-decoxy groups and *tert*-butoxy groups were present in the interlayer space, indicating that the alcohol-exchange-type reaction had proceeded only partially. These results suggest that the bulkiness of reactant molecules influences alcohol-exchange-type reactions. The reaction with ethylene glycol also led to the occurrence of an alcohol-exchange-type reaction. Only one of the two hydroxy groups of ethylene glycol was reacted, as shown by solid-state ^{13}C CP/MAS NMR. Thus, the reactions between alkoxy derivatives and various organic molecules possessing OH groups led to the formation of various organic derivatives of $HLaNb_2O_7 \cdot xH_2O$, which could not be prepared by direct reaction.[50,110] An overview of these alcohol-exchange-type reactions for organic derivatization is shown in Figure 7.

These *n*-alkoxy derivatives had been known only for $HLaNb_2O_7 \cdot xH_2O$. We recently reported the formation of *n*-alkoxy derivatives of another Dion-Jacobson phase, $HCa_2Nb_3O_{10} \cdot xH_2O$.[51] The direct reactions of $HCa_2Nb_3O_{10} \cdot xH_2O$ with methanol at 100°C and with ethanol at 150°C in an autoclave led to the formation of single-phase methoxy and ethoxy derivatives, respectively. A single-phase *n*-propoxy derivative was obtained through the reaction of an intermediate methoxy derivative with *n*-propanol in an autoclave at 150°C. Use of the *n*-propoxy derivative as an intermediate made it possible to obtain single-phase products of various *n*-alkoxy derivatives through

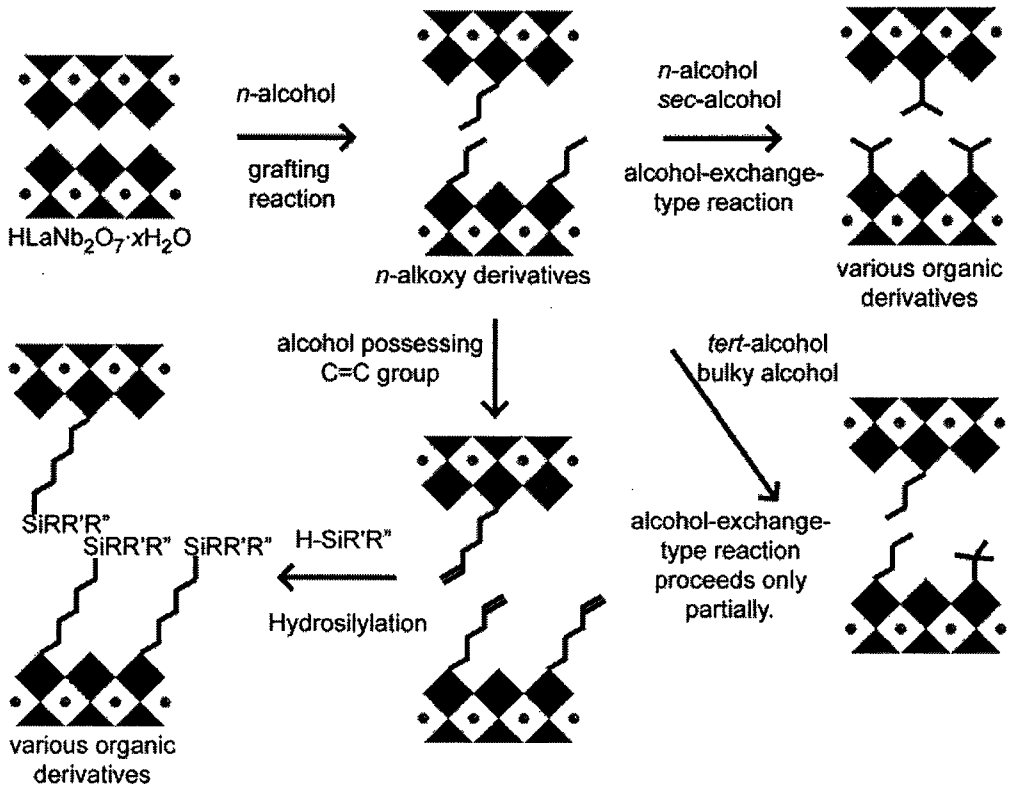

Figure 7. Preparation of various organic derivatives of layered perovskites using alcohol-exchange-type reactions or hydrosilylation reactions on the interlayer surface.

reactions with various *n*-alcohols ($C_nH_{2n+1}OH$; n = 4, 6, 8, 10, 12, 14, 16, 18) in the autoclave at 150°C. Solid-state ^{13}C CP/MAS NMR spectra showed downfield shifts of α-carbon signals, clear evidence for the formation of *n*-alkoxy groups.[36] As concerns the state of the alkyl chains, the IR spectra[111] and solid-state ^{13}C CP/MAS NMR spectra[112] suggested that the *n*-alkyl chains of *n*-alkoxy groups ($n \geq 10$) in the interlayer space were *all-trans* conformation. The interlayer distances of the *n*-alkoxy derivatives increased linearly with the increase in the number of carbon atoms, and the slope of this linear relationship indicated that the *n*-alkyl chains in the interlayer space formed bilayer arrangements with a tilt angle of 41°.

We investigated the reaction process between the *n*-alkoxy derivatives of ion-exchangeable layered perovskites and alcohols on the interlayer surface. Two reaction mechanisms are possible for reactions on the interlayer surface. In one possible mechanism,[105] an alcohol (R'OH) molecule attacks the $(RO)NbO_5$ site as a nucleophilic reaction, and ROH is subsequently released to form the $(R'O)NbO_5$ site. The other mechanism proceeds in two steps, hydrolysis and esterification; the $(HO)NbO_5$ site forms *via* hydrolysis of the

$(RO)NbO_5$ site by water, which is present as an impurity, and a subsequent reaction of the $(HO)NbO_5$ site with an alcohol (R'OH) molecule leads to the formation of the $(R'O)NbO_5$ site. To investigate this mechanism, we studied a reaction of the *n*-propoxy derivative of $HLaNb_2O_7 \cdot xH_2O$ with distilled *n*-decanol or an *n*-decanol-water mixture (containing 3 mass% of water). While the reaction with distilled *n*-decanol did not proceed, the reaction with the *n*-decanol-water mixture led to the formation of an *n*-decoxy derivative through reaction at 80°C. In a similar manner, we examined a reaction between the *n*-propoxy derivative of an m = 3 member of the Dion-Jacobson phase, $HCa_2Nb_3O_{10} \cdot xH_2O$, and *n*-decanol at 80°C. The *n*-propoxy derivative of $HCa_2Nb_3O_{10} \cdot xH_2O$ and distilled *n*-decanol did not react, while the reaction of the *n*-propoxy derivative of $HCa_2Nb_3O_{10} \cdot xH_2O$ with the *n*-decanol-water mixture (containing 1 mass% of water) led to the formation of a single-phase *n*-decoxy derivative of $HCa_2Nb_3O_{10} \cdot xH_2O$. These results clearly indicate that the reactions of *n*-alkoxy derivatives with other alcohols on the interlayer surface require water in the system. Thus, it is highly likely that these reactions proceed through a hydrolysis-esterification mechanism, as shown in Figure 8.

Interestingly, although an *n*-propoxy derivative of $HLaNb_2O_7 \cdot xH_2O$ and *n*-decanol were capable of a reaction at 80°C, the reaction of *n*-propoxy derivatives of $HCa_2Nb_3O_{10} \cdot xH_2O$ with *n*-decanol requires a reaction temperature of 150°C. To investigate the difference between these two ion-exchangeable layered perovskites, we studied the hydrolysis behavior of *n*-propoxy derivatives of $HLaNb_2O_7 \cdot xH_2O$ and $HCa_2Nb_3O_{10} \cdot xH_2O$ with a 2-pentanone-water mixture (containing 3 mass% of water). For the hydrolysis of the *n*-propoxy derivative of $HCa_2Nb_3O_{10} \cdot xH_2O$, the product hydrolyzed at 80°C contained the hydrated phase, $HCa_2Nb_3O_{10} \cdot xH_2O$ (which possesses water molecules in the interlayer space), and the product hydrolyzed at 150°C contained the anhydrous phase, $HCa_2Nb_3O_{10}$ (with no water molecules present in the interlayer space). Hydrolysis of the *n*-propoxy derivative of $HLaNb_2O_7 \cdot xH_2O$ at 80°C, on the contrary, led to the formation of the anhydrous phase, $HLaNb_2O_7$. These results indicate that the hydration behavior

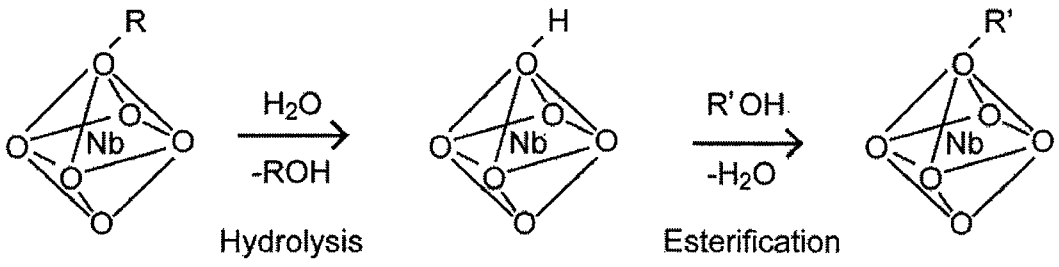

Figure 8. The proposed reaction process of the alcohol-exchange-type reaction.

depended on both the reaction temperature and the protonated forms. Such differences in hydrolysis behavior can, therefore, provide a reasonable explanation for differences in reaction temperatures. For the reaction of the *n*-propoxy derivative of $HCa_2Nb_3O_{10}\cdot xH_2O$ with *n*-decanol at 150°C or the reaction of the *n*-propoxy derivative of $HLaNb_2O_7\cdot xH_2O$ with *n*-decanol at 80°C, the presence of a sufficient amount of water in the system without incorporation in the interlayer space of the protonated form is considered necessary. For the reaction of an *n*-propoxy derivative of $HCa_2Nb_3O_{10}\cdot xH_2O$ with *n*-decanol at 80°C, on the contrary, hydrolysis of $(RO)NbO_5$ with a small amount of water produces the $(HO)NbO_5$ site, and water molecules are assumed to be readily incorporated into the interlayer space to form the hydrated phase, $HCa_2Nb_3O_{10}\cdot xH_2O$. It is likely that the incorporation of water significantly reduces the amount of free water available to suppress the reaction between the $(RO)NbO_5$ site and water. As a consequence, the hydrolysis-esterification does not proceed at 80°C. This explanation is well consistent with the aforementioned proceeding the alcohol-exchange-type reaction of $HCa_2Nb_3O_{10}\cdot xH_2O$ at 80°C in the presence of water. The reaction processes occurring between the *n*-propoxy derivatives of $HCa_2Nb_3O_{10}\cdot xH_2O$ and *n*-decanol at 80°C and 150°C are summarized in Figure 9.

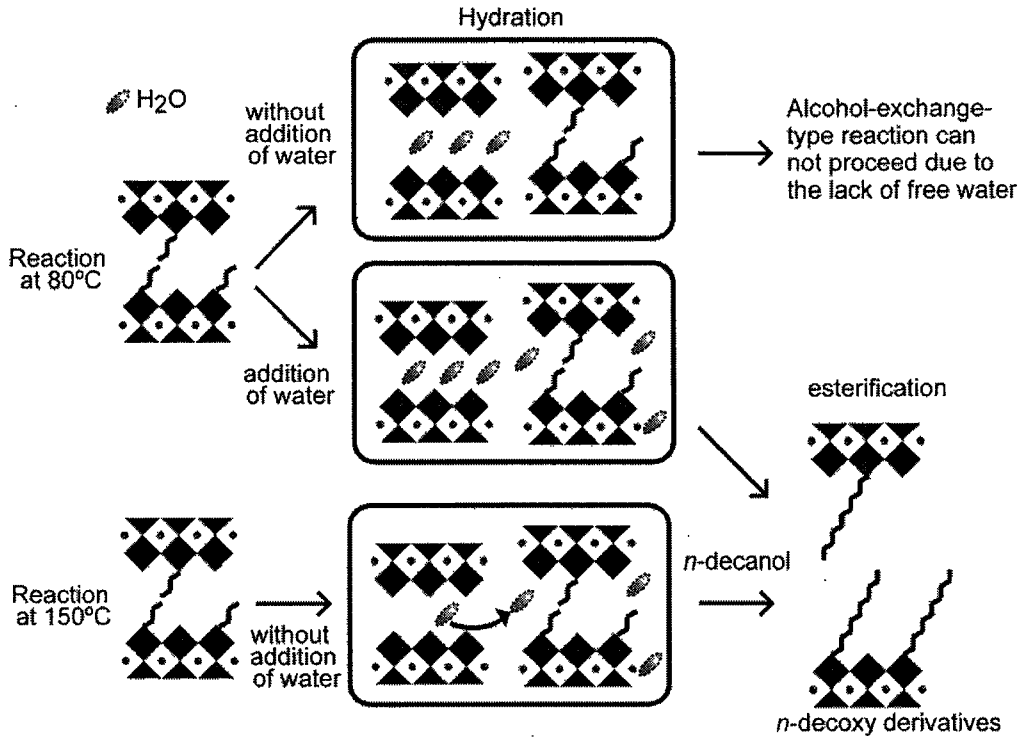

Figure 9. Reaction between the *n*-propoxy derivative of $HCa_2Nb_3O_{10}\cdot xH_2O$ and *n*-decanol at 80°C or 150°C.

Although the hydrolysis-esterification reactions led to the formation of various organic derivatives of ion-exchangeable layered perovskites, bulky alcohols such as *tert*-butanol were only partially grafted on the interlayer surface. The preparation of various organic derivatives of ion-exchangeable layered perovskites consequently requires a versatile alternative method. We therefore propose the use of hydrosilylation reactions for the preparation of organic derivatives of ion-exchangeable layered perovskites. Hydrosilylation reactions are ideal for the organic derivatization occurring in the interlayer space, since addition reactions such as hydrosilylation do not form by-products.[113] We reported that an alcohol molecule with C=C groups can be dissociatively bound to the interlayer surface of $HLaNb_2O_7 \cdot xH_2O$ and that a subsequent hydrosilylation reaction between the C=C groups and SiH groups of chlolosilane can proceed, as shown in Figure 7.[52]

The reaction of the *n*-propoxy derivative of $HLaNb_2O_7 \cdot xH_2O$ with 4-penten-1-ol [CH_2=$CH(CH_2)_3OH$] led to the formation of a CH_2=$CH(CH_2)_3O$-derivative. For the hydrosilylation reaction, the CH_2=$CH(CH_2)_3O$-derivative and $Cl_x(H)SiMe_{3-x}$ (x = 1–3) were reacted using a Pt-catalyst, $H_2PtCl_6 \cdot 6H_2O$. The reaction with x = 1 silane, $Cl(H)SiMe_2$, scarcely proceeded. The reactions with x = 2 silane, $Cl_2(H)SiMe$, and x = 3 silane, $HSiCl_3$, on the contrary, led to successful hydrosilylation reactions. Conversion of a part of the Si-Cl groups into Si-(O-) groups by hydrolysis with impurity water also proceeded during the hydrosilylation reactions and/or washing, since Si-Cl groups are known to be easily hydrolyzed. It is worth noting that the structures of the perovskite-like slabs did not change during the hydrosilylation reactions. These results suggest that the hydrosilylation reactions could be employed for the preparation of various organic derivatives of ion-exchangeable layered perovskites.

Conclusions

In this review, we demonstrated that the *Chimie Douce* approach is widely applicable to layered perovskites. Selective leaching of bismuth oxide sheets of the Aurivillius phases by acid treatment led to the formation of protonated forms of ion-exchangeable layered perovskites and layered tungstic acid possessing novel compositions. These protonated forms exhibited intercalation behavior and photocatalytic activities. To date, although Aurivillius phases possessing a variety of compositions have been prepared, the conversion of the Aurivillius phases into protonated forms has been achieved only for those with B-site cations of Nb^{5+}, Ta^{5+}, W^{6+} and Mn^{4+}.[4,43-47] Conversion of Aurivillius phases with various cations at the A-site and B-site potentially provides a variety of novel compounds, therefore, which could exhibit improved properties. These conversions also appear to be important for ferroelectric

materials, since selective leaching provided direct evidence of disordering between A-site cations in perovskite-like slabs and bismuth ions in bismuth oxide sheets.

We also demonstrated the preparation of organic derivatives of Dion-Jacobson-type niobates. Various organic derivatives of Dion-Jacobson phases were prepared by the reaction of *n*-alkoxy derivatives with organic molecules possessing OH groups through the hydrolysis-esterification mechanism, and hydrosilylation in the interlayer space led to the formation of organic derivatives. This strategy, the combination of an alcohol-exchange-type reaction and hydrosilylation reaction, is expected to enable us to prepare numerous organic derivatives, which could generate various properties originating in organic molecules.

Acknowledgement

This work was supported in part by a Grant-in-Aid for Scientific Research (No. 14350462) from the Ministry of Education, Science, Sports, and Culture, Japan, and by 21COE "Practical Nano-Chemistry" from MEXT, Japan. The authors express their gratitude to Prof. Kazuyuki Kuroda, Department of Applied Chemistry, Waseda University, Dr. Yuko Uchimaru, National Institute of Advanced Science and Technology, AIST, and Dr. Wataru Sugimoto, Department of Fine Materials Engineering, Shinshu University, for their valuable discussion. We also thank Mr. Masashi Shirata, Mr. Kazuya Notsu, Mr. Hajime Ohkawa, Mr. Yu Tsunoda, Ms. Hiromi Suzuki, Mr. Manabu Kudo, Mr. Yosuke Takeda, Mr. Satoru Yoshioka and Ms. Saki Tsuzuki for their contributions to experiments conducted during the research.

References

1. Figlarz, M., Gérand, B., Delahaye-Vidal, A., Dumont, B., Harb, F., Coucou, A. and Fievet, F. 1990, Solid State Ionics, 43, 143.
2. Rouxel, J. 1992, ACS Symp. Ser., 499, 88.
3. Gopalakrishnan, J. 1995, Chem. Mater., 7, 1265.
4. Schaak, R. E. and Mallouk, T. E. 2002, Chem. Mater., 14, 1455.
5. Sanchez, C., Soler-Illia, G. J. d. A. A., Ribot, F., Lalot, T., Mayer, C. R. and Cabuil, V. 2001, Chem. Mater., 13, 3061.
6. Ganguli, D. and Chatterjee, M. 1997 Ceramic Powder Preparation: A Handbook, Kluwer Academic Publishers, Boston, 42.
7. Sanchez, C. and Ribot, F. 1994, New Jounal of Chermistry, 18, 1007.
8. Corriu, R. J. P. and Leclercq, D. 1996, Angew. Chem. Int. Ed. Engl., 35, 1420.
9. Judeinstein, P. and Sanchez, C. 1996, J. Mater. Chem., 6, 511.
10. Alexandre, M. and Dubois, P. 2000, Mater. Sci. Eng., R28, 1.
11. Laaziz, PI., Larbot, A., Guizard, C., Durand, J., Cot, L. and Joffre, J. 1990, Acta Crystallogr., Sect. C; Cryst. Struct. Commun., 46, 2332.

12. Hubert-Pfalzgraf, L. G., Abada, V., Halut, S. and Roziere, J. 1997, Polyhedron, 16, 581.
13. Choy, J.-H. 2004, J. Phys. Chem. Solid, 65, 373.
14. Izawa, H., Kikkawa, S. and Koizumi, M. 1982, J. Phys. Chem., 86, 5023.
15. Rebbah, H., Hervieu, M. and Reveau, B. 1981, Meter. Res. Bull., 16, 149.
16. Largaly, G. and Beneke, K. 1976, J. Inorg. Nucl. Chem, 38, 1513.
17. Rebbah, H., Borel, M. M., Bernard, M. and Reveau, B. 1981, Rev. Chim. Miner., 81, 109.
18. Reveau, B. 1984, Rev. Chim. Miner., 21, 391.
19. Cross, L. E., 1993, Ferroelectric Ceramics, Setter, N. and Colla, E. L. (Eds.), Brinkhauser Verlag, Basel.
20. Du, X. F. and Chen, I.-W. 1998, Ferroelectrics, 208, 237.
21. Goodenough, J. B. and Longo, J. M. 1970, "Landolt-Börnstein" New Series, Group III, Vol. 4, Part a, Springer. Berlin.
22. Kurtz, S. K. and Perry, T. T. 1968, J. Appl. Phys., 39, 3798.
23. Rao, C. N. R. and Reveau, B. 1995 Transition Metal Oxides, VCH, New York.
24. Yoshimura, J., Ebina, Y., Kondo, J. N., Domen, K. and Tanaka, A. 1993, J. Phys. Chem., 97, 1970.
25. Takata, T., Tanaka, A., Kondo, J. N. and Domen, K. 1998, Catal. Today, 44, 17.
26. Sato, M., Abo, J., Jin, T. and Ohta, M. 1993, J. Alloys Compd., 192, 81.
27. Gopalakrishnan, J., Bhat, V. and Raveau, B. 1987, Mater. Res. Bull., 22, 413.
28. Jacobson, A. J., Johnson, J. W. and Lewandouski, J. T. 1985, Inorg. Chem., 24, 3727.
29. Gopalakrishnan, J. and Bhat, V. 1987, Inorg. Chem., 26, 4299.
30. Jacobson, A. J., Johnson, J. W. and Lewandouski, J. T. 1987, Mater. Res. Bull., 22, 45.
31. Mohan-Ram, R. A. and Clearfield, A. 1991, J. Solid State Chem., 94, 45.
32. Gopalakrishnan, J., Uma, S. and Bhat, V. 1993, Chem. Mater., 5, 132.
33. Uma, S., Raju, A. R. and Gopalakrishnan, J. 1993, J. Mater. Chem., 3, 709.
34. Nakato, T., Nakade, M., Kuroda, K. and Kato, C. 1994, Stud. Surf. Sci. Catal. Lett., 90, 285.
35. Zhong, Z., Ding, W., Hou, W., Chen, Y., Chen, X., Zhu, Y. and Min, N. 2001, Chem. Mater., 13, 538.
36. Takahashi, S., Nakato, T., Hayashi, S., Sugahara, Y. and Kuroda, K. 1995, Inorg. Chem., 34, 5065.
37. Suzuki, M. 1995, J. Ceram. Soc. Jpn., 103, 1099.
38. Araujo, C. A. P. d., Cuchlaro, J. D., McMillan, L. D., Scott, M. C. and Scott, J. F. 1995, Nature, 374, 627.
39. Dobal, P. S. and Katiyar, R. S. 2002, J. Raman Spectrosc., 33, 405.
40. Aurivillius, B. 1949, Ark. Kemi, 463, 1.
41. Aurivillius, B. 1949, Ark. Kemi, 499, 1.
42. Aurivillius, B. 1950, Ark. Kemi, 519, 2.
43. Sugimoto, W., Shirata, M., Sugahara, Y. and Kuroda, K. 1999, J. Am. Chem. Soc., 121, 11601.
44. Shirata, M., Tsunoda, Y., Sugimoto, W. and Sugahara, Y. 2001, Mat. Res. Soc. Symp. Proc., 658, GG.6.24.1.

45. Sugimoto, W., Shirata, M., Kuroda, K. and Sugahara, Y. 2002, Chem. Mater., 14, 2946.
46. Tsunoda, Y., Shirata, M., Sugimoto, W., Liu, Z., Terasaki, O., Kuroda, K. and Sugahara, Y. 2001, Inorg. Chem., 40, 5768.
47. Kudo, M., Ohkawa, H., Sugimoto, W., Kumada, N., Liu, Z., Terasaki, O. and Sugahara, Y. 2003, Inorg. Chem., 42, 4479.
48. Kudo, M., Tsuzuki, S., Katshumata, K., Yasumori, A. and Sugahara, Y. 2004, Chem. Phys. Lett., 393, 12.
49. Tsunoda, Y., Sugimoto, W. and Sugahara, Y. 2003, Chem. Mater., 15, 632.
50. Suzuki, H., Notsu, K., Takeda, Y., Sugimoto, W. and Sugahara, Y. 2003, Chem. Mater., 15, 636.
51. Tahara, S. and Sugahara, Y. 2003, Langmuir, 19, 9473.
52. Yoshioka, S., Takeda, Y., Uchimaru, Y. and Sugahara, Y. 2003, J. Organomet. Chem., 686, 145.
53. Bhuvanesh, N. S. P., Crosnier-Lopez, M.-P., Duroy, H. and Fourquet, J.-L. 2000, J. Mater. Chem., 10, 1685.
54. Richard, M., Brohan, L. and Tournoux, M. 1994, J. Solid State Chem., 112, 345.
55. Ollivier, P. J. and Mallouk, T. E. 1998, Chem. Mater., 10, 2585.
56. Thangadurai, V., Shukla, A. K. and Gopalakrishnan, J. 1994, Solid State Ionics, 73, 9.
57. Dion, M., Ganne, M. and Tournoux, M. 1986, Rev. Chim. Miner., 23, 61.
58. Jacobson, A. J., Lewandouski, J. T. and Johnson, J. W. 1986, J. Less-Common Met., 116, 137.
59. 1964, Gmelins Handbuch der Anorganischen Chemie: Bismuth, Splinger-Verlag, Berlin.
60. 1921, A Dictionary of Chemical Solubilities; Inorganic, Comey, A. M. and Hahn, D. A. (Eds.), Macmillan, New York.
61. Suzuki, M., Nagasawa, N., Machida, A. and Ami, T. 1996, Jpn. J. Appl. Phys., 35, L564.
62. Macquart, R., Kennedy, B. J. and Shimakawa, Y. 2001, J. Solid State Chem., 160, 174.
63. Srikanth, V., Idink, H., White, W. B., Subbarao, E. C., Rajagopal, H. and Sequeira, A. 1996, Acta Crystallogr., B52, 432.
64. Blake, S. M., Falconer, M. J., McCreedy, M. and Lightfoot, P. 1997, J. Mater. Chem., 7, 1609.
65. Ismunandar, Hunter, B. A. and Kennedy, B. J. 1998, Solid State Ionics, 112, 281.
66. Ismunandar and Kennedy, B. J. 1999, J. Mater. Chem., 9, 541.
67. Park, B. H., Kang, B. S., Bu, S. D., Noh, T. W., Lee, J. and Jo, W. 1999, Nature, 401, 682.
68. Palacín, M. R., Lira, M., García, J. L., Caldés, M. T., Casañ-Pastor, N., Fuertes, A. and Gómez-Romero, P. 1996, Mater. Res. Bull., 31, 217.
69. Schaak, R. E. and Mallouk, T. E. 2000, J. Solid State Chem., 155, 46.
70. Watanabe, A. and Goto, M. 1978, J. Less-Common Met., 61, 265.
71. Champarnaud-Mesjard, J. C., Frit, B. and Watanabe, A. 1999, J. Mater. Chem., 9, 1319.
72. Schaak, R. E. and Mallouk, T. E. 2002, Chem. Commun., 706.
73. Gopalakrishnan, J. 1988, Rev. Solid State Sci., 1, 515.

74. Toda, K. and Sato, M. 1996, J. Mater. Chem., 6, 1067.
75. Gopalakrishnan, J., Sivakumar, T., Ramesha, K., Thangadurai, V. and Subbanna, G. N. G. 2000, J. Am. Chem. Soc., 122, 6237.
76. Kudo, A. 2001, J Ceram. Soc. Jpn., 109, S81.
77. Tanaka, A., Kondo, J. N. and Domen, K. 1995, Crit. Rev. Surf. Chem., 5, 305.
78. Domen, K., Kondo, J. N., Hara, M. and Takata, T. 2000, Bull. Chem. Soc. Jpn., 73, 1307.
79. Domen, K., Yoshimura, J., Sakine, T., Tanaka, A. and Onishi, T. 1990, Catal. Lett., 4, 339.
80. Machida, M., Yabunaka, J. and Kijima, T. 2000, Chem. Mater., 12, 812.
81. Machida, M., Yabunaka, J., Kijima, T., Matsushima, S. and Arai, M. 2001, Int. J. Inorg. Mater., 3, 545.
82. Machida, M., Miyazaki, K., Matsushima, S. and Arai, M. 2003, Chem. Mater., 13, 1433.
83. Takata, T., Furumi, Y., Shinohara, K., Tanaka, A., Hara, M., Kondo, J. N. and Domen, K. 1997, Chem. Mater., 9, 1063.
84. Ebina, Y., Tanaka, A., Kondo, J. N. and Domen, K. 1996, Chem. Mater., 8, 2534.
85. Ebina, Y., Sasaki, T., Harada, M. and Watanabe, M. 2002, Chem. Mater., 14, 4390.
86. Kudo, A. and Hijii, S. 1999, Chem. Lett., 1103.
87. Stachiotti, M. G., Rodriguez, C. O., Ambrosch-Draxl, C. and Christensen, N. E. 2000, Phys. Rev. B, 61, 14434.
88. Robertson, J., Chen, C. W., Warren, W. L. and Gutleben, C. D. 1996, Appl. Phys. Lett., 69, 1704.
89. Tsai, M.-H. and Dey, S. K. 2000, IEEE Trans. Ultrason. Ferroelectr., 47, 929.
90. Shimizu, A., Takada, S., Shimooka, H., Takahashi, S., Kohiki, S., Arai, M. and Oku, M. 2002, Chem. Mater., 14, 3971.
91. Whittingham, M. S. and Jacobson, A. J. 1982 Intercalation Chemistry, Academic Press, New York.
92. O'Hare, D. 1996 Inorganic Materials, 2nd ed, John Wiley & Sons, Chichester, 171.
93. Ogawa, M. and Kuroda, K. 1997, Bull. Chem. Soc. Jpn., 70, 2593.
94. Hong, Y.-S. and Kim, S.-J. 1996, Bull. Korean Chem. Soc., 17, 730.
95. Uma, S. and Gopalakrishnan, J. 1995, Mater. Sci. Eng., B34, 175.
96. Schaak, R. E. and Mallouk, T. E. 2000, Chem. Mater., 12, 3427.
97. Goñi, A., Rius, J., Insausti, M., Lezama, L. M., Pizarro, J. L., Arriortua, M. I. and Rojo, T. 1996, Chem. Mater., 8, 1052.
98. Bhat, V. and Gopalakrishnan, J. 1988, J. Solid State Ionics., 26, 25.
99. Sasaki, T., Izumi, F. and Watanabe, M. 1996, Chem. Mater., 8, 777.
100. Ruiz-Hitzky, E. and Rojo, J. M. 1980, Nature, 287, 28.
101. Ogawa, M., Okutomo, S. and Kuroda, K. 1998, J. Am. Chem. Soc., 120, 7361.
102. Tunney, J. J. and Detellier, C. 1996, J. Mater. Chem., 6, 1679.
103. Kikkawa, S., Kanamaru, F. and Koizumi, M. 1976, Inorg. Chem., 15, 2195.
104. Yamanaka, S. 1976, Inorg. Chem., 15 2811.
105. Bradley, D., Mehrotra, R. C., Rothwell, I. and Singh, A., 2001, Alkoxo and Aryloxo Derivatives of Metals, Academic Press, San Diego.
106. Bradley, D. C., Chakravarti, B. N. and Wardlaw, W. 1956, J. Chem. Soc., 4439.
107. Bradley, D. C., Chakravarti, B. N., Chatterjee, A. K., Wardlaw, W. and Whitley, A. 1958, J. Chem. Soc., 99.

108. Mehrotra, R. C. and Kapoor, P. N. 1965, J. Less-Common Met., 8, 419.
109. Kapoor, R. N., Prakash, S. and Kapoor, P. N. Z. 1967, Anorg. Allg. Chem., 351, 219.
110. Matsuda, T., Miyamae, N. and Takeuchi, M. 1993, Bull. Chem. Soc. Jpn., 66, 1551.
111. Vaia, R. A., Teukolsky, R. K. and Giannelis, E. P. 1994, Chem. Mater., 6, 1017.
112. Pursch, M., Brindle, R., Ellwanger, A., Sander, L. C., Bell, C. M., Händel, H. and Albert, K. 1997, Solid State Nucl. Magn. Reson., 9, 191.
113. Speier, J. L. 1979 Advances in Organometallic Chemistry, Academic Press, New York, Vol. 17, 407.

Preparation of Organic−Inorganic Hybrids Possessing Nanosheets with Perovskite-Related Structures via Exfoliation during a Sol−Gel Process

Seiichi Tahara, Yosuke Takeda, and Yoshiyuki Sugahara*

Department of Applied Chemistry, School of Science and Engineering, Waseda University, Shinjuku-ku, Ohkubo-3, Tokyo 169-8555, Japan

Received July 8, 2005. Revised Manuscript Received September 13, 2005

Organic−inorganic hybrids containing exfoliated nanosheets with a perovskite-related structure have been prepared from an *n*-decoxy derivative of an ion-exchangeable layered perovskite, $HLaNb_2O_7 \cdot xH_2O$ (HLaNb) or $HCa_2Nb_3O_{10} \cdot xH_2O$ (HCaNb), silanol-terminated poly(dimethylsiloxane) (PDMS), and tetramethoxysilane (TMOS) via a sol−gel process involving the reaction of the *n*-decoxy derivative with a PDMS−TMOS mixture and subsequent intentional hydrolysis with hydrochloric acid. The X-ray diffraction (XRD) patterns of the resultant products after intentional hydrolysis indicate both preservation of the perovskite-like slab structure and disappearance of stacking order. Partial exfoliation of layered perovskites is correspondingly observed by transmission electron microscopy (TEM). The formation of a polysiloxane network composed of PDMS chains and Q^n units ($(RO)_{4-n}Si(OSi)_n$: R = H, CH_3) via intentional hydrolysis is shown by the solid-state ^{29}Si CP/MAS (cross-polarization and magic angle spinning) NMR spectroscopy. These products are expected to possess the Nb−O−Si linkage interface since a signal assignable to the $(SiO)Si(CH_3)_2O$−Nb environment is present in the ^{29}Si CP/MAS NMR spectra of products prepared from an *n*-decoxy derivative of HLaNb (or HCaNb), PDMS, and TMOS in a similar manner without intentional hydrolysis and the Nb−O−Si bonds are expected to be preserved during hydrolysis. The exfoliated structures should be formed during the intentional hydrolysis process since the products prepared without intentional hydrolysis clearly exhibit a stacking order along the *c* axis.

Introduction

Organic−inorganic hybrids have been attracting significant attention as a new class of materials since the combination of an inorganic component and an organic component has the potential to provide improved and tunable properties.[1−5] Transition metal oxides are attractive inorganic components for hybrids since they exhibit a wide variety of properties.[4,6,7] Sol−gel processing is one of the promising routes to organic−inorganic hybrids since metal−oxygen networks can be formed using a "*Chimie Douce*" approach involving hydrolysis and polycondensation.[1−4,8−16] Thus, a large number of hybrids containing transition metal oxides have been prepared from transition metal alkoxides. It should be noted that crystalline transition metal oxides are generally favorable for enhancing the properties of hybrids.[4]

In addition to selection of an appropriate combination of inorganic and organic components, achieving desirable properties requires that their interfaces and nanostructures are carefully designed. Organic−inorganic hybrids can be classified into two groups, based on their interfaces:[1,2,4] class I hybrids with weak interactions and class II hybrids with strong bonds such as covalent bonds. For the production of class II hybrids,[1] selection of the preparation process and starting compounds is extremely important. In sol−gel processes, Si−C and Sn−C bonds are widely utilized as interfacial covalent bonds.[4] For hybrids containing transition metal oxides, on the contrary, M−O−Si bonds (M = transition metal) are frequently introduced at their interfaces[4] since covalent M−C and M−O−C bonds are unstable against hydrolysis.[17,18] One of the ideal nanostructures is a structure containing inorganic components with a well-defined domain size. The sol−gel process requires significant modification for the preparation of such structures since it

* To whom correspondence should be addressed. E-mail: ys6546@waseda.jp.

(1) Sanchez, C.; Ribot, F. *New. J. Chem.* **1994**, *18*, 1007.
(2) Judeinstein, P.; Sanchez, C. *J. Mater. Chem.* **1996**, *6*, 511.
(3) Corriu, R. J. P.; Leclercq, D. *Angew. Chem., Int. Ed. Engl.* **1996**, *35*, 1420.
(4) Sanchez, C.; Soler-Illia, G. J. de. A. A.; Ribot, F.; Lalot, T.; Mayer, C. R.; Cabuil, V. *Chem. Mater.* **2001**, *13*, 3061.
(5) Alexandre, M.; Dubois, P. *Mater. Sci. Eng.* **2000**, *R28*, 1.
(6) Schaudel, B.; Guermeur, C.; Sanchez, C.; Nakatani, K.; Delaire, J. A. *J. Mater. Chem.* **1997**, *7*, 61.
(7) Itou, T.; Matsuda, H. *Key Eng. Mater.* **1998**, *150*, 67.
(8) Wilkes, G. L.; Orler, B.; Huang, H. H. *Polym. Prepr.* **1985**, *26*, 300.
(9) Schmidt, H. *J. Non-Cryst. Solids* **1985**, *73*, 681.
(10) Philipp, G.; Schmidt, H. *J. Non-Cryst. Solids* **1984**, *63*, 283.
(11) Schmidt, H.; Scholze, H.; Kaiser, A. *J. Non-Cryst. Solids* **1984**, *63*, 1.
(12) Sanchez, C.; Ribot, F.; Lebeau, B. *J. Mater. Chem.* **1999**, *9*, 35.
(13) Beecroft, L. L.; Ober, C. K. *Chem. Mater.* **1997**, *9*, 1302.
(14) Schmidt, H.; Seiferling, B. *Mater. Res. Soc. Symp. Proc.* **1986**, *73*, 739.
(15) Mackenzie, J. D.; Chung, Y. J.; Hu, Y. *J. Non-Cryst. Solids* **1992**, *147*, 271.
(16) Babonneau, F. *Polyhedron* **1994**, *13*, 1123.
(17) Bradley, D.; Mehrotra, R. C.; Rothwell, I.; Singh, A. *Alkoxo and Aryloxo Derivatives of Metals*; Academic Press: San Diego, 2001.
(18) Sanchez, C.; Livage, J.; Henry, M.; Babonneau, F. *J. Non-Cryst. Solids* **1988**, *100*, 65.

10.1021/cm0514793 CCC: $30.25
Published on Web 10/29/2005

is generally very difficult to control the polycondensation process of metal alkoxides precisely. One of the proposed modifications is the use of well-defined oxo-clusters bearing alkoxy groups as inorganic nanobuilding blocks (NBBs),[4] but the relatively low stability of their core structures with respect to hydrolysis has limited their applicability to sol–gel processes. Instead, organic–inorganic hybrids have been prepared with NBBs bearing polymerizable groups, such as methacrylate groups, via copolymerization with organic monomers.[4,19,20]

The exfoliation of layered materials is another "*Chimie Douce*" technique for obtaining nanosheets with well-defined nanoscaled thicknesses, and if nanosheets possess reactive groups on their surfaces, they can be attractive candidates for inorganic NBBs for class II hybrids. As class I hybrids, layered material/polymer hybrids containing inorganic nanosheets have been extensively prepared through exfoliation.[5,21] Literature describing the preparation of class II layered material/polymer hybrids possessing interfacial covalent bonds, on the contrary, has been limited to date. A class II hybrid was prepared, for example, by polymerization of cyclo-siloxane in the interlayer space of a tetramethylammonium-$HTiNbO_5$ intercalation compound.[22] Another approach to preparation of class II hybrids was modification of the edges of the nanosheets of hectorite, with silanol-terminated polysiloxane[23] or with γ-methacryloxypropyl trimethoxysilanes or γ-methacryloxypropyl dimethyl ethoxysilanes, followed by polymerization.[24]

Here we report a novel sol–gel process for preparation of class II hybrids using crystalline nanosheets with perovskite-related structures as transition metal oxide NBBs. The *n*-alkoxy derivatives of ion-exchangeable layered perovskites, $HLaNb_2O_7 \cdot xH_2O$ (HLaNb) and $HCa_2Nb_3O_{10} \cdot xH_2O$ (HCaNb), consisting of stacked perovskite-like slabs (the compositions originally present in the protonated forms are $[LaNb_2O_7]^-$ and $[Ca_2Nb_3O_{10}]^-$) bearing surface decoxy groups were utilized.[25–28] Cohydrolysis of an *n*-decoxy derivative of HLaNb (or HCaNb), silanol-terminated poly(dimethylsiloxane) $[HO(Si(CH_3)_2O)_nH$; PDMS], and tetramethoxysilane $[Si(OCH_3)_4$, TMOS] led to simultaneous occurrence of the formation of a condensed polysiloxane network (so-called organically modified silicates[15,16]) and exfoliation to form class II hybrids where nanosheets were dispersed in a condensed polysiloxane network with an Nb–O–Si linkage interface (Scheme 1).

Scheme 1. Overview of the Reaction of an *n*-Decoxy Derivative of an Ion-Exchangeable Layered Perovskite with a PDMS–TMOS Mixture and Subsequent Intentional Hydrolysis

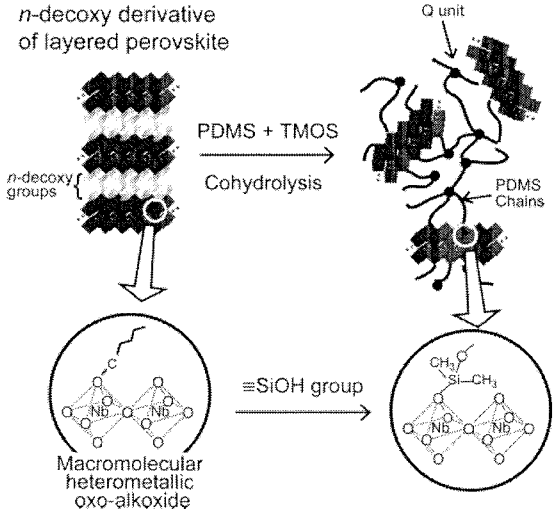

Experimental Section

Preparation of the Organic–Inorganic Hybrids. Preparation of the intermediates, *n*-decoxy derivatives of HLaNb[27] and HCaNb,[28] was conducted based on previous reports. Typically, 0.1 g of the *n*-decoxy derivative was dispersed in a mixture of 3.0 mL of PDMS (molecular mass: ~400–700) and 0.79 g of TMOS [$((CH_3)_2SiO)$ unit (in PDMS):TMOS = 1:1 in a molar ratio], and the resulting suspension was stirred at 80 °C for 7 d. Hydrochloric acid (ca. 0.6 M) was then added dropwise to the suspension to achieve a nominal molar ratio of $TMOS:H_2O:HCl = 1:4:0.045$. After the mixture was stirred for 1 d under ambient atmosphere, the resultant product was dried under reduced pressure (*hydrolyzed* HLaNb–PDMS–TMOS or *hydrolyzed* HCaNb–PDMS–TMOS). For the investigation of the interfaces between the layered perovskites and polysiloxanes, 0.1 g of the *n*-decoxy derivative was dispersed in a mixture of 3.0 mL of PDMS and 0.79 g of TMOS at 80 °C for 7 d with no intentional hydrolysis procedure. The resultant product was then centrifuged, washed with tetrahydrofuran (THF), and dried at room temperature (HLaNb–PDMS–TMOS and HCaNb–PDMS–TMOS). In a similar fashion, typically 0.1 g of the *n*-decoxy derivative was dispersed in 5 mL of PDMS at 80 °C for 7 d. The resultant product was then centrifuged, washed with THF, and dried at room temperature (HLaNb–PDMS and HCaNb–PDMS).

For the investigation of the reaction process, 0.1 g of the *n*-decoxy derivative and 5 mL of trimethysilyl-terminated poly(dimethylsiloxane) $\{(CH_3)_3SiO[Si(CH_3)_2O]_mSi(CH_3)_3\}$ (average molecular mass: ~550) were stirred at 80 °C for 7 d. The resultant product was centrifuged, washed with THF, and dried at room temperature. In a similar fashion, 0.1 g of an *n*-decoxy derivative of a layered perovskite, HLaNb, was dispersed in 5 mL of TMOS at 80 °C for 7 d. The resultant product was then centrifuged, washed with THF, and dried at room temperature.

Instrumentation. The X-ray diffraction (XRD) patterns of the products were recorded with a Mac Science M03XHF[22] diffractometer with Mn-filtered Fe Kα radiation. The solid-state ^{13}C and ^{29}Si nuclear magnetic resonance (NMR) spectra were obtained using a JEOL CMX-400 spectrometer operated at 100.54 MHz (^{13}C) and 79.427 MHz (^{29}Si) using cross-polarization and magic angle spinning techniques (CP/MAS). The sample spinning rate was about 5 kHz. The contact time was 2 ms (^{13}C) or 5 ms (^{29}Si), and the

(19) Hubert-Pfalzgraf, L. G.; Abada, V.; Halut, S.; Roziere, J. *Polyhedron* **1997**, *16*, 581.
(20) Laaziz, I.; Larbot, A.; Guizard, C.; Durand, J.; Cot, L.; Joffre, J. *Acta Crystallogr. C* **1990**, *46*, 2332.
(21) Lappas, A.; Zorko, A.; Wortham, E.; Das, R. N.; Giannelis, E. P.; Cevc, P.; Arčon, D. *Chem. Mater.* **2005**, *17*, 1199.
(22) Bruzaud, S.; Levesque, G. *Chem. Mater.* **2002**, *14*, 2421.
(23) Bourlinos, A. B.; Jiang, D. D.; Giannelis, E. P. *Chem. Mater.* **2004**, *16*, 2404.
(24) Herrera, N. N.; Letoffe, J. M.; Putaux, J. L.; David, L.; Bourgeat-Lami, E. *Langmuir* **2004**, *20*, 1564.
(25) Tahara, S.; Sugahara, Y. *Recent Res. Dev. Inorg. Chem.* **2004**, *4*, 13.
(26) Takahashi, S.; Nakato, T.; Hayashi, S.; Sugahara, Y.; Kuroda, K. *Inorg. Chem.* **1995**, *34*, 5065.
(27) Suzuki, H.; Notsu, K.; Takeda, Y.; Sugimoto, W.; Sugahara, Y. *Chem. Mater.* **2003**, *15*, 636.
(28) Tahara, S.; Sugahara, Y. *Langmuir* **2003**, *19*, 9473.

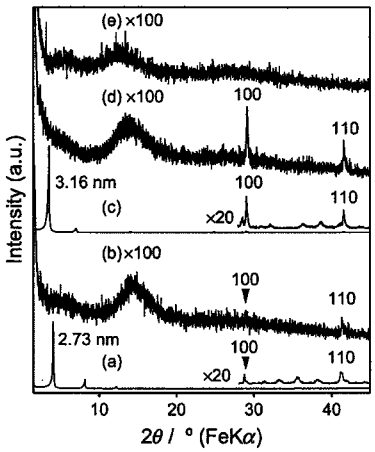

Figure 1. XRD patterns of (a) the *n*-decoxy derivative of HLaNb, (b) the reaction product of the *n*-decoxy derivative of HLaNb and PDMS-TMOS mixture with intentional hydrolysis (*hydrolyzed* HLaNb−PDMS−TMOS), (c) the *n*-decoxy derivative of HCaNb, (d) the reaction product of the *n*-decoxy derivative of HCaNb and PDMS−TMOS mixture with intentional hydrolysis (*hydrolyzed* HCaNb−PDMS−TMOS), and (e) the hydrolyzed PDMS−TMOS mixture.

pulse delay was 5 s. Transmission electron microscopy (TEM) images were obtained using a JEOL JEM-100CX microscope operated at 100 kV. Infrared (IR) adsorption spectra were recorded with a Perkin-Elmer Spectrum One instrument using the KBr disk technique.

Results and Discussion

Preparation of Organic−Inorganic Hybrids. Figure 1 demonstrates the XRD patterns of the *n*-decoxy derivatives of HLaNb and HCaNb as well as those of *hydrolyzed* HLaNb−PDMS−TMOS and *hydrolyzed* HCaNb−PDMS−TMOS. The interlayer distances of the *n*-decoxy derivatives are 2.73 nm (HLaNb) and 3.16 nm (HCaNb), consistent with the previous reports.[27,28] After cohydrolysis of the products obtained from the *n*-decoxy derivatives, PDMS and TMOS, the (00*l*) reflections of the *n*-decoxy derivatives disappear, while the (100) reflections at $2\theta = 28.9°$ (HLaNb) and 29.1° (HCaNb) and the (110) reflections at $2\theta = 41.4°$ (HLaNb) and 41.7° (HCaNb) are clearly present. Thus, although the long-range stacking order along the *c* axis disappears, the perovskite-like slab structures are preserved. A broad diffraction at around $2\theta = 13°$ can be ascribed to the condensed polysiloxane network based on a comparison with the XRD pattern of the hydrolyzed PDMS−TMOS mixture (Figure 1e).

The solid-state ^{29}Si CP/MAS NMR spectra of *hydrolyzed* HLaNb−PDMS−TMOS and *hydrolyzed* HCaNb−PDMS−TMOS are shown in Figure 2. Both the spectra show four signals at −19, −22, −100, and −109 ppm, and the signals at −22, −100, and −109 ppm are assignable to D^2 [$(CH_3)_2Si(OSi)_2$] (PDMS chain), Q^3 [$(RO)Si(OSi)_3$] [R = H, CH_3 (derived from TMOS)], and Q^4 [$Si(OSi)_4$] (derived from TMOS) environments, respectively.[29] The signal at −19 ppm can be ascribed to a D^2-Q [$(CH_3)_2Si(OSi)(OSi(O\text{-})_3)$] environment, indicating the successful formation of condensed polysiloxanes possessing a certain amount of bonds between the Q units and the PDMS chains via cohydrolysis.[16]

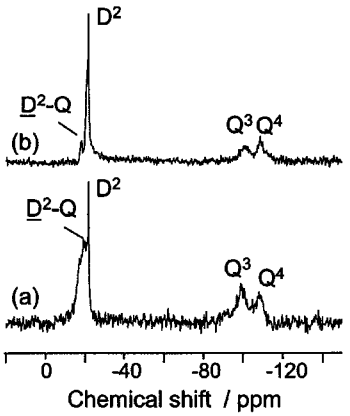

Figure 2. Solid-state ^{29}Si CP/MAS NMR spectra of (a) the reaction product of the *n*-decoxy derivative of HLaNb and the PDMS−TMOS mixture with intentional hydrolysis (*hydrolyzed* HLaNb−PDMS−TMOS) and (b) the reaction product of the *n*-decoxy derivative of HLaNb and the PDMS−TMOS mixture with intentional hydrolysis (*hydrolyzed* HCaNb−PDMS−TMOS).

Figures 3a and 3b show TEM images of *hydrolyzed* HLaNb−PDMS−TMOS and *hydrolyzed* HCaNb−PDMS−TMOS, respectively. Dark lines are clearly observed in the TEM images, and the thicknesses of the dark lines in both the images of *hydrolyzed* HLaNb−PDMS−TMOS (~1 nm) and *hydrolyzed* HCaNb−PDMS−TMOS (~1.5 nm) are closely consistent with the thickness of the individual perovskite-like slabs. Thus, it is clearly demonstrated that the perovskite-like slabs (dark lines) are dispersed in the polysiloxane network, a finding indicative of the formation of exfoliated hybrid structures. In addition to these structures, partially exfoliated particles consisting of stacked 3−5 perovskite-like slabs are also present; an example observed in *hydrolyzed* HCaNb−PDMS−TMOS is shown in Figure 3c.

Interfaces Formed between Perovskite-like Slabs and the Polysiloxane Network. To investigate the interfaces between perovskite-like slabs and the polysiloxane network, the reactions between the *n*-decoxy derivatives and PDMS are investigated. The XRD patterns of these products, HLaNb−PDMS and HCaNb−PDMS, are shown in Figure 4. After the reactions with PDMS, the new reflections appear at 1.41 nm (HLaNb−PDMS) and 1.85 nm (HCaNb−PDMS), which correspond to the interlayer distances. The presence of reflections at $2\theta = 28.8°$ (HLaNb−PDMS) and 29.1° (HCaNb−PDMS) indicates the preservation of the perovskite-like slab structures. These XRD results show that nanosheets (perovskite-like slabs) are stacked along the *c* axis in an ordered state.

Figure 5 shows the solid-state ^{13}C CP/MAS NMR of HLaNb−PDMS and HCaNb−PDMS. Both the spectra exhibit signals at 1 ppm, which are ascribable to methyl groups in the PDMS chain [$(CH_3)_2SiO$].[30] It is also notable with respect to both the spectra that the signals due to the

(29) Marsmann, H. NMR 17, Basic Principals and Progress, Oxygen-17 and Silicon-29. In *NMR 17, Basic Principals and Progress, Oxygen-17 and Silicon-29*; Diehl, P., Fluck, E., Cosfeld, R., Eds.; Springer-Verlag: Berlin, 1981.

(30) Julián, B.; Gervais, C.; Cordoncillo, E.; Escribano, P.; Babonneau, F.; Sanchez, C. *Chem. Mater.* **2003**, *15*, 3026.

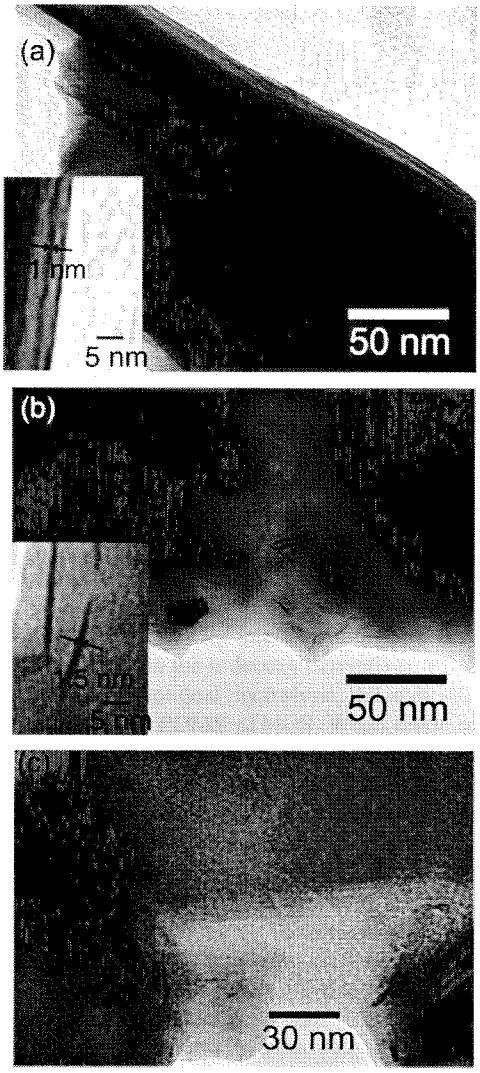

Figure 3. TEM images of (a) the reaction product of the *n*-decoxy derivative of HLaNb and the PDMS–TMOS mixture with intentional hydrolysis (*hydrolyzed* HLaNb–PDMS–TMOS), (b) the reaction product of the *n*-decoxy derivative of HCaNb and the PDMS–TMOS mixture with intentional hydrolysis (*hydrolyzed* HCaNb–PDMS–TMOS), and (c) partially exfoliated particles with layer stacking of 3–5 perovskite-like slabs of HLaNb. The inset images are magnifications of (a) and (b).

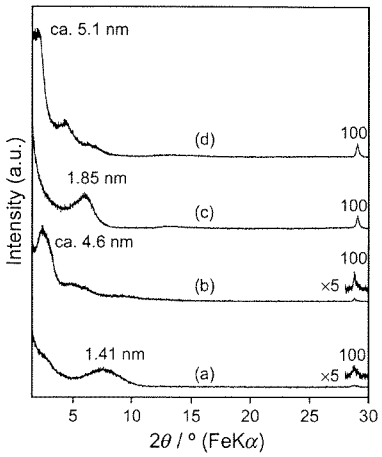

Figure 4. XRD patterns of (a) the reaction product of the *n*-decoxy derivative of HLaNb and PDMS (HLaNb–PDMS), (b) the reaction product of the *n*-decoxy derivative of HLaNb and the PDMS–TMOS mixture with no intentional hydrolysis (HLaNb–PDMS–TMOS), (c) the reaction product of the *n*-decoxy derivative of HCaNb and PDMS (HCaNb–PDMS), and (d) the reaction product of the *n*-decoxy derivative of HCaNb and the PDMS–TMOS mixture with no intentional hydrolysis (HCaNb–PDMS–TMOS).

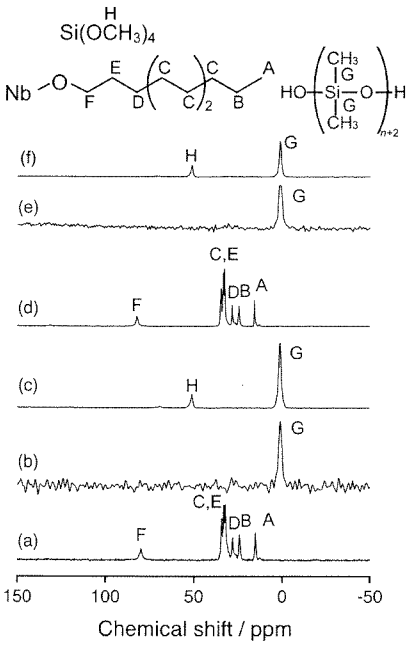

Figure 5. Solid-state ^{13}C CP/MAS NMR spectra of (a) the *n*-decoxy derivative of HLaNb, (b) the reaction product of the *n*-decoxy derivative of HLaNb and PDMS (HLaNb–PDMS), (c) the reaction product of the *n*-decoxy derivative of HLaNb and the PDMS–TMOS mixture with no intentional hydrolysis (HLaNb–PDMS–TMOS), (d) the *n*-decoxy derivative of HCaNb, (e) the reaction product of the *n*-decoxy derivative of HCaNb and PDMS (HCaNb–PDMS), and (f) the reaction product of the *n*-decoxy derivative of HCaNb and the PDMS–TMOS mixture with no intentional hydrolysis (HCaNb–PDMS–TMOS).

n-decoxy groups have disappeared, indicating that the *n*-decoxy groups on the interlayer surface are removed during the reaction. The IR spectra of HLaNb–PDMS and HCaNb–PDMS (not shown) revealed the presence of the bands at 1260, 1100–1000, and 800 cm^{-1}. These three bands can be ascribed to $\delta(Si-CH_3)$ (1260 cm^{-1}), $\nu(Si-O-Si)$ (1100–1000 cm^{-1}), and $\gamma(Si-CH_3)$ (800 cm^{-1}) modes, a finding consistent with the presence of PDMS chains in the products.[31]

Solid-state ^{29}Si MAS NMR spectra of HLaNb–PDMS and HCaNb–PDMS are shown in Figure 6. Both the spectra show two signals at −5 and −22 ppm, the latter of which is ascribable to the D^2 environment of the PDMS chain $[(CH_3)_2Si(OSi)_2]$.[29] The chemical shift of the broad signal (−5 ppm) is not consistent with the terminal D^1 environment of PDMS $[(SiO)Si(CH_3)_2OH]$ (−11.0 ppm in a ^{29}Si NMR spectrum), and based on the reported chemical shift of an $(SiO)Si(CH_3)_2O-Nb$ environment (−6.8 ppm),[30] it should be ascribed to the $(SiO)Si(CH_3)_2O-Nb$ environment; the Nb–O–Si covalent bonds are formed between the interlayer surface of the layered perovskites and the end of PDMS chains.

(31) Marchand, A.; Valade, J. *J. Organomet. Chem.* **1968**, *12*, 305.

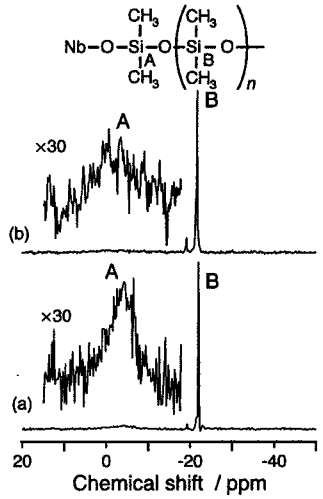

Figure 6. Solid-state ^{29}Si MAS NMR spectra of (a) the reaction product of the *n*-decoxy derivative of HLaNb with PDMS (HLaNb–PDMS) and (b) the reaction product of the *n*-decoxy derivative of HCaNb with PDMS (HCaNb–PDMS).

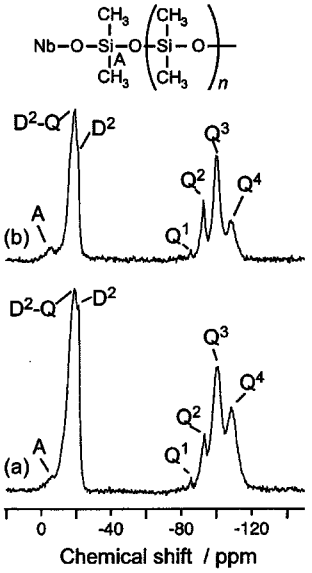

Figure 7. Solid-state ^{29}Si CP/MAS NMR spectra of (a) the reaction product of the *n*-decoxy derivative of HLaNb and the PDMS–TMOS mixture with no intentional hydrolysis (HLaNb–PDMS–TMOS) and (b) the reaction product of the *n*-decoxy derivative of HCaNb and the PDMS–TMOS mixture with no intentional hydrolysis (HCaNb–PDMS–TMOS).

We further investigated the interface of organic–inorganic hybrids prepared from the *n*-decoxy derivatives, PDMS and TMOS without intentional hydrolysis, HLaNb–PDMS–TMOS and HCaNb–PDMS–TMOS. When crude reaction products from the *n*-decoxy derivative and the PDMS–TMOS mixture were washed with THF without the addition of any water, the XRD patterns of the resulting products showed new reflections at ca. 4.6 nm (HLaNb) and ca. 5.1 nm (HCaNb), as shown in Figure 4. These interlayer distances could not be determined precisely since the broad reflections are expected to be composed of overlapping reflections with different interlayer distances, as indicated by a shoulder appearing at 2.8° in HLaNb–PDMS–TMOS. The presence of the (100) reflections at 28.8° (HLaNb–PDMS–TMOS) and 29.1° (HCaNb–PDMS–TMOS) indicates the preservation of perovskite-like slab structures. These results exhibit the presence of a stacking order along the *c* axis before intentional hydrolysis.

Solid-state ^{13}C CP/MAS NMR spectra of HLaNb–PDMS–TMOS and HCaNb–PDMS–TMOS are shown in Figure 5. No signals due to *n*-decoxy groups are observed, a result similar to the reactions with PDMS. Instead, the signals of methyl groups in the PDMS chains, a [(*C*H$_3$)$_2$-SiO] environment (1 ppm),[30] and methoxy groups originating from TMOS, an [≡Si(O*C*H$_3$)] environment (51 ppm), are detected. These results indicate that the *n*-decoxy groups on the interlayer surface are completely removed before the intentional hydrolysis.

Solid-state ^{29}Si CP/MAS NMR spectra of HLaNb–PDMS–TMOS and HCaNb–PDMS–TMOS are shown in Figure 7. Both the spectra exhibit D^2-Q (−19 ppm), D^2 (−22 ppm), Q^1 [(RO)$_3$*Si*(OSi)] (R = H, CH$_3$) (−85 ppm), Q^2 [(RO)$_2$*Si*(OSi)$_2$] (−93 ppm), Q^3 (−101 ppm), and Q^4 (−108 ppm) environments, indicating the formation of a polysiloxane network via hydrolysis–condensation, probably initiated by water present as an impurity and/or produced by condensation of a part of PDMS.[16,29] Signals due to the Q^1 and Q^2 environments are observed in the products without intentional hydrolysis, while the polysiloxane network of the hydrolyzed products, *hydrolyzed* HLaNb–PDMS–TMOS and *hydrolyzed* HCaNb–PDMS–TMOS, consists of Q^3 and Q^4 environments only, indicating that the Q units are in a highly condensed state after intentional hydrolysis. In addition, broad shoulders are detected at around −5 ppm, presenting clear evidence for the presence of the (SiO)-*Si*(CH$_3$)$_2$O–Nb environment in the hybrids.[30] The products without intentional hydrolysis, HLaNb–PDMS–TMOS and HCaNb–PDMS–TMOS, can therefore be classified as graft-type class II hybrids.

Mechanism of the Reaction between Layered Perovskites and the PDMS-TMOS Mixture. We first discuss the reaction of the *n*-decoxy derivative of HLaNb (or HCaNb) with PDMS. The Nb–O–Si bonds are formed by the reaction between ≡SiOH groups of PDMS and the surface of perovskite-like slabs, as shown in the ^{29}Si CP/MAS NMR spectra of the products, HLaNb–PDMS and HCaNb–PDMS. When we attempted a reaction between an *n*-decoxy derivative of HLaNb and trimethylsilyl-terminated poly(dimethylsiloxane), {(CH$_3$)$_3$SiO[Si(CH$_3$)$_2$O]$_m$Si(CH$_3$)$_3$}, the XRD pattern of the product showed reflections due to an *n*-decoxy derivative of HLaNb only, indicating that no intercalation nor exfoliation occurs; the ≡SiOH groups are required for the reaction between an *n*-decoxy derivative and PDMS.

Reactions between *n*-decoxy derivatives and PDMS are, therefore, expected to be similar to those between *n*-alkoxy derivatives and alcohols, the so-called alcohol-exchange-type reactions,[25,27,28] that require the presence of water in the system. Since water must be present as an impurity and/or produced by condensation between the ≡SiOH groups of PDMS in the present system, the reaction is expected to proceed in two steps: a part of the (*n*-C$_{10}$H$_{21}$O)NbO$_5$ group is hydrolyzed to form an (HO)NbO$_5$ site, and the subsequent

reaction between the $(HO)NbO_5$ site and PDMS leads to the formation of $\{-O[Si(CH_3)_2O]_{n-1}\}-Si(CH_3)_2O-NbO_5$ groups. The reaction between an *n*-decoxy derivative and PDMS can therefore be expressed as follows:

$$(n\text{-}C_{10}H_{21}O)NbO_5 + H_2O \rightarrow (HO)NbO_5 + n\text{-}C_{10}H_{21}OH \quad (1)$$

$$\{-O[Si(CH_3)_2O]_{n-1}\}-Si(CH_3)_2OH + (HO)NbO_5 \rightarrow \{-O[Si(CH_3)_2O]_{n-1}\}-Si(CH_3)_2O-NbO_5 + H_2O \quad (2)$$

The products of the reaction between an *n*-decoxy derivative of HLaNb (or HCaNb) and PDMS–TMOS mixture without intentional hydrolysis, HLaNb–PDMS–TMOS and HCaNb–PDMS–TMOS, also possess Nb–O–Si bonds, as shown in their ^{29}Si CP/MAS NMR spectra, indicating that the reaction mechanism is very similar to that between an *n*-alkoxy derivative of HLaNb (or HCaNb) and PDMS. Since the Nb–O–Si bonds are stable against hydrolysis,[4] the Nb–O–Si bonds, once formed in the products of a reaction between an *n*-decoxy derivative of HLaNb (or HCaNb) and PDMS–TMOS mixture before intentional hydrolysis (see previous section "Interfaces Formed between Perovskite-like Slabs and the Polysiloxane Network"), should be preserved in the exfoliated hybrids prepared via intentional hydrolysis, *hydrolyzed* HLaNb–PDMS–TMOS and *hydrolyzed* HCaNb–PDMS–TMOS. The exfoliated hybrids, *hydrolyzed* HLaNb–PDMS–TMOS and *hydrolyzed* HCaNb–PDMS–TMOS, should consequently also be classified as class II hybrids.

Based on a report on a reaction between PDMS and tetraethoxysilane (TEOS),[15] cohydrolysis between PDMS and TEOS leads to the formation of a silica-like region, which provides cross-linking points. Since the solid-state ^{29}Si CP/MAS NMR spectra of *hydrolyzed* HLaNb–PDMS–TMOS and *hydrolyzed* HCaNb–PDMS–TMOS are very similar to those of cohydrolysis products from PDMS–TEOS mixtures (not shown), silica-like regions providing a cross-linking point are also expected to be present in *hydrolyzed* HLaNb–PDMS–TMOS and *hydrolyzed* HCaNb–PDMS–TMOS.

The interactions of Q^n environments with the *n*-decoxy derivatives are also investigated through the reaction between *n*-decoxy derivative of HLaNb and TMOS without intentional hydrolysis. An XRD pattern of the product of a reaction between the *n*-decoxy derivative of HLaNb and TMOS without intentional hydrolysis showed a decrease in the interlayer distance from 2.73 to 1.46 nm. Solid-state ^{13}C CP/MAS NMR spectroscopy showed the presence of no *n*-decoxy groups. The solid-state ^{29}Si CP/MAS NMR spectrum of the product showed signals due to the Q^1 and Q^2 environment, indicating the formation of oligomeric and/or polymeric polysiloxane through hydrolysis–condensation of TMOS by impurity water. These results indicate that TMOS molecules and/or silicate polymer derived from TMOS can be intercalated into the interlayer space of HLaNb. We cannot find spectroscopic evidence, however, for the presence of Nb–O–Si bonds formed by the reaction involving *n*-decoxy derivative of HLaNb and TMOS only, mainly because no clear shift of ^{29}Si NMR signals has been reported upon the formation of M–O–Si bonds.

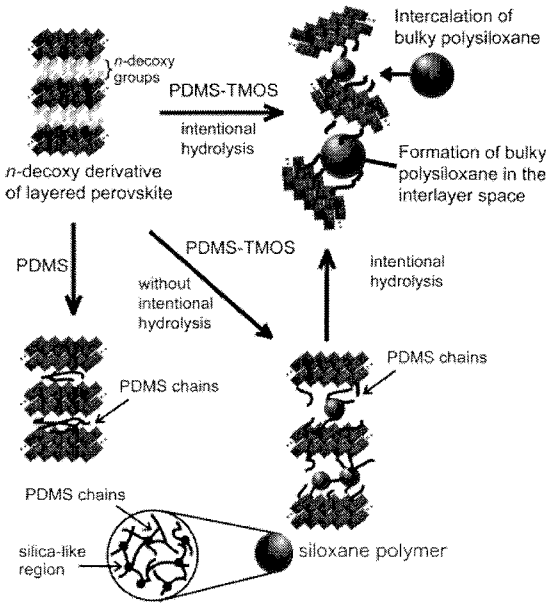

Figure 8. Proposed model for exfoliation behavior.

Exfoliation Behavior of Layered Perovskites. The XRD patterns and TEM images of hydrolyzed products, *hydrolyzed* HLaNb–PDMS–TMOS and *hydrolyzed* HCaNb–PDMS–TMOS, show that the stacking order disappears along the *c* axis (a characteristic typically observed with exfoliated hybrids[32]), while the products without intentional hydrolysis, HLaNb–PDMS–TMOS and HCaNb–PDMS–TMOS, possess a stacking order along the *c* axis (graft-type hybrids). Since intentional hydrolysis leads to the formation of a condensed polysiloxane network, the intercalation of condensed polysiloxane and/or development of a polysiloxane network in the interlayer space are expected to occur during intentional hydrolysis to induce exfoliation of the layered perovskite. Figure 8 demonstrates the proposed model for the exfoliation process.

When we attempted a reaction of HLaNb, or of an *n*-propoxy derivative of HLaNb possessing a smaller interlayer distance than that of the *n*-decoxy derivative of HLaNb, with PDMS, the XRD patterns of the reaction products showed a reflection due to unreacted HLaNb at 10.6° (1.05 nm) or *n*-propoxy derivative of HLaNb at 7.21° (1.54 nm) only, indicating no intercalation of PDMS in the interlayer space of HLaNb or the *n*-propoxy derivative of HLaNb. We also attempted a reaction of HLaNb or the *n*-propoxy derivative of HLaNb with the PDMS–TMOS mixture with subsequent intentional hydrolysis. The XRD pattern of the reaction product from HLaNb showed a reflection of HLaNb only at 10.6° (1.05 nm), indicating that the reaction did not occur. When the *n*-propoxy derivative of HLaNb was used as an intermediate, the XRD pattern showed a reflection at 10.2° (1.09 nm). Based on the interlayer distance of HLaNb (1.05 nm), this reflection at 10.2° seems to be assignable to HLaNb, suggesting that the *n*-propoxy groups on the interlayer surface are hydrolyzed to form HLaNb; the reaction between the *n*-propoxy derivative of HLaNb and

(32) Giannelis, E. P. *Adv. Mater.* **1996**, *8*, 29.

the PDMS−TMOS mixture also failed to occur. The use of an intermediate with a larger interlayer distance is consequently important for exfoliation of layered perovskites.

Conclusions

We have demonstrated a new sol−gel approach involving exfoliation of the *n*-decoxy derivatives of ion-exchangeable layered perovskites to prepare class II hybrids. Cohydrolysis of the *n*-decoxy derivative of an ion-exchangeable layered perovskite (HLaNb or HCaNb), PDMS, and TMOS by hydrochloric acid leads to the formation of organic−inorganic hybrids possessing exfoliated perovskite-like slabs, nanosheets with perovskite-related structures. Nb−O−Si covalent bonds, which bind PDMS chains to the exfoliated perovskite-like slabs, are formed during the reaction of an *n*-decoxy derivative of an ion-exchangeable layered perovskite with PDMS or a PDMS−TMOS mixture with no intentional hydrolysis process. Since the Nb−O−Si bonds are expected to be stable with respect to hydrolysis, the reaction products of the *n*-decoxy derivatives of ion-exchangeable layered perovskites with a PDMS−TMOS mixture with an intentional hydrolysis process should also be class II hybrids with an Nb−O−Si linkage interface. Since the product obtained with no intentional hydrolysis possesses the stacking order of perovskite-like slabs along the *c* axis, the hydrolysis process must induce the exfoliation of layered perovskites. Although class-I-type layered material/polymer hybrids created through exfoliation have been extensively studied, the present approach appears to be applicable to a variety of class II hybrids whose properties can be tuned by selecting appropriate nanosheets, as NBBs.

Acknowledgment. The authors thank Prof. Kazuyuki Kuroda of Waseda University, Department of Applied Chemistry, for his valuable discussions. This work was financially supported by the Grant-in-Aid for Scientific Research (No. 14350462) from the Ministry of Education, Science, Sports, and Culture, Japan, and by 21COE "Practical Nano-Chemistry" from MEXT, Japan.

CM0514793

Hydrosilylation of the CH_2=CH- Groups Immobilized on the Interlayer Surface of Ion-exchangeable Layered Perovskite with Hydorochlorosilanes and Oligosiloxanes

Seiichi Tahara[a], Kazuyoshi Ohta[a], Satoru Yoshioka[a], Yosuke Takeda[a], Yuko Uchimaru[b] and Yoshiyuki Sugahara[a,*]

[a] Department of Applied Chemistry, School of Science and Engineering, Waseda University, Ohkubo-3, Shinjuku-ku, Tokyo 169-8555, Japan

[b] National Institute of Advanced Industrial Science and Technology, AIST Tsukuba Central 5-2, Tsukuba, Ibaraki 305-8565, Japan

Abstract

The novel preparation of inorganic-organic hybrids using ion-exchangeable layered perovskite *via* hydrosilylation has been explored. The CH_2=CH- groups were immobilized on the interlayer surface through the alcohol-exchange-type reaction of an *n*-propoxy derivative of $HLaNb_2O_7 \cdot xH_2O$ (HLaNb) with 4-penten-1-ol or 9-decen-1-ol to form a $CH_2=CH(CH_2)_nO$-derivative of HLaNb (n = 3 or 8), and hydrosilylation of the CH_2=CH- groups of the $CH_2=CH(CH_2)_nO$- groups with SiH groups in hydrochlorosilanes, hydride-terminated polydimethylsiloxane (H-PDMS) or octahydridosilsesquioxane (OHSQ) was subsequently conducted. When the $CH_2=CH(CH_2)_nO$-derivative of HLaNb was reacted with dichloromethylsilane, trichlorosilane or H-PDMS, X-ray diffraction (XRD) patterns, infrared (IR) adsorption, and ^{13}C and ^{29}Si CP/MAS nuclear magnetic resonance (NMR) spectra showed the occurrence of hydrosilylation in the interlayer space. Although the XRD pattern of the reaction product between the $CH_2=CH(CH_2)_8O$-derivative of HLaNb and OHSQ did not show a notable increase in interlayer distance, the IR and ^{13}C and ^{29}Si CP/MAS NMR spectra suggested the occurrence of hydrosilylation. The occurrence of hydrosilylation between the CH_2=CH- groups and OHSQ in the interlayer space was also indicated by a comparison of the pyrolysis behavior of the reaction product from the $CH_2=CH(CH_2)_8O$-derivative of HLaNb and OHSQ with those of HLaNb and the pyrolyzed $CH_2=CH(CH_2)_8O$-derivative of HLaNb. These results clearly demonstrate that hydrosilylation in the interlayer space could potentially be a new method of

preparing the various organic derivatives of ion-exchangeable layered perovskites.

Introduction

Extensive research on the preparation of inorganic-organic hybrids has been conducted with a focus on to achievement of novel structures, compositions and tunable properties.[1-8] The preparation of inorganic-organic hybrids has been widely studied employing various techniques, including intercalation [1,7-10] and the sol-gel process.[3,5,6] "Intercalation" is utilized to accommodate organic ions and/or molecules in the interlayer space of layered compounds to form intercalation compounds, which consist of alternatively stacked inorganic nano-sheets and layers of organic ions/molecules. Since the intercalation compounds exhibit not only photofunctional properties[7,8] and anisotropic electro/ion conductivities[1,11,12] based on the properties of guest ions/molecules but also enhanced properties based on the inorganic sheets[13] and adsorptive properties[7,8], various functional organic ions/molecules have been intercalated in the interlayer space. The interfaces between interlayer surfaces and organic ions and/or molecules generally consist of weak interactions such as ionic bonds and hydrogen bonds. The organic ions/molecules are therefore easily removed under appropriate conditions. Some layered compounds can bind organic and organometallic groups on the interlayer surface by covalent bonds, on the other hand, through "grafting" reactions to form stable interfaces. Layered polysilicate can react with chlorosilanes or alkoxysilanes to form Si-O-Si bonds,[14,15] for expamle, and kaolinite can react with alcohols to form Al-O-C bonds.[16,17] In addition, immobilization of organic or organometallic groups is reported for FeOCl[18] and zirconium phosphate.[19]

Perovskite and perovskite-related compounds are interesting materials, since these compounds exhibit magnetic,[20] dielectric[21,22] and optical properties,[23] which originate in the perovskite-related structure and the composition. Ion-exchangeable layered perovskites consist of interlayer cations, M, and perovskite-like slabs, $[A_{m-1}B_mO_{3m+1}]$, (such as $[LaNb_2O_7]$ where A = La, B = Nb and m = 2.)[24] Perovskite-like slabs, $[A_{m-1}B_mO_{3m+1}]$, possess a (100) sliced perovskite structure with an A-site cation coordinated by 12 oxygen atoms and a B-site cation positioned at the center of the BO_6 octahedra. The thickness of the perovskite-like slab

is expressed by m. Based on the number of exchangeable cations, M, per $[A_{m-1}B_mO_{3m+1}]$, ion-exchangeable layered perovskites can be classified into two phases: Dion-Jacobson phases, $M[A_{m-1}B_mO_{3m+1}]$, and Ruddlesden-Popper phases, $M_2[A_{m-1}B_mO_{3m+1}]$.[24] Acid treatment of these phases easily leads to formation of the protonated forms of ion-exchangeable layered perovskites, $H[A_{m-1}B_mO_{3m+1}]$ and $H_2[A_{m-1}B_mO_{3m+1}]$. The protonated forms of ion-exchangeable layered perovskites have been reported to exhibit photocatalytic activities[25,26] and proton conductivities.[27]

Intercalation of organic bases into the protonated forms of ion-exchangeable layered perovskites *via* acid-base reactions has been attracting attention, since the intercalation compounds could exhibit enhanced properties based on the perovskite-related structures.[24] Intercalation of *n*-alkylamine into $HSr_2Nb_3O_{10}$ leads, for example, to excellent fatigue behavior of the dielectric properties.[28] Dion-Jacobson type niobates, $HLaNb_2O_7 \cdot xH_2O$ (HLaNb) and $HCa_2Nb_3O_{10} \cdot xH_2O$ (HCaNb), on the other hand, can react with *n*-alcohols to form *n*-alkoxy derivatives of HLaNb and HCaNb possessing Nb-O-C covalent bonds.[29-31] These *n*-alkoxy derivatives of HLaNb and HCaNb are stable compared to the intercalation compounds, since covalent bonds are more stable than ionic and hydrogen bonds. The reactions of *n*-alkoxy derivatives of HLaNb with other alcohols, such as *sec*-alcohol and alkanediol, lead to the formation of organic derivatives of HLaNb through alcohol-exchange-type reactions.[32] Although the alcohol-exchange-type reactions enable us to prepare additional organic derivatives, bulky alcohols, such as *tert*-alcohol, are grafted onto the interlayer surface only partially. These facts suggest that an additional method for binding organic molecules in the interlayer space of layered perovskites is required.

Hydrosilylation has been well known for decades in silicon chemistry and industry.[33-35] For hydrosilylation, transition metal complex catalysts, such as chloroplatinic acid and $Pt_2(dvs)_3$ (dvs = 1,3-divinyl-1,1,3,3-tetramethyl-1,3-disiloxane), are used to obtain hydrosilylated products with high yields. Hydrosilylation of CH_2=CHR groups with ≡SiH groups generally proceeds to give a large amount of $\equiv SiCH_2CH_2R$ *via* β-addition, but the structure of hydrosilane compounds, the R group in CH_2=CHR groups and the selection of catalysts could affect the distribution of adducts formed *via* α- and β-addition.[33,36] Since hydrosilylation usually forms no by-products, it is applied extensively to surface modification of solids possessing ≡SiH and CH_2=CH- groups on their surface to form inorganic-organic hybrids.

Hydrosilylation has therefore been applied extensively to surface modification of solids possessing SiH and CH_2=CH- groups on their surfaces.[37-39] In addition, hydrosilylation between alkenyl groups bound on the interlayer surface and pentametyldisiloxane using a layered mineral, appophlite, has been also reported.[40,41] Application of hydrosilylation to appropriate organic group (such as CH_2=CH-, CH≡C- and SiH groups) immobilized on the interlayer surface of ion-exchangeable layered perovskites is therefore expected to form new organic derivatives of ion-exchangeable layered perovskites.

Here, we report the immobilization of CH_2=CH- groups in the interlayer space through a reaction between an *n*-propoxy derivative of HLaNb and 4-penten-1-ol or 9-decen-1-ol and subsequent hydrosilylation between CH_2=CH- groups immobilized on the interlayer surface of HLaNb and hydrochlorosilanes, $(CH_3)_{3-x}(H)SiCl_x$ (x = 2, 3),[42] hydride-terminated polydimethylsiloxane (H-PDMS), $HSi(CH_3)_2O$-$[Si(CH_3)_2O]_n$-$(CH_3)_2SiH$, and octahydridosilsesquioxane (OHSQ), $H_8Si_8O_{12}$. (Scheme 1) Successful formation of these hydrosilylated products indicates that hydrosilylation is a versatile method for the preparation of novel inorganic-organic hybrids.

Scheme 1

Experimental section

Instrumentation. The X-ray diffraction (XRD) patterns of the products were recorded on a Mac Science M03XHF[22] diffractometer with Mn-filtered FeK_α radiation. The solid-state ^{13}C and ^{29}Si nuclear magnetic resonance (NMR) spectra were obtained using a JEOL CMX-400 spectrometer operated at 100.54 MHz (^{13}C) and 79.427 (^{29}Si) MHz with cross-polarization (CP) and magic angle spinning (MAS) techniques. The contact time was 1.5 ms (^{13}C) and 5 ms (^{29}Si). The sample spinning rate was about 5 kHz and the pulse delay was 5 s. In the solid-state ^{29}Si MAS NMR measurement without cross-polarization techniques, the pulse delay was set for 250 s. The infrared (IR) adsorption spectra of the reaction products were recorded with a Perkin-Elmer Spectrum One instrument or a JASCO FT/IR-460 Plus instrument with KBr disc techniques. The amounts of carbon were determined by an internal service at the Waseda University Materials Characterization Center. The Si/Nb ratios of the products

were determined by X-ray fluorescence (XRF) (Rigaku RIX-2100) analysis employing the fundamental parameter method.

Starting Materials. $RbLaNb_2O_7$ and $HLaNb_2O_7 \cdot xH_2O$ were prepared based on the previous reports.[32,43] A mixture of Rb_2CO_3, La_2O_3 and Nb_2O_5 (with 30-mol% excess amount of Rb_2CO_3) was calcined at 1200°C for 48 h with intermittent grinding after 24 h . After calcination, the product was washed with distilled water to remove the residual Rb and dried at 120°C. The XRD pattern of the product was indexed for a tetragonal cell with a = 0.3888(4) nm and c = 1.0991(6) nm, parameters consistent with the previous report (a = 0.3885(2) nm and c = 1.0989(3) nm).[43] Inductively coupled plasma emission spectrometry (ICP) showed that the cation ratio of the product was consistent with $RbLaNb_2O_7$. To prepare $HLaNb_2O_7 \cdot xH_2O$ (HLaNb), $RbLaNb_2O_7$ was treated with 6 mol/L HNO_3 at 60°C for 3 d. After acid treatment, the product was centrifuged, washed with distilled water and dried at ambient temperature. The XRD pattern of the product after drying at 120°C was indexed for a tetragonal cell with a = 0.3896(5) nm and c = 1.045(1) nm, parameters consistent with the reported values for anhydrous $HLaNb_2O_7$ (a = 0.3894(3) nm and c = 1.0479(7) nm).[43] ICP showed that all the Rb ions were essentially removed by acid treatment and that the La/Nb ratio was consistent with $HLaNb_2O_7$. The amount of protons estimated by thermogravimetry (TG) was 1.0 per $[LaNb_2O_7]$.

For the preparation of an *n*-propoxy derivative of HLaNb, 3 g of HLaNb were typically refluxed with a mixture of *n*-propanol and distilled water (10mass% of water) for 3 d.[32] After centrifugation, the product was washed with acetone and dried at room temperature. The XRD pattern of the product was assigned to the *n*-propoxy derivative of HLaNb with lattice parameters, a = 0.389(1) nm and c = 1.540(3) nm. The solid-state ^{13}C CP/MAS NMR spectrum of the product exhibited a signal at 80 ppm, which was indicative of the formation of Nb-O-C bonds.[32] All the analytical results indicated that an *n*-propoxy derivative of HLaNb was obtained.[32]

Trichlorosilane was supplied by Tokyo Kasei Kogyo Co., and dichloromethylsilane and H-PDMS, $HSi(CH_3)_2O$-$[Si(CH_3)_2O]_n$-$(CH_3)_2Si$-H (number average molecular weight, M_w, = 580 and $n \approx 6$) and $Pt_2[(CH_2{=}CH(CH_3)_2Si)_2O]_3$ (0.1M in xylene) were purchased from Aldrich. Trichlorosilane and dichloromethylsilane were distilled under reduced pressure. Toluene, *n*-hexane and tetrahydrofuran were

supplied by Kanto Kagaku Co. Methanol, $FeCl_3$, $CaCl_2$, *p*-xylene and $H_2PtCl_6 \cdot 6H_2O$ were purchased from Wako Pure Chemical Industries. Distillation of toluene, *p*-xylene and tetrahydrofuran was performed with sodium and benzophenone.

Octahydridosilsesquioxane (OHSQ) was prepared under a protective nitrogen atmosphere based on the previous report.[44] Typically, 50 g of anhydrous $FeCl_3$, 20 mL of 12 mol/L HCl, 40 mL of methanol, 350 mL of *n*-hexane and 50 mL of toluene were mixed in a round-bottomed flask. This suspension was stirred vigorously with a mechanical stirrer. A mixture of trichlorosilane (25 mL) and *n*-hexane (150 mL) was added dropwise to the suspension over a period of 9 h. After an additional 30-min stirring, the suspension was filtered to remove $FeCl_3$. Fourteen g of K_2CO_3 and 10 g of $CaCl_2$ were then added to the filtrated solution and stirred overnight. The solution was filtrated and the solvent was removed under reduced pressure to obtained a crude product. The crude product was recrystallized from a mixture of 20 mL of tetrahydrofuran and 30 mL of *n*-hexane and washed with *n*-hexane. The ^1H NMR spectrum (C_6D_6) of the product showed the presence of a signal at 4.2 ppm. The ^{29}Si NMR (C_6D_6) spectrum (DEPT) showed a signal at –84 ppm assignable to an $H\underline{Si}(OSi)_3$ environment. These NMR results indicated the formation of OHSQ.[45] In addition, the IR spectrum of the product showed the presence of a weak band at 3416 cm^{-1} due to the $\nu_{(OH)}$ mode, indicating the formation of impurities containing the ≡SiOH group.

Immobilization of 4-penten-1-ol and 9-decen-1-ol on the interlayer surface of $HLaNb_2O_7 \cdot xH_2O$ (HLaNb). For the reaction between the *n*-propoxy derivative of HLaNb and 4-penten-1-ol, 1.3 g of the *n*-propoxy derivative of HLaNb and 40 mL of 4-penten-1-ol were sealed in a glass ampoule and heated at 80°C for 7 d. After centrifugation, the product was washed with acetone and dried at ambient temperature (CH_2=$CH(CH_2)_3O$-HLaNb). For the reaction between the *n*-propoxy derivative of HLaNb and 9-decen-1-ol, 2 g of the *n*-propoxy derivative of HLaNb were reacted with 25 mL of 9-decen-1-ol in a glass ampoule at 80°C for 7 d. The product was centrifuged and washed with acetone. The product was dried at ambient temperature (CH_2=$CH(CH_2)_8O$-HLaNb).

Reaction of immobilized CH_2=CH- groups on the interlayer surface with hydrochlorosilanes, H-PDMS or OHSQ. The reaction procedures with

hydrochlorosilanes and OHSQ were performed using the standard Schlenk technique under a protective nitrogen atmosphere[46] or in a globe box filled with nitrogen.

For the reactions with hydrochlorosilanes, about 0.3 g of CH_2=$CH(CH_2)_3$O-HLaNb and 20 mL of $Cl_x(H)Si(CH_3)_{3-x}$ (x = 2, 3) were refluxed for 3 d. As a catalyst, $H_2PtCl_6 \cdot 6H_2O$ (as an acetonitrile solution) was added with a Pt/Si ratio of 5×10^{-4}. The resultant product was washed with *n*-hexane and dried under reduced pressure.

For the reaction with H-PDMS, about 0.3 g of CH_2=$CH(CH_2)_8$O-HLaNb and 17 mL of H-PDMS (with an approximate HSi≡/CH_2=$CH(CH_2)_8$O-molar ratio of 100) were stirred at 80°C for 10 d under a nitrogen atmosphere. CH_2=$CH(CH_2)_8$O-HLaNb was used after drying under reduced pressure for 1 h, and the water was removed from H-PDMS using molecular sieves 3A before use. As a catalyst, $Pt_2[(CH_2=CH(CH_3)_2Si)_2O]_3$ (as a *p*-xylene solution) was added with a Pt/CH_2=CH- ratio of 5×10^{-2}. After centrifugation, the resultant product was washed with *p*-xylene and tetrahydrofuran and dried under reduced pressure.

For the reaction with OHSQ, about 0.3 g of CH_2=$CH(CH_2)_8$O-HLaNb and 0.4 g of OHSQ (with an approximate $H_8Si_8O_{12}$/CH_2=$CH(CH_2)_8$O- molar ratio of 2) were refluxed in toluene at 110°C for 10 d. CH_2=$CH(CH_2)_8$O-HLaNb and OHSQ were used after drying under reduced pressure for 1 h. As a catalyst, $H_2PtCl_6 \cdot 6H_2O$ was added with a Pt/CH_2=CH- ratio of about 5×10^{-2}. The resultant product was washed with *p*-xylene and tetrahydrofuran and dried under reduced pressure.

The pyrolysis of HLaNb, CH_2=$CH(CH_2)_8$O-HLaNb and the reaction product of CH_2=$CH(CH_2)_8$O-HLaNb with OHSQ using a tube furnace was performed at 350°C and 400°C for 10 min in air with a heating rate of 5°C/min.

Results and Discussions

Immobilization of 4-penten-1-ol and 9-decen-1-ol on the interlayer surface of $HLaNb_2O_7 \cdot xH_2O$ (HLaNb). The XRD patterns of the *n*-propoxy derivative of HLaNb and the products of the *n*-propoxy derivative of HLaNb with 4-penten-1-ol and 9-decen-1-ol are shown in Figure 1 (CH_2=$CH(CH_2)_3$O-HLaNb) and Figure 2 (CH_2=$CH(CH_2)_8$O-HLaNb). The *d* values for the low-angle reflections correspond to the interlayer distances. The interlayer distance increases from 1.53 nm to 1.85

(4-penten-1-ol) or 2.67 nm (9-decen-1-ol). The (100) reflections at $2\theta = 28.8°$, reflecting the crystal structure of the perovskite-like slabs, do not shift after the reactions, thus indicating the preservation of the perovskite-like slab structure.

Figure 1

Figure 2

The IR spectra of the products, $CH_2=CH(CH_2)_3O$-HLaNb and $CH_2=CH(CH_2)_8O$-HLaNb, are shown in Figure 3 and Figure 4, respectively. The IR spectrum of $CH_2=CH(CH_2)_3O$-HLaNb shows new bands at 3074 and 1641 cm^{-1}. These bands are assignable to the $\nu_{(CH)}$ mode (3074 cm^{-1}) and the $\nu_{(C=C)}$ (1640 cm^{-1}) mode of the $CH_2=CH$- groups. In the IR spectrum of $CH_2=CH(CH_2)_8O$-HLaNb, the $\nu_{(CH)}$ band (3075 cm^{-1}) and $\nu_{(C=C)}$ band (1640 cm^{-1}) of the $CH_2=CH$- groups are observed in a similar fashion.

Figure 3

Figure 4

The ^{13}C CP/MAS NMR spectra of the *n*-propoxy derivative of HLaNb and its reaction products with 4-penten-1-ol and 9-decen-1-ol are shown in Figure 5 ($CH_2=CH(CH_2)_3O$-HLaNb) and Figure 6 ($CH_2=CH(CH_2)_8O$-HLaNb). The A, B and C signals in the spectrum of the *n*-propoxy derivative of HLaNb are assigned to *n*-propoxy groups (Figure 5-a). The spectra of both $CH_2=CH(CH_2)_3O$-HLaNb and $CH_2=CH(CH_2)_8O$-HLaNb show the disappearance of these signals due to the *n*-propoxy groups. New signals at 31 (signal F), 33 (signal G), 80 (signal H), 115 (signal D) and 140 (signal E) ppm appear in the spectrum of $CH_2=CH(CH_2)_3O$-HLaNb, on the other hand, and are assignable to the $CH_2=CH(CH_2)_3O$- groups, as shown in Figure 5(b). The spectrum of $CH_2=CH(CH_2)_8O$-HLaNb also shows new signals at 28 (signal O), 31 (signal M), 32 (signal N), 34 (signal P), 35 (signal L), 80 (signal Q), 115 (signal J) and 139 (signal K). These signals can be assigned to the $CH_2=CH(CH_2)_8O$- groups, as shown in Figure 6-a. The chemical shifts for the carbon atoms attached to oxygen atoms (-$\underline{C}H_2O$-) are 80 ppm for both of the reaction products with 4-penten-1-ol and 9-decen-1-ol. The typical chemical shifts in liquid-state ^{13}C NMR spectra of 4-penten-1-ol and 9-decen-1-ol molecules, on the contrary, were 62 and 63

ppm, respectively, and downfield shifts for the -$\underline{C}H_2O$- environments were reported to be indicative of the formation Nb-O-C bonds.[30] With increases in the interlayer distances and IR results taken into account, the ^{13}C CP/MAS NMR results provide sufficient evidence for the successful immobilization of 4-penten-1-ol or 9-decen-1-ol on the interlayer surface.

Figure 5

Figure 6

The amounts of the $CH_2=CH(CH_2)_nO$- groups are estimated from the carbon contents, 9.96 ($CH_2=CH(CH_2)_4O$-) and 19.23 mass% ($CH_2=CH(CH_2)_4O$-). Thus, the amount of the $CH_2=CH(CH_2)_4O$- groups is 0.81per [$LaNb_2O_7$] and that of the $CH_2=CH(CH_2)_8O$- groups is 0.90 per [$LaNb_2O_7$].

Hydrosilylation of $CH_2=CH(CH_2)_3O$-HLaNb with hydrochlorosilanes. The XRD patterns of the reaction products of $CH_2=CH(CH_2)_3O$-HLaNb with hydrochlorosilanes are shown in Figure 1. The XRD patterns of the reaction products with dichloromethylsilane, [$CH_3(H)SiCl_2$], and trichlorosilane, ($HSiCl_3$), show the disappearance of the reflection due to $CH_2=CH(CH_2)_3O$-HLaNb, and new low-angle reflections at d = 2.41 nm (trichlorosilane) and d = 2.07 nm (trichlorosilane) are observed. In addition, these XRD patterns of the products with dichloromethylsilane and trichlorosilane show (100) reflections at 28.8°, indicating preservation of the perovskite-like slab structure after the reactions. We also attempted a reaction with dimethylchlorosilane [$(CH_3)_2(H)SiCl$], but the XRD pattern of the reaction product (not shown) showed a low-angle reflection corresponding to the interlayer distance of $CH_2=CH(CH_2)_3O$-HLaNb at d = 1.85 nm with a very weak shoulder at d = 2.43 nm, indicating much lower reactivity, which seems to be ascribable to an electronic effect of the chlorine substitute on the hydrosilanes.[35,47]

The solid-state ^{13}C CP/MAS NMR spectra of the reaction products with hydrochlorosilanes are shown in Figure 5. In the spectrum of the reaction product with dichloromethylsilane, the signals due to the $CH_2=CH$- groups disappear and new signals appear at 4 (signal I), 21 (signal D'), 27 (signal E'), 30 (signal F' and G') and 82 (signal H') ppm. These signals are assignable to carbon atoms in an expected hydrosilylated product, [$CH_3(Cl)_2Si(CH_2)_5$-O-Nb], as shown in Figure 5-c. In a similar

fashion, the signals due to the CH_2=CH- groups disappear in the spectrum of the reaction product with trichlorosilane, and new signals appear at 22 (signal D''), 27 (signal E''), 31 (signal F'' and G'') and 83 (signal H'') ppm. These signals are assignable to carbon atoms in an expected hydrosilylated product, [$Cl_3Si(CH_2)_5$-O-Nb], as shown in Figure 5-d. No signals assignable to α-addition-type hydrosilylated products are detected, indicating the occurrence of β-addition only.

The IR spectra of the reaction products with hydrochlorosilanes are shown in Figure 3. In a spectrum of the reaction product with dichloromethylsilane, a new band is observed at 1259 cm^{-1}, which is assignable to the $\delta_{(Si\text{-}CH_3)}$ mode.[48] Both the spectra show the disappearance of the $\nu_{(CH)}$ mode of the CH_2=CH- groups, indicating the occurrence of hydrosilylation. In addition, both the spectra show the $\nu_{(SiH)}$ band at 2160 cm^{-1} (dichloromethylsilane) or at 2238 and 2248 cm^{-1} (trichlorosilane).[48] In the spectrum of the reaction product with trichlorosilane, a weak shoulder assignable to the $\nu_{(Si\text{-}O\text{-}Si)}$ mode is detected at 1039 cm^{-1}. The presence of the $\nu_{(SiH)}$ and $\nu_{(Si\text{-}O\text{-}Si)}$ bands is discussed below.

Figure 7 shows the solid-state ^{29}Si CP/MAS NMR spectra of the reaction products with hydrochlorosilanes. Both the spectra show signals assignable to expected hydrosilylation products, a $Cl_2(CH_3)\underline{Si}CH_2$- environment at 33 ppm (dichloromethylsilane) and a $Cl_3\underline{Si}CH_2$- environment at 14 ppm (trichlorosilane),[49] which are consistent with solid-state ^{13}C CP/MAS NMR results. Some additional signals are also observed, however, in upfield regions of both of the spectra. In the solid-state ^{29}Si CP/MAS NMR spectrum of the reaction product with dichloromethylsilane, the signals at 6, –20 and –35 ppm are ascribable to the $CH_3\underline{Si}(O\text{-})_2CH_2$-, $(CH_3)Cl\underline{Si}(O\text{-})CH_2$- and $H(CH_3)\underline{Si}(O\text{-})_2$ environments, respectively. The solid-state ^{29}Si CP/MAS NMR spectrum of the reaction product with trichlorosilane shows signals at –35, –62 and –86 ppm, which can be assigned to the $H\underline{Si}Cl_2(O\text{-})$, $H\underline{Si}Cl(O\text{-})_2$ and $H\underline{Si}(O\text{-})_3$ environments, respectively. These environments observed in both the spectra indicate the occurrence of hydrolysis and condensation reactions to form siloxane bonds, which are consistent with the presence of the $\nu_{(Si\text{-}O\text{-}Si)}$ band observed in the IR results. In addition, ≡Si-H groups are present in the silyl groups formed by the hydrolysis and condensation reactions without hydrosilylation. These results are consistent with the observation of the $\nu_{(SiH)}$ bands in the IR spectra of the reaction products with dichloromethylsilane and trichlorolsilane. The hydrolysis

and condensation reaction is expected to occur during the synthesis and/or washing procedure with impurity water, since the ≡SiCl groups are very moisture-sensitive.

Figure 7

Hydrosilylation of CH_2=CH$(CH_2)_8$O-HLaNb with H-PDMS. The XRD pattern of the reaction product of CH_2=CH$(CH_2)_8$O-HLaNb with H-PDMS, HSi$(CH_3)_2$O-[Si$(CH_3)_2$O]$_n$-$(CH_3)_2$Si-H ($n \approx 6$), is shown in Figure 2. The XRD pattern of the reaction product with H-PDMS shows the disappearance of the reflection of CH_2=CH$(CH_2)_8$O-HLaNb, and new broad reflections are observed at d = 3.33 nm and d = 1.61 nm. These reflections are indexed as (001) and (002), respectively, to give an approximate interlayer distance of ca. 3.3 nm. The interlayer distance is not determined precisely, however, since weak reflections at ca. 9.1° (ca. 1.2 nm) and ca. 12.1° (ca. 0.92 nm) (marked by arrows) overlap, indicating that the reaction product with H-PDMS is conposed of compounds with different interlayer distances. Preliminary analysis of the BET specific surface area of CH_2=CH$(CH_2)_8$O-HLaNb and the reaction product of CH_2=CH$(CH_2)_8$O-HLaNb with H-PDMS also showed non-porous features for these products. The (100) reflection at 28.8° is observed at the same position, indicating preservation of the perovskite-like slab structure.

The IR spectrum of the reaction product of CH_2=CH$(CH_2)_8$O-HLaNb with H-PDMS is shown in Figure 4. Bands are observed at 1260 cm^{-1} and 1090–1020 cm^{-1} due to the $\delta_{(Si\text{-}CH_3)}$ and $\nu_{(Si\text{-}O\text{-}Si)}$ modes of the PDMS chain,[50] while the band due to the $\nu_{(SiH)}$ mode of H-PDMS at 2160 cm^{-1} disappears (Figures 4-b and -c). The band due to the $\nu_{(CH)}$ mode of the CH_2=CH- groups at 3074 cm^{-1} is also not observed. These observations suggest the occurrence of hydrosilylation.

The solid-state ^{13}C CP/MAS NMR spectrum of the reaction product of CH_2=CH$(CH_2)_8$O-HLaNb with H-PDMS is shown in Figure 6. Signals at 115 and 139 ppm due to the $\underline{C}H_2$=CH(CH_2)- and CH_2=$\underline{C}$H(CH_2)- groups disappear, and new signals appear at 18 (signal J') and 24 (signal K') ppm. These new signals can be assigned to the -OSi$(CH_3)_2\underline{C}H_2CH_2$- (18 ppm) and -OSi$(CH_2)_2CH_2\underline{C}H_2$- (24 ppm) environments,[51] providing additional evidence for the occurrence of β-addition-type hydrosilylation.

The solid-state ^{29}Si CP/MAS NMR spectrum of the reaction product of

CH_2=$CH(CH_2)_8$O-HLaNb with H-PDMS is shown in Figure 8. A new signal at –22 ppm is assignable to a $(CH_3)_2\underline{Si}(OSi)_2$ environment of the PDMS chains.[49] Another new signals at 8 ppm can be assigned to a $(CH_3)_2\underline{Si}(OSi)CH_2$- environment (signal B'),[49] which is consistent with the occurrence of hydrosilylation. The $H(CH_3)_2\underline{Si}(OSi)$- environment (signal B) at –7 ppm is not detected, moreover, indicating that all the SiH groups in H-PDMS are involved in the hydrosilylation with immobilized CH_2=CH- groups. The additional weak signals at 2 and 29 ppm (marked by asterisks) could not be assigned so far.

Figure 8

The expansion of the interlayer distance demonstrated by the XRD results and the presence of the $\delta_{(Si\text{-}CH_3)}$ and $\nu_{(Si\text{-}O\text{-}Si)}$ modes of the PDMS chains in the IR spectra indicate the presence of PDMS chains in the interlayer space of HLaNb. The disappearance of the $\nu_{(SiH)}$ band suggests, moreover, that all the SiH groups attached to the PDMS chains are involved in hydrosilylation. The proposed reactions are illustrated as Scheme 2 and can also be expressed by the following equation:

$$2\{CH_2{=}CH(CH_2)_8\text{-}\}_{0.9}H_{0.1}\text{-}[LaNb_2O_7] + x HSi(CH_3)_2O\text{-}[Si(CH_3)_2O]_n\text{-}(CH_3)_2SiH \rightarrow [LaNb_2O_7]H_{0.1}[\text{-}(CH_2)_8\text{-}CH{=}CH_2]_{0.9-x}\{\text{-}(CH_2)_{10}\text{-}Si(CH_3)_2O\text{-}[(CH_3)_2SiO]_n(CH_3)_2Si\text{-}(CH_2)_{10}\text{-}\}_x[CH_2{=}CH(CH_2)_8\text{-}]_{0.9-x}H_{0.1}[LaNb_2O_7] \quad (1)$$

Scheme 2

Although the intercalation compound with polymers generally exhibits its own uniform interlayer distances,[1] XRD analysis demonstrates that the interlayer distance is not uniform. The absence of a uniform interlayer environment seems to be characteristic of the grafting reactions of polymer chains: since intercalated H-PDMS is involved in hydrosilylation, the formation of a variety of interlayer configurations of PDMS chains is likely.

The XRF results showed that the Si/Nb ratio was 0.60. The amount of the PDMS chain per $[LaNb_2O_7]$ cannot be determined precisely, however, since unidentified side reactions occurred, as shown by solid-state ^{29}Si CP/MAS NMR. The

amount of the PDMS chain is therefore estimated roughly by assuming that the product consists of the hydrosilylated product only. From the XRF results, the x value of equation (1) is calculated as $0.60\times4/(n+2) = 0.30$. (Since four Nb atoms are present in two [$LaNb_2O_7$] units, the 0.60×4 Si atoms are present. The average number of Si atoms in a PDMS chain is expressed by '(n+2)'. The calculation is performed with $n = 6$). This result indicates that about 30% of the CH_2=CH groups originally present in the CH_2=CH$(CH_2)_8$O- derivative of HLaNb react with H-PDMS. The ^{13}C CP/MAS NMR shows the absence of unreacted CH_2=CH- groups, however, which is inconsistent with the estimated amount of reacted CH_2=CH- groups. We tentatively interpret these observations as resulting from the hydrolysis of the unreacted CH_2=CH$(CH_2)_8$O- groups during the experimental process.

Hydrosilylation of CH_2=CH$(CH_2)_8$O-HLaNb with OHSQ. The XRD pattern of the reaction product of CH_2=CH$(CH_2)_8$O-HLaNb with OHSQ is shown in Figure 2. The low-angle reflection corresponds to a d value of 2.70 nm, indicating that the interlayer distance of the product increases only slightly. The intensity of the low-angle reflection of the CH_2=CH$(CH_2)_8$O-HLaNb decreases drastically, however, after the reaction with OHSQ. The (100) reflection at 28.8° is observed in the same position, indicating preservation of the perovskite-like slab structure.

The IR spectra of OHSQ and the reaction product of CH_2=CH$(CH_2)_8$O-HLaNb with OHSQ are shown in Figures 4-d and 4-e, respectively. In the IR spectrum of OHSQ, the $\nu_{(SiH)}$ band at 2280 cm^{-1}, the $\delta_{(SiH)}$ band at 864 cm^{-1}, and the broad $\nu_{(Si\text{-}O\text{-}Si)}$ band centered at 1120 cm^{-1} are observed.[52] The IR spectrum of the reaction product of CH_2=CH$(CH_2)_8$O-HLaNb with OHSQ shows the $\nu_{(SiH)}$ band at 2250 cm^{-1}, the $\delta_{(SiH)}$ band at 850 cm^{-1}, and the $\nu_{(Si\text{-}O\text{-}Si)}$ band at 1124 cm^{-1}, indicating the presence of OHSQ in the product. The relative intensity of the $\nu_{(CH)}$ bands of the CH_2=CH- groups at 3075 cm^{-1} with respect to the $\nu_{(Nb\text{-}O\text{-}Nb)}$ band at 608 cm^{-1}[53] decreases, suggesting the occurrence of hydrosilylation.

The ^{13}C CP/MAS NMR spectrum of the reaction product of CH_2=CH$(CH_2)_8$O-HLaNb with OHSQ is shown in Figure 6. Signals at 13 (signal J") and 23 ppm (signal K"), which are assignable to $(SiO)_3Si\underline{C}H_2CH_2$- (13 ppm) and $(SiO)_3SiCH_2\underline{C}H_2$- (23 ppm) environments formed by β-addition-type hydrosilylation, are detected.[54,55] A signal at 18 ppm (marked by asterisk) may be assigned to

$(SiO)_3SiCH(\underline{C}H_3)$- groups, moreover, indicating the simultaneous occurrence of the α-addition reaction. Signals are also detected at 115 and 139 ppm, indicating that the presence of unreacted CH_2=CH- groups.

The ^{29}Si CP/MAS NMR spectrum of OHSQ and the reaction product of CH_2=$CH(CH_2)_8$O-HLaNb with OHSQ are shown in Figure 8. In the ^{29}Si CP/MAS NMR spectrum of OHSQ, a signal due to an $H\underline{Si}(OSi)_3$ environment is observed at –84 ppm (signal C). The ^{29}Si CP/MAS NMR spectrum of the reaction product of CH_2=$CH(CH_2)_8$O-HLaNb with OHSQ shows a new signal at –65 ppm (signal C''). This signal can be assigned to an $-CH_2\underline{Si}(OSi)_3$ environment,[56] which is consistent with the occurrence of hydrosilylation. A signal due to the $H\underline{Si}(OSi)_3$ environment is present at –84 ppm. Since the $-CH_2\underline{Si}(OSi)_3$: $H\underline{Si}(OSi)_3$ ratio was estimated by ^{29}Si MAS NMR (not shown) to be ca. 1 : 4.9, 1.4 SiH groups in an OHSQ molecule are involved in hydrosilylation, on average. Signals at –100 and –110 ppm are assignable to $\underline{Si}(OSi)_3(O^-)$ and $\underline{Si}(OSi)_4$ environments, respectively.[49] These signals originate from impurities in the starting OHSQ, as described in the experimental section.

Although the occurrence of hydrosilylation is shown by ^{13}C and ^{29}Si CP/MAS NMR, the interlayer distance does not clearly increase after the reaction, as shown by the XRD results (Figure 2). For the investigation of the presence of OHSQ in the interlayer space, HLaNb, CH_2=$CH(CH_2)_8$O-HLaNb and the reaction product of CH_2=$CH(CH_2)_8$O-HLaNb with OHSQ were pyrolyzed at 350°C and 400°C. The XRD pattterns of the pyrolyzed products are shown in Figure 9. The XRD pattern of HLaNb does not change after the pyrolysis (Figure 9-a), because the TG curves of HLaNb showed the onset temperature of dehydroxylation for HLaNb as ca. 400°C.[57,58] The XRD patterns of both the pyrolyzed residues from CH_2=$CH(CH_2)_8$O-HLaNb show decreases in the interlayer distance from 2.67nm to 1.08 (350°C) and 1.06 nm (400°C), indicating the decomposition of CH_2=$CH(CH_2)_8$O- groups in the interlayer space. Broad reflections (1.84 nm in Figures 9-b and 9-c) are also observed (marked by arrows), indicating that the decomposition is not complete. On the other hand, the XRD pattern of the reaction product (CH_2=$CH(CH_2)_8$O-HLaNb with OHSQ) pyrolyzed at 350° shows a new reflection at 1.60 nm (Figure 9-d). In the residue of the reaction product of CH_2=$CH(CH_2)_8$O-HLaNb with OHSQ pyrolyzed at 400°C, a reflection is observed at ca. 1.3 nm (Figure 9-e). In addition, (100) reflections due to the crystal structures of perovskite-like slabs are observed in the XRD patterns of all pyrolyzed

products at 28.9°. These results clearly indicate that the pyrolysis behavior of the reaction product of CH_2=CH(CH_2)$_8$O-HLaNb with OHSQ is different from that of HLaNb and CH_2=CH(CH_2)$_8$O-HLaNb, a finding ascribable to the presence of OHSQ in the interlayer space of HLaNb. Based on the ^{13}C and ^{29}Si CP/MAS NMR results, therefore, the presence of OHSQ in the interlayer space strongly suggests the occurrence of hydrosilylation in the interlayer space.

The reason for the very small change in the interlayer distance is attributable to the alkyl chain conformation. The ^{13}C CP/MAS NMR spectrum (Figure 6) of CH_2=CH(CH_2)$_8$O-HLaNb shows signals of -CH_2- chains (signal N) at 32 ppm, (We do not discuss the position of signal M, since the CH_2=CH bond may affect the environment of carbon atoms, CH_2=CH$CH_2$$\underline{C}H_2$$\underline{C}H_2$-$CH_2$-), and the signals of the -CH_2- chains of the reaction product of CH_2=CH(CH_2)$_8$O-HLaNb with OHSQ are detected at 31 ppm (signals M" and N"). The chemical shifts of the -CH_2- groups generally reflect the conformation of -CH_2- chains; signals for trans-conformation are detected at 32.6 ppm, while the presence of a larger amount of the gauche-conformations leads to a larger upfield shift.[59,60] The conformation of the -CH_2- chains should change, therefore, after the occurrence of hydrosilylation between CH_2=CH(CH_2)$_8$O-HLaNb and OHSQ to form a substantial amount of gauche-conformation. Consequently, gauche-conformation formation could lead to a decrease in the length of the CH_2=CH(CH_2)$_8$O- groups to cancel an expected increase in the interlayer distance due to the presence of OHSQ in the interlayer space.

Figure 10

When OHSQ is assumed to be a cube (Figure 10), the length of one side is estimated by the Si-O bond length, Si-O-Si bond angle and ionic diameter of oxygen to be 0.635 nm.[61,62] The volume of OHSQ is therefore estimated to be $0.635^3 = 0.256$ nm^3. Since the diagonal length of the OHSQ is $0.635 \times \sqrt{3} = 1.10$ nm, a maximum cross-section is estimated by assuming a circle with a diameter of 1.10 nm to be 0.951 nm^2, an area corresponding to 6.28 [$LaNb_2O_7$] units. The volume of the space between

two adjacent nano-sheets for 6.28 [$LaNb_2O_7$] units is calculated as follows:

Δd×(area of 6.28 [$LaNb_2O_7$] units) = (2.70−1.03) × 0.389^2×6.28 = 1.60 nm^3

(The thickness of the perovskite-like slab is calculated to be

1.03 = 0.389×2+0.25 nm (ionic diameter of oxygen)[62])

The volume of the CH_2=$CH(CH_2)_8$- group is roughly estimated to be 0.186×0.127×10 = 0.24 nm^3 (a cross-section area of the -CH_2- chains is 0.186 nm^2[63] and the increase in the *all-trans* -CH_2- chain is 0.127 nm[64]). Since the 6.28×0.9 of CH_2=$CH(CH_2)_8$- groups are present in 6.28 [$LaNb_2O_7$] units (the average amount of CH_2=$CH(CH_2)_8$- group per [$LaNb_2O_7$] is '0.9'), the estimated free volume is 0.263 (=1.60−0.24×6.28×0.9) nm^3, which is larger than the estimated volume of OHSQ (0.256 nm^3). An OHSQ molecule could therefore fit into 6.28 [$LaNb_2O_7$] units bearing the CH_2=$CH(CH_2)_8$- groups, corresponding to an Si/Nb ratio of 0.64. (0.16 OHSQ per [$LaNb_2O_7$].) The XRF results, on the contrary, showed the Si/Nb ratio to be 0.51, indicating that OHQS can be spatially accommodated in the space between two adjacent nano-sheets. From the Si/Nb ratio, the amount of OHSQ is estimated to be 0.13 per [$LaNb_2O_7$], indicating that OHSQ occupies 80% (0.51/0.64) of the total free volume (0.263 nm^3). The actual amount of OHSQ per [$LaNb_2O_7$] seems to be lower, impurities are also present to a certain extent in OHSQ.

On the other hand, the amount of carbon is determined by CHN analysis to be 18.1%. After the reaction of CH_2=$CH(CH_2)_8$-HLaNb with OHSQ, the general formula is expressed by $\{(H_7Si_8O_{12}\text{-}(CH_2)_{10}\}_x\{CH_2{=}CH(CH_2)_8\text{-}\}_{0.9-x}H_{0.1}LaNb_2O_7$. The amount of OHSQ is therefore calculated by the following equation:

$10\times0.9\times(\text{atomic weight of C})/[Mw_{\{(H_7Si_8O_{12}\text{-}(CH_2)_{10}\}_x\{CH_2=CH(CH_2)_8\text{-}\}_{0.9-x}H_{0.1}LaNb_2O_7}] = 0.181$

The amount of OHSQ, x value, is estimated to be 0.09 per [$LaNb_2O_7$], which is smaller than the value estimated from the XRF results (0.13). This difference could be partially attributed to the presence of silicon containing impurities. Based on the two types of estimations, we assume that the space between two adjacent nano-sheets is occupied by the CH_2=$CH(CH_2)_8$- groups (~85%) and hydrosilylated OHSQ (~9–14%).

Conclusions

We have investigated the hydrosilylation of the CH_2=CH- groups immobilized on the interlayer surface of layered perovskite, $HLaNb_2O_7 \cdot xH_2O$, with SiH groups in hydrochlorosilanes, hydride-terminated polydimethylsiloxane or octahydridosilsesquioxane. Immobilization of the CH_2=CH- groups on the interlayer surface was conducted by reacting the *n*-propoxy derivative of $HLaNb_2O_7 \cdot xH_2O$ with 4-penten-1-ol or 9-decen-1-ol to form the $CH_2=CH(CH_2)_nO$-derivative (n = 3 or 8) of $HLaNb_2O_7 \cdot xH_2O$. The CH_2=CH- groups on the interlayer surface can be reacted with hydrochlorosilanes, hydride-terminated polydimethylsiloxane and octahydridosilsesquioxane to give a hydrosilylated product. The spectroscopic analyses and the increases in the interlayer distances clearly indicate that hydrosilylation with hydrochlorosilanes and hydride-terminated polydimethylsiloxane occurs in the interlayer space. Although the XRD pattern of the reaction product of the $CH_2=CH(CH_2)_nO$-derivative of HLaNb with octahydridosilsesquioxane shows a slight increase in the interlayer distance, ^{13}C and ^{29}Si CP/MAS NMR spectra indicate the occurrence of hydrosilylation. The hydrosilylation with octahydridosilsesquioxane in the interlayer space is demonstrated by its pyrolysis behavior, and the lack of an increase in the interlayer distance is explained by the conformation change of the $-CH_2-$ chain. In addition, the XRD results for all the hydrosilylated products show the (100) reflection at 28.8°, indicating the preservation of the perovskite-like slab structure during the hydrosilylation. This study, therefore, clearly demonstrates that grafting of the $CH_2=CH(CH_2)_n$-O groups and subsequent hydrosilylation is a versatile approach for grafting the functional groups on the interlayer surface of the ion-exchangeable layered perovskites. Various inorganic-organic hybrids are expected to be prepared via hydrosilylation by applying other reactions involving various organic and organometallic molecules.

Acknowledgements.

The authors express their gratitude to Prof. Kazuyuki Kuroda of Waseda University, Department of Applied Chemistry, for his valuable discussions. Experimental technical supports by Dr. Ichiro Fujiwara and Mr. Yusuke Mori are also acknowledged. This work was financially supported by the Grant-in-Aid for Scientific Research (No. 14350462) from the Ministry of Education, Science, Sports, and Culture, Japan, and by 21COE "Practical Nano-Chemistry" from MEXT, Japan.

Figure captions

Figure 1 XRD patterns of (a) *n*-propoxy derivatives of HLaNb, (b) CH_2=CH$(CH_2)_3$O-HLaNb, (c) the reaction product of CH_2=CH$(CH_2)_3$O-HLaNb with dichloromethylsilane and (d) the reaction product of CH_2=CH$(CH_2)_3$O-HLaNb with trichlorolsilane.

Figure 2 XRD patterns of (a) CH_2=CH$(CH_2)_8$O-HLaNb, (b) the reaction product of CH_2=CH$(CH_2)_8$O-HLaNb with H-PDMS and (c) the reaction product of CH_2=CH$(CH_2)_3$O-HLaNb with OHSQ.

Figure 3 IR spectra of (a) *n*-propoxy derivatives of HLaNb, (b) the CH_2=CH$(CH_2)_3$O-HLaNb, (c) the reaction product of CH_2=CH$(CH_2)_3$O-HLaNb with dichloromethylsilane and (d) the reaction product of CH_2=CH$(CH_2)_3$O-HLaNb with trichlorolsilane.

Figure 4 IR spectra of (a) CH_2=CH$(CH_2)_8$O-HLaNb, (b) H-PDMS, (c) the reaction product of CH_2=CH$(CH_2)_8$O-HLaNb with H-PDMS, (d) OHSQ and (e) the reaction product of CH_2=CH$(CH_2)_3$O-HLaNb with OHSQ.

Figure 5 Solid-state ^{13}C CP/MAS NMR spectra of (a) *n*-propoxy derivatives of HLaNb, (b) CH_2=CH$(CH_2)_3$O-HLaNb, (c) the reaction product of CH_2=CH$(CH_2)_3$O-HLaNb with dichloromethylsilane and (d) the reaction product of CH_2=CH$(CH_2)_3$O-HLaNb with trichlorolsilane.

Figure 6 Solid-state ^{13}C CP/MAS NMR spectra of (a) CH_2=CH$(CH_2)_8$O-HLaNb, (b) PDMS, (c) the reaction product of CH_2=CH$(CH_2)_8$O-HLaNb with H-PDMS and (d) the reaction product of CH_2=CH$(CH_2)_3$O-HLaNb with OHSQ. The figure in the box (right) is the image expanded in the range 20–40 ppm.

Figure 7 Solid-state ^{29}Si CP/MAS NMR spectra of (a) the reaction product of CH_2=CH$(CH_2)_3$O-HLaNb with dichloromethylsilane and (b) the reaction product of CH_2=CH$(CH_2)_3$O-HLaNb with trichlorolsilane.

Figure 8 Solid-state ^{29}Si CP/MAS NMR spectra of (a) H-PDMS, (b) the reaction product of $CH_2=CH(CH_2)_8O$-HLaNb with H-PDMS, (c) OHSQ and (d) the reaction product of $CH_2=CH(CH_2)_3O$-HLaNb with OHSQ.

Figure 9 The XRD patterns of (a) the pyrolyzed HLaNb at 400°C, (b) the pyrolyzed $CH_2=CH(CH_2)_8O$-HLaNb at 350°C, (c) the pyrolyzed $CH_2=CH(CH_2)_8O$-HLaNb at 400°C, (d) the pyrolyzed reaction product with OHSQ at 350°C and (e) the pyrolyzed reaction product with OHSQ at 400°C. The inset patterns in (d) and (e) are recorded at a scan speed of 0.3°/min in the range of 5–12°.

Figure 10 The length on the side assuming OHSQ as a cube and the cross-section area of OHSQ are demonstrated. The area of the $[LaNb_2O_7]$ unit is shown (right).

Scheme 1 Overview of the reaction of hydrochlorosilanes and oligosiloxanes *via* the hydrosilylation.

Scheme 2 Proposed reaction of $CH_2=CH(CH_2)_8$-HLaNb with H-PDMS.

References

1. Alexandre, M.; Dubois, P. *Mater. Sci. Eng.* **2000,** *R28*, 1-63.
2. Choy, J.-H. *J. Phys. Chem. Solid* **2004,** *65*, 373-383.
3. Corriu, R. J. P.; Leclercq, D. *Angew. Chem. Int. Ed. Engl.* **1996,** *35*, 1420-1436.
4. Judeinstein, P.; Sanchez, C. *J. Mater. Chem.* **1996,** *6*, 511-525.
5. Sanchez, C.; Ribot, F. *New Jounal of Chermistry* **1994,** *18*, 1007-1047.
6. Sanchez, C.; Soler-Illia, G. J. d. A. A.; Ribot, F.; Lalot, T.; Mayer, C. R.; Cabuil, V. *Chem. Mater.* **2001,** *13*, 3061-3083.
7. Ogawa, M.; Kuroda, K. *Chem. Rev.* **1995,** *95*, 399-438.
8. Ogawa, M.; Kuroda, K. *Bull. Chem. Soc. Jpn.* **1997,** *70*, 2593.
9. *Intercalation Chemistry*. Academic Press: New York, 1982.
10. O'Hare, D., *Inorganic Materials, 2nd ed.* John Wiley & Sons: Chichester, 1996; p 171.
11. Kanatzidis, M. G.; Wu, C. G.; Marcy, H.; Kannewurf, C. B. *J. Am. Chem. Soc.* **1989,** *111*, 4139-4141.
12. Mehrotra, V.; Giannelis, E. P. *Solid State Ionics* **1992,** *51*, 115-122.
13. Ebina, Y.; Tanaka, A.; Kondo, J. N.; Domen, K. *Chem. Mater.* **1996,** *8*, 2534-2538.
14. Ruiz-Hitzky, E.; Rojo, J. M. *Nature* **1980,** *287*, 28-30.
15. Ogawa, M.; Okutomo, S.; Kuroda, K. *J. Am. Chem. Soc.* **1998,** *120*, 7361-7362.
16. Tunney, J. J.; Detellier, C. *J. Mater. Chem.* **1996,** *6*, 1679-1685.
17. Komori, Y.; Enoto, H.; Takenawa, R.; Hayashi, S.; Sugahara, Y.; Kuroda, K. *Langmuir* **2000,** *16*, 5506-5508.
18. Kikkawa, S.; Kanamaru, F.; Koizumi, M. *Inorg. Chem.* **1976,** *15*, 2195-2197.
19. Alberti, G.; Casciola, M.; Constantino, U.; Vivani, R. *Adv. Mater.* **1996,** *8*, 291-303.
20. Goodenough, J. B.; Longo, J. M., *"Landolt-Börnstein" New Series, Group III, Vol. 4, Part a*. Springer: Berlin, 1970.
21. Cross, L. E., *Ferroelectric Ceramics*. Brinkhauser Verlag: Basel, 1993.
22. Du, X.; Chen, I.-W. *Ferroelectrics* **1998,** *208*, 237-256.
23. Kurtz, S. K.; Perry, T. T. *J. Appl. Phys.* **1968,** *39*, 3798-3813.
24. Schaak, R. E.; Mallouk, T. E. *Chem. Mater.* **2002,** *14*, 1455-1471.

25. Yoshimura, J.; Ebina, Y.; Kondo, J. N.; Domen, K.; Tanaka, A. *J. Phys. Chem.* **1993,** *97*, 1970-1973.
26. Kudo, M.; Tsuzuki, S.; Katshumata, K.; Yasumori, A.; Sugahara, Y. *Chem. Phys. Lett.* **2004,** *393*, 12-16.
27. Sato, M.; Abo, J.; Jin, T.; Ohta, M. *J. Alloys Compd.* **1993,** *192*, 81-83.
28. Zhong, Z.; Ding, W.; Hou, W.; Chen, Y.; Chen, X.; Zhu, Y.; Min, N. *Chem. Mater.* **2001,** *13*, 538-542.
29. Tahara, S.; Sugahara, Y., Novel Materials Derived from Layered Perovskites using a *Chimie Douce* Appproach. In *Recent Res. Devel. Inorganic Chemistry*, Pandalai, S. G., Ed. Transworld Reseach Network: India, 2004; Vol. 4, pp 13-34.
30. Takahashi, S.; Nakato, T.; Hayashi, S.; Sugahara, Y.; Kuroda, K. *Inorg. Chem.* **1995,** *34*, 5065-5069.
31. Tahara, S.; Sugahara, Y. *Langmuir* **2003,** *19*, 9473-9478.
32. Suzuki, H.; Notsu, K.; Takeda, Y.; Sugimoto, W.; Sugahara, Y. *Chem. Mater.* **2003,** *15*, 636-641.
33. Speier, J. L., *Advances in Organometallic Chemistry*. Academic Press: New York, 1979; Vol. 17, p 407-447.
34. Ojima, I., *The Chemistry of Organic Silicon compounds (Chapter 25)*. Wiley: Chichester, 1989.
35. Marciniec, B.; Gulinski, J.; Urbaniak, W.; Kornetka, Z. W., *Comprehensive Handbook on Hydrosilylation*. Pergamon press: Oxford, 1992.
36. Musolf, M. C.; Speier, J. L. *J. Org. Chem.* **1964,** *29*, 2519-2524.
37. Buriak, J. M. *Chem. Commun.* **1999**, 1051-1060.
38. Boukherroub, R.; Morin, S.; Bensebaa, F.; Wayner, D. D. M. *Langmuir* **1999,** *15*, 3831-3835.
39. Fyfe, C. A.; Niu, J.; 3894., M. *Macromol.* **1995,** *28*, 3894-3897.
40. Katsoulis, D. E.; Chao, T. C.-S.; McQuiston, E. A.; Chen, C.; Kenney, M. E. *Mater. Res. Soc. Symp.* **1998,** *519*, 321-326.
41. Chao, T. C.; Katsoulis, D. E.; Kenney, M. E. *Chem. Mater.* **2001,** *13*, 4269-4277.
42. Yoshioka, S.; Takeda, Y.; Uchimaru, Y.; Sugahara, Y. *J. Organomet. Chem.* **2003,** *686*, 145-150.

43. Gopalakrishnan, J.; Bhat, V.; Raveau, B. *Mater. Res. Bull.* **1987,** *22*, 413-417.
44. Agaskar, P. A. *Inorg. Chem.* **1991,** *30*, 2707-2708.
45. Agaskar, P. A. *Inorg. Chim. Acta* **1995,** *229*, 355-364.
46. Shriver, D. F.; Drezdzon, M. A., *The Manipulation of Air-Sensitive Compounds, second ed.* Wiley-Interscience: New York, 1986.
47. Eaborn, C.; Bott, B. W., *Organometallic Compounds of the Group IV Elements Part 2.* Marcel Dekker: New York, 1986; Vol. 1, p 1968.
48. Shurvell, H. F., Sample Characterization and Spectral Data Processing. In *Handbook of Vibrational Spectroscopy*, Chalmers, J. M.; Griffiths, P. R., Eds. Wiley: Chichester, 2002; Vol. 3, p 1783.
49. Marsmann, H., NMR 17, Basic Principals and Progress, Oxygen-17 and Silicon-29. In *NMR 17, Basic Principals and Progress, Oxygen-17 and Silicon-29*, Diehl, P.; Fluck, E.; Cosfeld, R., Eds. Springer-Verlag: Berlin, 1981.
50. Marchand, A.; Valade, J. *J. Organomet. Chem* **1968,** *12*, 305-322.
51. Henkensmeier, D.; Abele, B. C.; Candussio, A.; Thiem, J. *Macromol. Chem. Phys.* **2004,** *205*, 1851-1857.
52. Fryfe, C. L.; Collins, W. T. *J. Am. Chem. Soc.* **1970,** *92*, 5586-5588.
53. Vandenborre, M. T.; Husson, E.; Chubb, M. *Spectrochim. Acta* **1984,** *40*, 361-365.
54. Tsuchida, A.; Bolln, C.; Sernetz, F. G.; Frey, H.; Mühaupt, R. *Macromol.* **1997,** *30*, 2818-2824.
55. Sellinger, A.; Laine, R. M. *Chem. Mater.* **1996,** *8*, 1592-1593.
56. Auner, N.; Bats, J. W.; Katsoulis, D. E.; Suto, M.; Tecklenburg, R. E.; Zank, G. A. *Chem. Mater.* **2000,** *12*, 3402-3418.
57. Ollivier, P. J.; Mallouk, T. E. *Chem. Mater.* **1998,** *10*, 2585-2587.
58. Jacobson, A. J.; Lewandouski, J. T.; Johnson, J. W. *J. Less-Common Met.* **1986,** *116*, 137-146.
59. Pursch, M.; Strohschein, S.; Händel, H.; Albert, K. *Anal. Chem.* **1996,** *68*, 386-393.
60. Pursch, M.; Brindle, R.; Ellwanger, A.; Sander, L. C.; Bell, C. M.; Händel, H.; Albert, K. *Solid State Nucl. Magn. Reson.* **1997,** *9*, 191-201.
61. Rattay, M.; Fenske, D.; Jutzi, P. *Organometallics* **1998,** *17*, 2930-2932.

62. Shannon, R. D. *Acta Crystallogr.* **1976,** *A32*, 751-767.

63. Goñi, A.; Ruis, J.; Insausti, M.; Lezama, L. M.; Pizarro, J. L.; Arriortua, M. I.; Rojo, T. *Chem. Mater.* **1996,** *8*, 1052-1060.

64. Jacobson, A. J.; Johnson, J. W.; Lewandouski, J. T. *Mater. Res. Bull.* **1987,** *22*, 45-51.

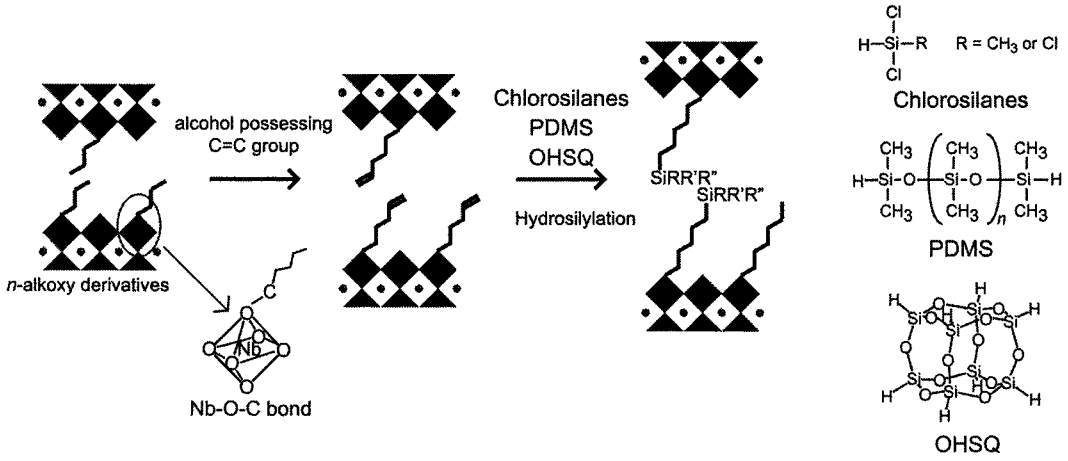

Scheme 1 Overview of the reaction of hydrochlorosilanes and oligosiloxanes *via* the hydrosilylation.

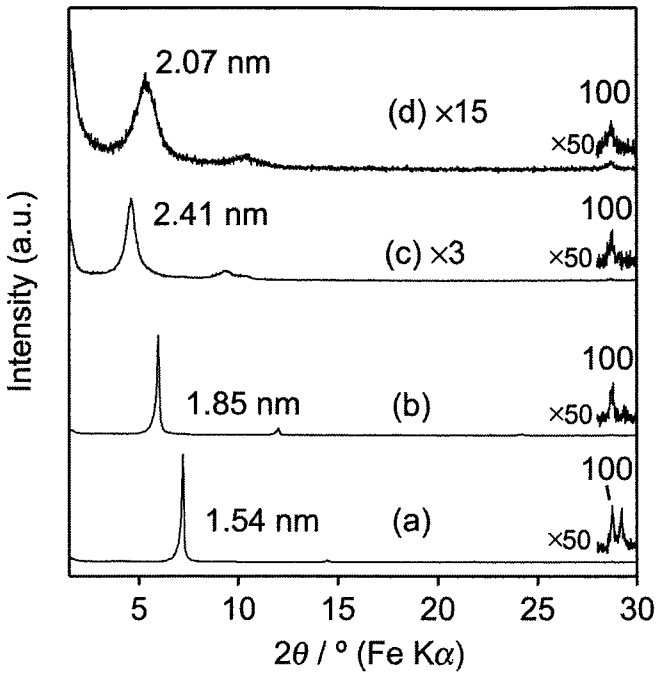

Figure 1 XRD patterns of (a) *n*-propoxy derivatives of HLaNb, (b) CH_2=CH$(CH_2)_3$O-HLaNb, (c) the reaction product of CH_2=CH$(CH_2)_3$O-HLaNb with dichloromethylsilane and (d) the reaction product of CH_2=CH$(CH_2)_3$O-HLaNb with trichlorolsilane.

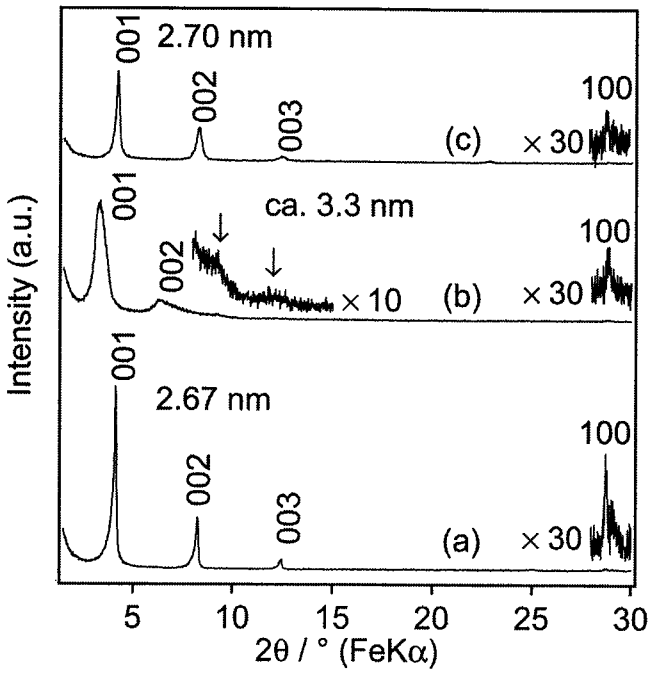

Figure 2 XRD patterns of (a) CH_2=CH$(CH_2)_8$O-HLaNb, (b) the reaction product of CH_2=CH$(CH_2)_8$O-HLaNb with H-PDMS and (c) the reaction product of CH_2=CH$(CH_2)_3$O-HLaNb with OHSQ.

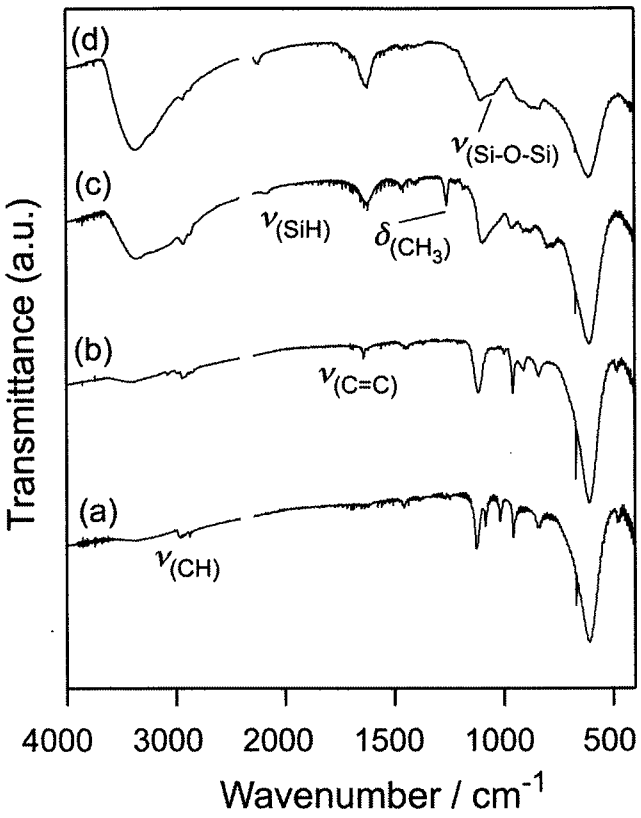

Figure 3 IR spectra of (a) *n*-propoxy derivatives of HLaNb, (b) the CH_2=$CH(CH_2)_3O$-HLaNb, (c) the reaction product of CH_2=$CH(CH_2)_3O$-HLaNb with dichloromethylsilane and (d) the reaction product of CH_2=$CH(CH_2)_3O$-HLaNb with trichlorolsilane.

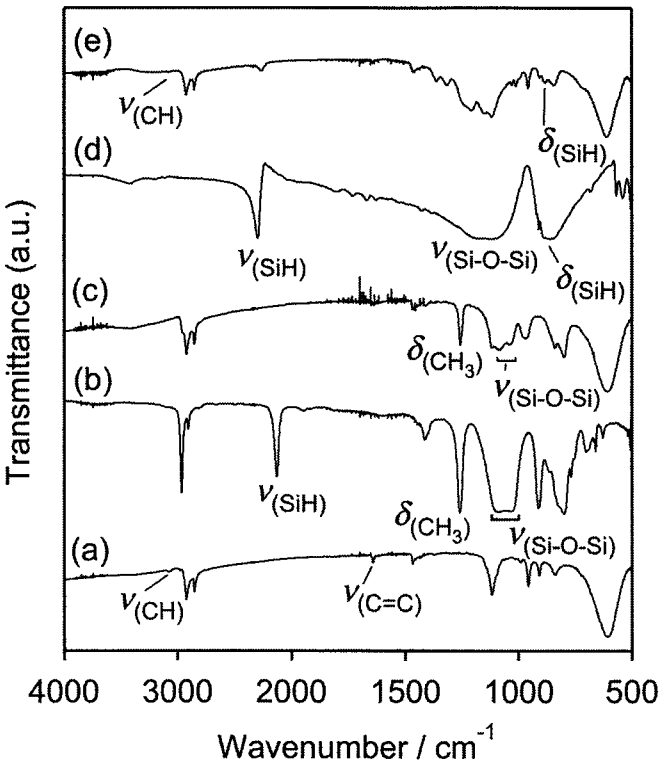

Figure 4 IR spectra of (a) CH_2=$CH(CH_2)_8O$-HLaNb, (b) H-PDMS, (c) the reaction product of CH_2=$CH(CH_2)_8O$-HLaNb with H-PDMS, (d) OHSQ and (e) the reaction product of CH_2=$CH(CH_2)_3O$-HLaNb with OHSQ.

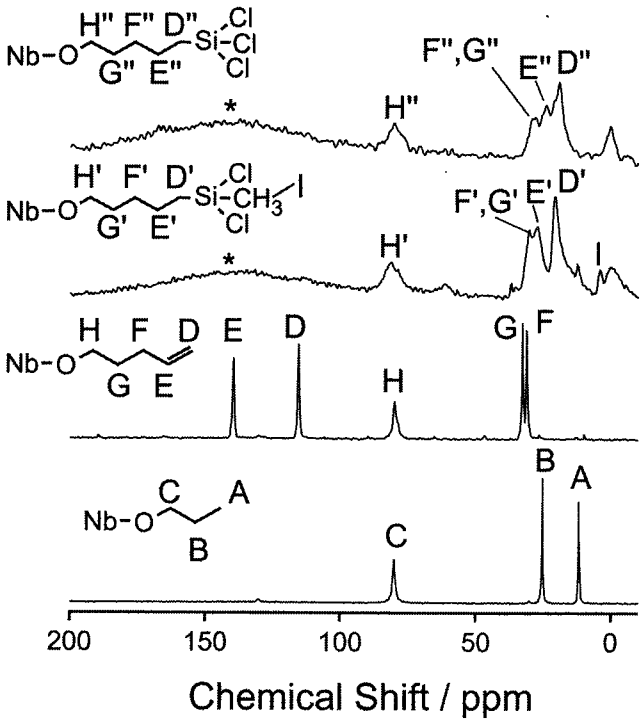

Figure 5 Solid-state ^{13}C CP/MAS NMR spectra of (a) *n*-propoxy derivatives of HLaNb, (b) CH_2=$CH(CH_2)_3O$-HLaNb, (c) the reaction product of CH_2=$CH(CH_2)_3O$-HLaNb with dichloromethylsilane and (d) the reaction product of CH_2=$CH(CH_2)_3O$-HLaNb with trichlorolsilane.

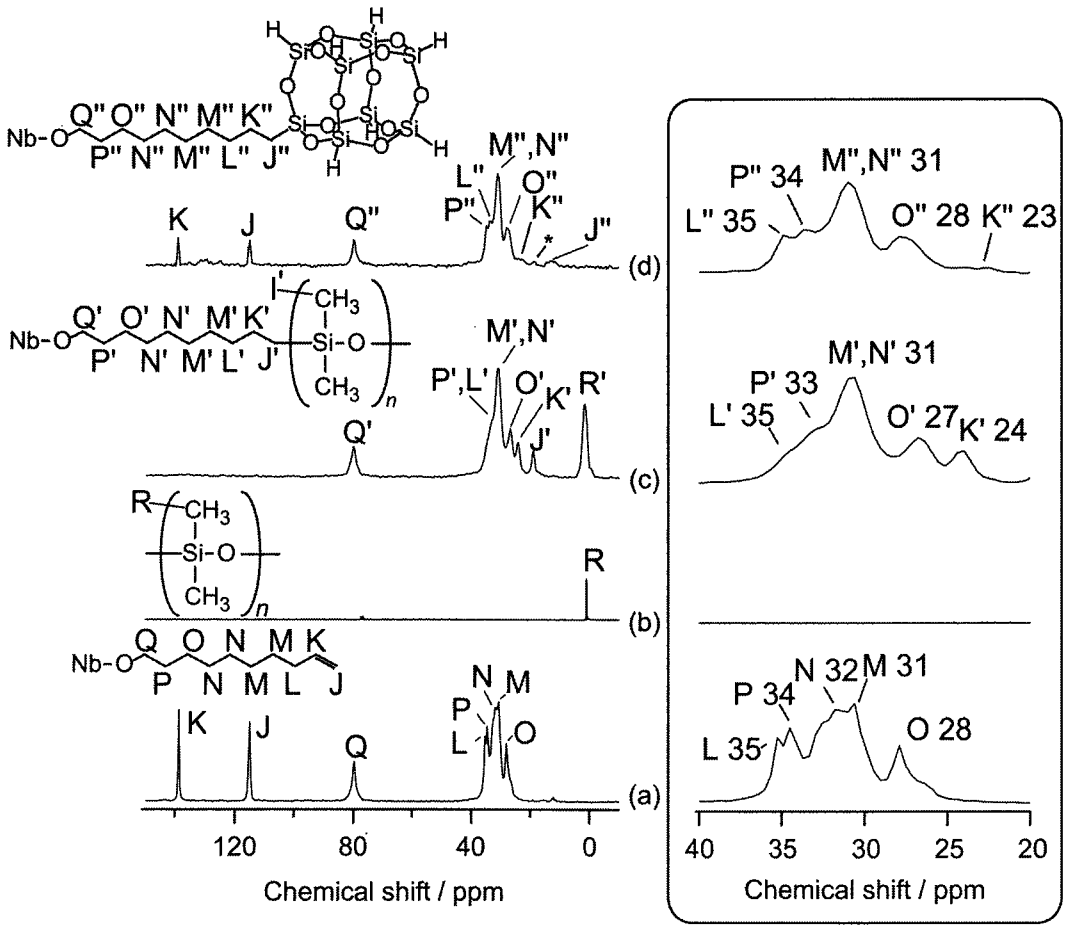

Figure 6 Solid-state ^{13}C CP/MAS NMR spectra of (a) $CH_2=CH(CH_2)_8O$-HLaNb, (b) PDMS, (c) the reaction product of $CH_2=CH(CH_2)_8O$-HLaNb with H-PDMS and (d) the reaction product of $CH_2=CH(CH_2)_3O$-HLaNb with OHSQ. The figure in the box (right) is the image expanded in the range 20–40 ppm.

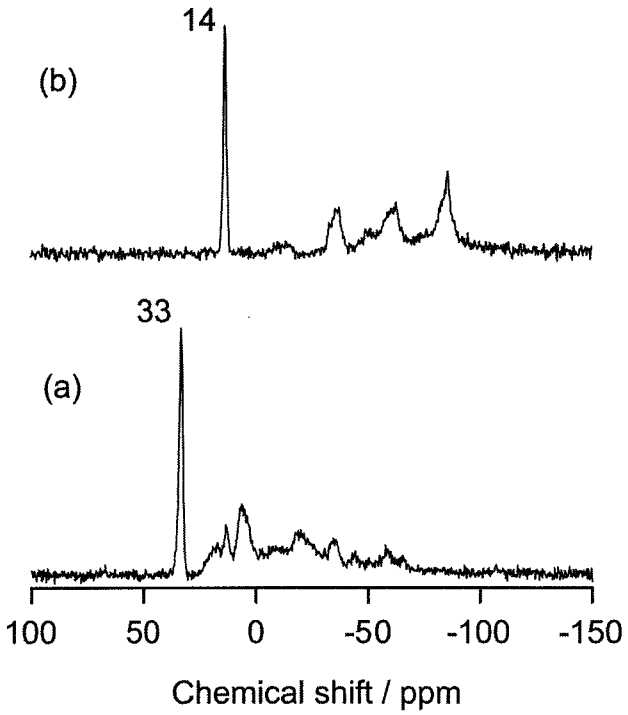

Figure 7 Solid-state ^{29}Si CP/MAS NMR spectra of (a) the reaction product of CH_2=CH$(CH_2)_3$O-HLaNb with dichloromethylsilane and (b) the reaction product of CH_2=CH$(CH_2)_3$O-HLaNb with trichlorolsilane.

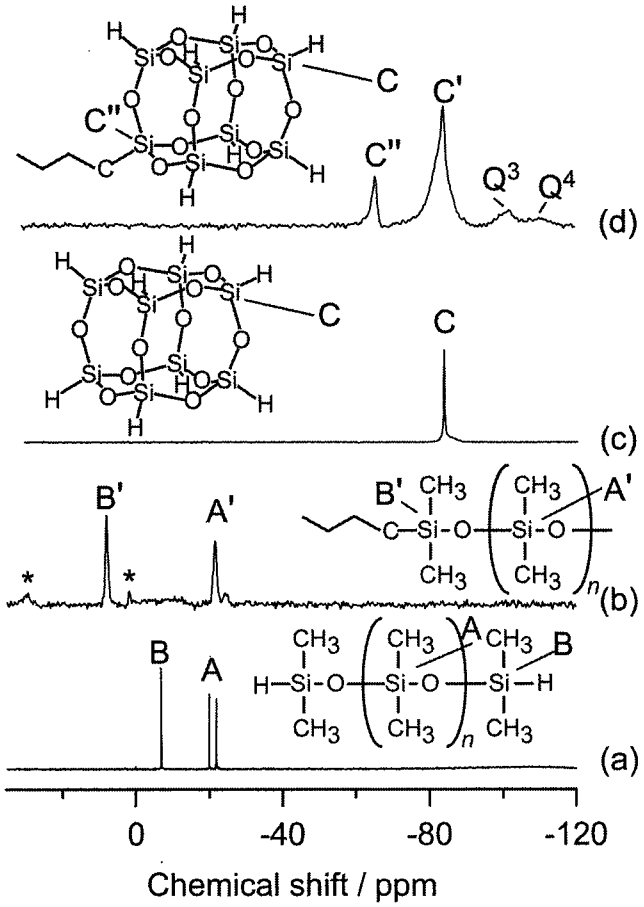

Figure 8 Solid-state ^{29}Si CP/MAS NMR spectra of (a) H-PDMS, (b) the reaction product of CH_2=CH$(CH_2)_8$O-HLaNb with H-PDMS, (c) OHSQ and (d) the reaction product of CH_2=CH$(CH_2)_3$O-HLaNb with OHSQ.

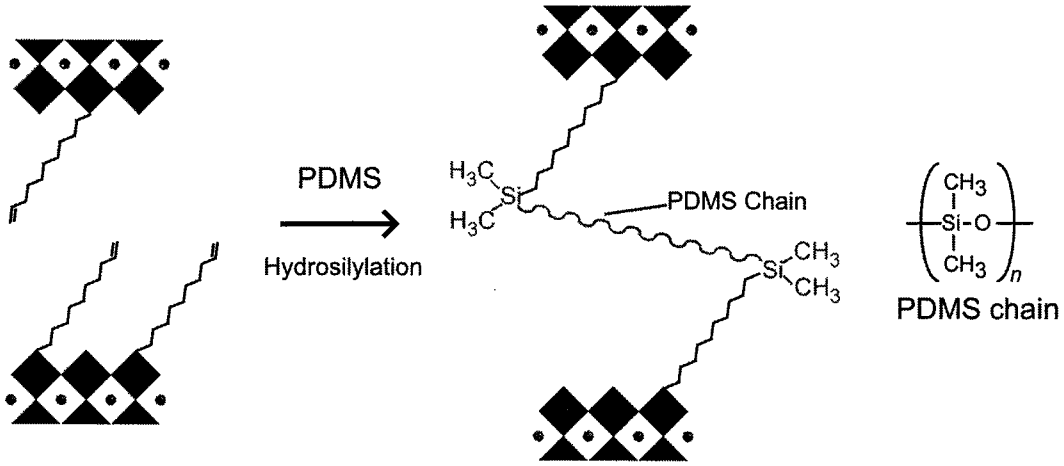

Scheme 2 Proposed reaction of CH_2=$CH(CH_2)_8$-HLaNb with H-PDMS.

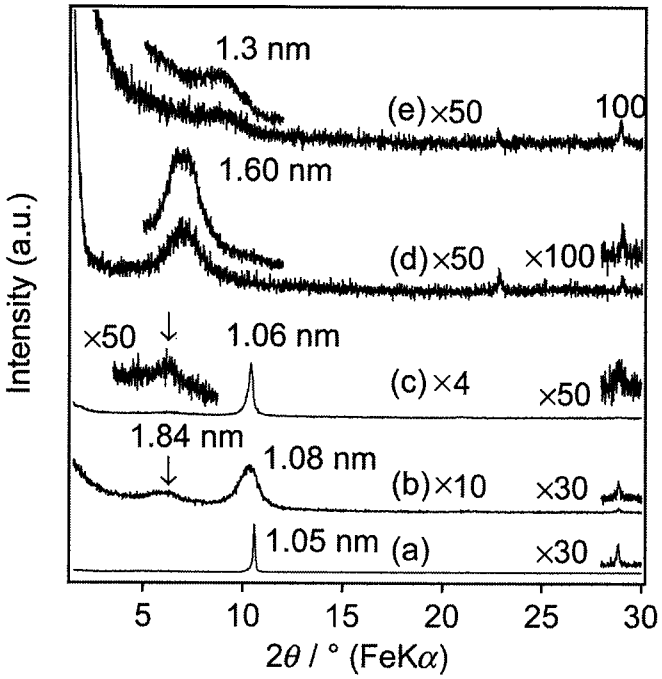

Figure 9 The XRD patterns of (a) the pyrolyzed HLaNb at 400°C, (b) the pyrolyzed CH_2=$CH(CH_2)_8O$-HLaNb at 350°C, (c) the pyrolyzed CH_2=$CH(CH_2)_8O$-HLaNb at 400°C, (d) the pyrolyzed reaction product with OHSQ at 350°C and (e) the pyrolyzed reaction product with OHSQ at 400°C. The inset patterns in (d) and (e) are recorded at a scan speed of 0.3°/min in the range of 5–12°.

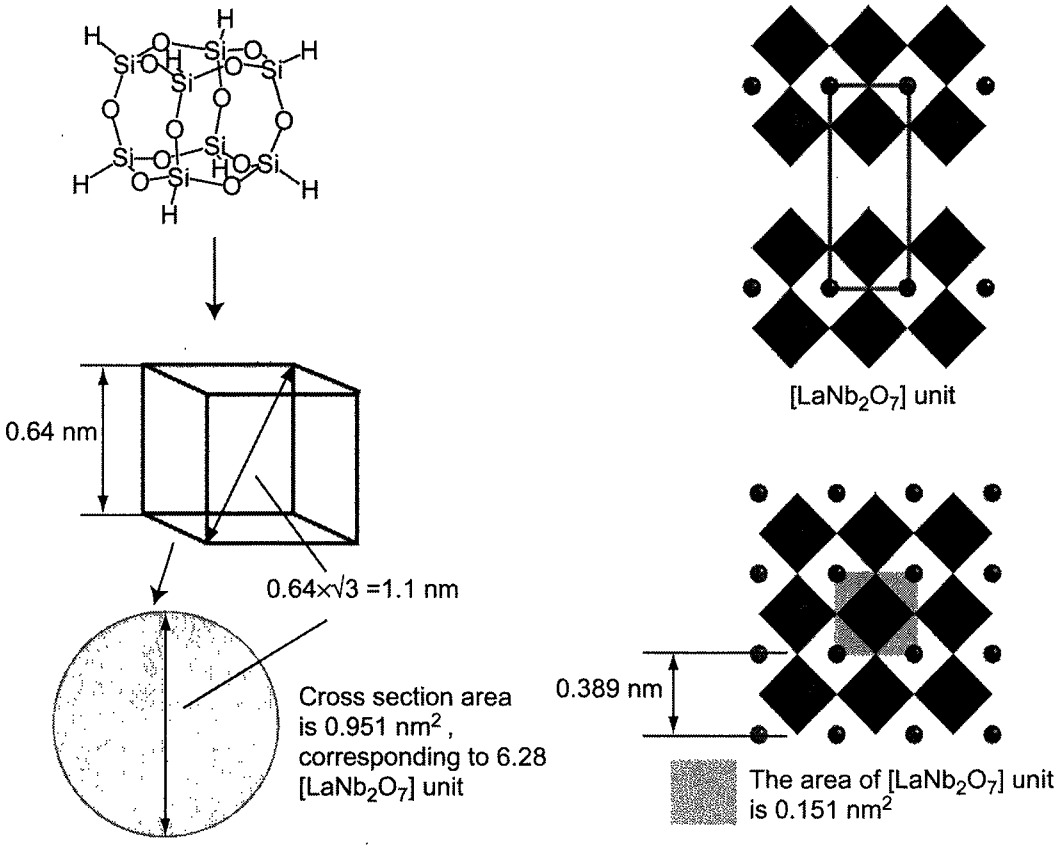

Figure 10 The length on the side assuming OHSQ as a cube and the cross-section area of OHSQ are demonstrated. The area of the $[LaNb_2O_7]$ unit is shown (right).